# BALANCE CONTROL OF CONSTRAINED BIPEDAL STANDING AND STABILITY ANALYSIS USING THE CONCEPT OF LYAPUNOV EXPONENTS

By

CAIXIA YANG

A thesis
Submitted to the Faculty of Graduate Studies
in Partial Fulfillment of the Requirement
for the Degree of

DOCTOR OF PHILOSOPHY

Department of Mechanical and Manufacturing Engineering
The University of Manitoba
Winnipeg, Manitoba
Canada

THE UNIVERSITY OF MANITOBA

FACULTY OF GRADUATE STUDIES

*****

COPYRIGHT PERMISSION

BALANCE CONTROL OF CONSTRAINED BIPEDAL

STANDING AND STABILITY ANALYSIS USING THE

CONCEPT OF LYAPUNOV EXPONENTS

BY

CAIXIA YANG

A Thesis/Practicum submitted to the Faculty of Graduate Studies of The University of

Manitoba in partial fulfillment of the requirement of the degree

DOCTOR OF PHILOSOPHY

To

My Parents

Husband

And Three Children

# Abstract

Balancing control of a constrained biped during standing is extremely challenging in that (1) the constraints between the feet and the ground impose bounds on the control torque, which makes balance controller design challenging, and (2) the lack of a single quantitative criterion and an effective tool for stability analysis prohibits the stability analysis of such highly nonlinear systems. There are two objectives of this thesis. The first objective is to systematically study balancing control of a simplified biped using the modeling approach, which includes (i) investigating the effects of the constraints between the feet and the ground during standing, (ii) designing a balancing controller satisfying the constraints, and (iii) analyzing the stability of the constrained bipedal control system using the concept of Lyapunov exponents, where the exponents are calculated from the mathematical model. The results show that the constraints between the feet and the ground have significant effects on balancing control design and thus they must be satisfied. The stability analysis reveals that the stability region determined using the concept of Lyapunov exponents is reasonably close to the one from previous work where the stability was defined based on clinical observations.

This thesis deals with a stability analysis of a constrained biped during standing. The problem is inherently difficult because the corresponding system is highly nonlinear. There is no simple methodology to determine the stability of the system. Lyapunov's stability theory has very limited applicability. Although Lyapunov exponents calculated from either the mathematical model or a time series can be used to characterize the type of stability of the potentially-stable system under consideration, the existing analytical

and numerical techniques have been developed for chaotic systems for which at least one exponent is positive. Since in potentially stable systems the largest exponent is either negative or zero, the existing techniques to compute the exponents are inaccurate. The second objective of this thesis is to develop a method for calculating negative Lyapunov exponents using a time series so that the stability of potential stable engineering systems can be studied using the concept of Lyapunov exponents. The balancing control system of the biped is used as an example to demonstrate the efficacy of the proposed method. The time series is generated by computer simulations from the mathematical model. The results show that: (1) The Lyapunov exponents calculated are more accurate. For nonlinear mapping, the minimum average relative error is 6.74%. For linear mapping, the minimum average relative error is 6.84%; (2) The calculated exponents' spectrum is not sensitive to the values of time lag, $T_{lag}$, and evolving time, $T_{evol}$, while, using linear mapping, the calculated exponents' spectrum is extremely sensitive to above key parameters; (3) No spurious Lyapunov exponents are generated. Some ground work has been laid on applying the concept of Lyapunov exponents to the analysis of stable systems.

The proposed method for calculating Lyapunov exponents based on time series is both systematic and constructive. It has a great potential for obtaining negative Lyapunov exponents and has significant practical applications in engineering systems. Furthermore, the method is not restricted to bipedal robotic systems. It can be used to general nonlinear potentially stable systems, especially for practical engineering systems.

# Acknowledgements

First and foremost, I would like to thank my advisor, Dr. Christine Q. Wu for giving me the opportunity to pursue my Ph.D. studies. Thank you for providing continuous guidance, stimulating suggestions, patience and encouragements that helped me go through every struggling moment throughout the course of my research.

My sincere appreciation goes to the members of my advisory committee members, Dr. Steve Onyshko, Dr. Witold Kinsner and Dr. A.B. Gumel, for their careful review, comments and suggestions with regard to this research. I also would like to thank Dr. Steve Onyshko, Dr. Nariman Sepehri, Dr. Witold Kinsner, Dr. A.B. Gumel and Dr. W.T.H. van Oers for providing me with the fundamental background knowledge in the areas of nonlinear stability analysis, control and robots, fractal and chaos, numerical stability analysis, and classical mechanics. Thanks also go to Dr. Hooshang Heimami, the external examiner of the thesis examination committee.

I thank Dr. Yushu Chen and Dr. Jian Xu, for their helpful and valuable discussions. I thank Dr. Zhu and Dr. Yu for their encouragement and help. I also thank my fellow students in the Nonlinear System Research Laboratory for making the environment comfortable and enjoyable. To all my friends whose names are not listed your support did not go unnoticed.

Finally, I wish to thank my husband for his love, encouragement, and confidence in my ability, spirit support and many sacrifices during my study. My deepest thanks go to my parents for their infinite love and support and the numerous sacrifices made on my behalf. I could not have accomplished my goals without any of them.

# Table of Contents

# List of Figures

# List of Tables

# Glossary

**accuracy** (a) A numerical measure of how close an approximation is to the truth;(b) Correctness, in the sence of lack of bias.

**anatomical position** For the purpose of universal comparison, there is a standard position - the anatomical position- that the patient or cadaver theoretically has assumed. This allows consistent description of body parts in relation to each other.

**attractor** The phase space point or set of points representing the various possible steady-state conditions of a system; in other words, an equilibrium state or group of states to which a dynamical system converges.

**autonomous** Independent of time

**basin of attraction** The group of all possible phase space points that can evolve onto a given attractor

**bilateral symmetry** A figure that has bilateral symmetry can be cut exactly into two identical mirror halves. The line along which a shape is cut is called the line of symmetry. The plane along which a solid is cut is called the plane of symmetry.

**bit** The unit of information when logs are taken to the base 2

**chaos** (a) Sustained and random-like long-term evolution that satisfies certain special mathematical criteria and that happens in deterministic, nonlinear, dynamical systems; (b) largely unpredictable long-term evolution occurring in a deterministic, nonlinear dynamical system because of sensitivity to initial conditions.

**constant** A quantity that does not vary under specified conditions.

**decomposition** The numerical expression of a quatity in terms of its simpler components

**delay-coordinate method** Same as time-delay method

**delay method** Same as time-delay method

**dynamical** Changing with time

**dynamical system** (a) Anything that moves or that evolves in time; (b) any process or model in which each successive state is a function of the preceding state.

**embedding** The preparation of a pseudo phase space graph to reconstruct a system's dynamics (attractor), using successively lagged values of a single variable

**embedding dimension** The total number of separate time series (consisting of the original series and subgroups obtained by lagging that series) used in a phase space plot or in a more rigorous mathematical analysis.

**equation of motion** An equation in which time is the independent variable.

**equilibrium point** Same as fixed point

**ergodic** (a) The property whereby statistical measures of an ensemble don't change with time and, in addition, all statistics are invariant from one time series to another within the ensemble; (b) said of a system for which spatial or ensemble averages are equal to time averages (meaning that time averages are independent of starting time and that most points visit every region of phase space with about equal probability); (c) said of a trajectory if it comes back arbitrarily close to itself after some time; (d) the property whereby averages computed from a date sample converge over time to ensemble average (i.e. statistics of all initial states ultimately lead to the same set of statistics).

**ergodic theory** The mathematical study of the long-term average behavior of dynamical systems

**exponential divergence** Temporal separation of two adjacent trajectories according to an exponential law, that is, by a straight-line relation between the log of separation distance (as the dependent variable) and time.

**false nearest neighbor** A point in lagged space that is close to another point only because the embedding dimension is too low

**fiducial** Referring to something used as a standard of reference for measurement or calculation. Examples: fiducial point, fiducial trajectory

**fiducial trajectory** A trajectory used as a reference trajectory from which to compute ordital gaps and the Laypunov exponent

**Gram-Schmidt orthogonalization** Same as orthogonalization

**hypercube** The multidimensional analog of a cube

**hyperspace** Space of more than three dimensions

**hypersphere** The multidimensional analog of a sphere

**identity line (or identity map)** A $45^0$ straight line on an arithmetic-scale two-coordinate graph, representing the relation $y = x$

**initial conditions** Values of variables at the beginning of any specified time

**invertible** Having a unique successor or predecessor, or in other words, capable of being solved uniquely either forwards or backwards in time.

**lag** The basic time interval or amount of offset between any two values being compared, within a time series.

**lag space** A special but very common type of pseudo phase space in which the axes or dimensions represent successive values of the same feature $(x)$ separated by a constant time interval.

**lagged phase space** See lag space

**local Lyapunov exponent** The exponential rate of trajectory convergence or divergence in a local region of an attractor

**Lyapunov characteristic exponent** Lyapunov exponent

**Lyapunov characteristic number** Lyapunov number

**Lyapunov exponent** The average of many local exponential rates of convergence or divergence of adjacent trajectories expressed in logarithms and measured over the entire attractor. As such, it reflects the average rate of expansion or contraction of neighboring trajectories with time

**Lyapunov number** The number whose logarithm, to a given base, equals the Lyapnov exponent

**map** A function, mathematical model, or rule specifying how a dynamical system evolves

**mapping** A function, correspondence, or transformation

**model** A simplified representation of a real phenomenon, in other words, a stripped-down or uncomplicated description or version of a real-world process. Models can be classified into physical (scale), mathematical, analog, and conceptual models.

**nearest neighbor** A pseudo phase space datum point that plots close to another point, for a particular embedding dimension

**nonautonomous** Time-dependent

**nonlinear** Not having a straight-line relationship, that is, referring to a response that is not directly (or inversely) proportional to a given variable

**nonlinear dynamics** The study of motion that does not follow a straight-line relation, that is, the study of nonlinear movement or evolution. As such, nonlinear dynamics is a broad field that includes chaos theory and many mathematical tools used in analyzing complex temporal phenomena.

**nonlinear system** A system in which the observations of a given variable do not plot as a straight-line (on arithmetic scales) against observations of a second (or lagged) variable.

**normalization** The process of adjusting or converting one or more values to some standard scale. The standard scale for a group of values usually is from zero to one. The conversion then consists of dividing each value of the original dataset by some maximum

reference quantity, such as the greatest value in the dataset or a theoretical maximum value. A vector is normalized by dividing it by its magnitude, yielding a so-called unit vector.

**observable** A physical quantity that an be measured.

**orbit** The path through space taken by a moving body or point. Examples: (a) a trajectory as represented in phase space

**origin** A reference point in ordinary space or phase space. Most often, it is the point at which all variables have a value of zero.

**orthogonal** (a) Perpendicular or normal (having to do with right angles); (b) unrelated or independent; (c) said of elements having the property that product of any pair of them is zero.

**orthogonalization** A procedure for realigning two or more nonorthogonal vectors into a set of an equal number of mutually orthogonal vectors, all of which have the same origin.

**orthonormal** Set of axes or vectors that are mutually perpendicular and of normalized (unit) length

**orthonormalization** The process of reducing mutually orthogonal vectors to unit length.

**phase space** An abstract mathematical space in which coordinates represent the variables needed to specify the phase (or state) of a dynamical system at any time

**phase space reconstruction** See reconstruction of phase space.

**projection** The image of a geometric object or vector superimposed on some other vector. As such, the projection is a new vector and is called the projection of the first vector onto the second.

**pseudo phase space** An imaginary graphical space in which the first coordinate represents a physical feature and the other coordinates represent lagged values of the feature.

**reconstruction dimension** The embedding dimension which an attractor is reconstructed.

**reconstruction of phase space** A pseudo (lagged) phase space plot in two or three dimensions, made with the hope of seeing an attractor (if there is one). Also known as pghase space reconsruction, state space reconstruction, phase portraint reconstruction, trajectory reconstruction, and samiliar expressions.

**renormalization** A mathematical scaling technique consisting of rescaling a physical variable and transforming a control parameter such that the properties of an equation a one scale can be related to those at another scale, and the properties at the limiting scale (infinity) can be determined.

**reorthonormalization** A procedure for again realigning all vectors to be mutually perpendicular and then making each vector of unit length.

**robust** Resistant to, or steady under, perturbation.

**sagittal plane** The sagittal plane in the anatomical position is any vertical anterior to posterior plane that passes through the body parallel to the median plane. It divides the body into unequal right and left halves.

**scalar** A number representing a magnitude only, as might be indicated on a simple scale.

**scalar time series** An ordinary time series, in which each successive measurement is recorded along with its time or order of measurement (and, hence, synonymous with the general meaning of time series.)

**sensitive dependence on initial conditions** (a) The quality whereby two slightly different values of an input variable evolve to two vastly different trajectories; (b) the quality whereby two initially nearby trajectories diverge exponentially with time.

**sensitivity to initial conditions** Sensitive dependence on initial conditions.

**singular system analysis** A phase space reconstruction technique in which orthonormal reconstruction axes near each point $x_t$ are a maximal set of linearly independent vectors that are derived from the local distribution of points near $x_t$ by singular value decomposition.

**smooth** In mathematical terms, is differentiable at every point.

**stable** Tending to dampen perturbations or initial differences, over time.

**stationary** Time-invariant, that is, (a) lacking a trend; or (b) (more rigidly), keeping a constant mean and variance with time; or (c) (more formally still), said of a randomlike process whose statistical properties are independent of time.

**steady state** (a) A condition that does not change with time; (b) the state toward which the system's behavior becomes asymptotic as time goes to infinity. The associated equation gives a constant solution.

**stretching** A topologist's interpretation of either (1) the amplification of a certain range of input to a large range of output values during iteration or (2) the phase space exponential divergence of two nearby trajectories.

**theoretic** (a) Restricted to theory; (b) lacking verification.

**time-delay method** A lag-time analytical technique that uses data of just one measured physical feature $(x)$ (regardless of any other features that may have been measured), whereby $x_t$ is compared to one or more lagged subseries, often with the aim of reconstructing an attractor.

**time domain** The representation of time series data in their raw or unaltered form.

**trajectory** (a) A path taken by a moving body or point ( and hence an orbit); (b) a sequence of measured values or list of successive states of a dynamical system; (c) a solution

to a differential equation; (d) graphically, a line on a phase space plot, connecting points in chronological order.

**truncate** (a) To shorten a number by keeping only the first few (significant) digits and discarding all others; (b) to approximate an infinite series by a finite number of terms; (c) to exclude sample values that are greater (or less) than a specified constant value.

**unit vector** A vector having a magnitude of one. It is usually obtained by dividing a vector by its length (magnitude).

**unstable** Tending to amplify perturbations or initial differences, over time.

**unstable orbit (unstable trajectory)** A trajectory for which,, arbitrarily close to any input value, there is another possible input which gives rise to a vastly different trajectory.

**variable** A characteristic or property that can have different numerical values.

# List of Symbols

| | |
|---|---|
| $a$, | The horizontal distance between the ankle and the heel |
| $a_i$, $b_i$, $c_i$, | Coefficients need to be determined in elements of Jacobian matrices |
| $b$, | The ankle height |
| $c$, | Horizontal distance between the mass center of foot and the ankle |
| $d$, | The number of Lyapunov exponents,<br>The dimension of the state space model of the system |
| $d_E$, | The embedding dimension |
| $g$, | The gravity acceleration ($9.80 ms^{-2}$) |
| $g_i(x)$, | The transition functions, defined based on the physical behaviour of the system, describe the transition conditions at each instant of discontinuity |
| $h$, | Time step-size used in nonstandard finite difference scheme |
| $h_i(x)$, | The indicator functions, defined based on the physical behaviour of the system, are at least one time continuously differentiable function and determine the instant of the discontinuity |
| $m$, | The mass of the inverted pendulum |
| $m_f$, | The mass of the both feet |
| $r$, | The distance between the mass center of inverted pendulum and the ankle |
| $x_{cop}$, | The distance between the center of pressure and the toe |
| $\dot{x} = \frac{dx}{dt}$, | First derivative with respect to time |
| $COP$ | The center of pressure |
| $F_{gx}$, | The horizontal ground reaction force |
| $F_{gy}$, | The vertical ground reaction force |
| $G_i(x)$, | The Jacobians of the transition functions |
| $GSR$ | The Gram-Schmidt reorthonormalizadtion |
| $H$, | The length of the whole body |
| $H_i(x)$, | The Jacobians of the indicator functions |
| $I$, | Moment of inertia of the inverted pendulum about mass center |
| $J_{ij}$, | Elements of Jacobian matrices |

$L = H - b$, The length of the inverted pendulum

$L_f$, The length of the feet

$M = I + mr^2$, Moment of inertia of the inverted pendulum about the ankle

$N$, The number of data points

$N_p$, The minimum number of nearest neighbors

$N_{Tay}$, The order of Taylor series

$SVD$ The singular value decomposition

$T_{evol}$, The evolving time

$T_{lag}$, The time-delay

$X_k(t)$, The set of variables actually taking part in nonlinear differential equations

$X_0(t)$, The time series data

$ZMP$ The zero moment point

$\theta$, Angular displacement of inverted pendulum (clockwise as "+")

$\theta_{cr1} = \theta^* = tan^{-1}(\frac{1}{\mu})$, Critical angle

$\theta_{cr2} = -\theta^* = -tan^{-1}(\frac{1}{\mu})$, Critical angle

$\dot{\theta}$, Angular velocity of inverted pendulum (clockwise as "+")

$\dot{\theta}_{cr1}(\theta)$, Critical angular velocity determined by friction constraint, detailed in Equation (3.11c)

$\dot{\theta}_{cr2}(\theta)$, Critical angular velocity determined by COP constraint, detailed in Equation (3.23b)

$\ddot{\theta}$, Angular acceleration of inverted pendulum (clockwise as "+")

$\lambda_i$, The Lyapunov exponents

$\mu$, The friction coefficient

$\tau$, Control torque applied at ankle

$\tau_{cop-heel}$, $\tau_{cop-toe}$, Control torque determined by COP constraint, detailed in Equation (3.22b), and (3.22c), respectively

$\tau_{lift}$, Control torque determined by gravity constraint, detailed in Equation (3.7c)

| | |
|---|---|
| $\tau_{slip-posterior}$, $\tau_{slip-anterior}$, | Control torque determined by friction constraint, detailed in Equation (3.12b), and (3.12c), respectively |
| $\Delta_1 = mr\sin\theta$, | Derived from gravity constraint |
| $\Delta_2 = mr(cos\theta - \mu sin\theta)$, | Derived from friction constraint |
| $\Delta_3 = mr(cos\theta + \mu sin\theta)$, | Derived from friction constraint |
| $\Delta_4 = mr(a\sin\theta - b\cos\theta) - (I + mr^2)$, | Derived from COP constraint |
| $\Delta_5 = (I + mr^2) + mr[(L_f - a)\sin\theta + b\cos\theta]$, | Derived from COP constraint |

# Chapter 1

# Introduction

## 1.1 Motivation

The balance control of disturbed bipedal standing is important for preventing falls of humans and bipedal robots. Stabilization of bipedal models has attracted much attention in the past two decades. In spite of much research effort, the progress has been slow due to the complexity of the structure of the bipedal robots and the lack of theoretical tools for stability analysis. Furthermore, bipedal standing is always subjected to constraints, such as the ground reaction force being upward (gravity constraint), friction between the foot and the ground being lower than the maximum friction (friction constraint), no tipping over about the toe and heel (tip-over constraint) and pressure center being within the foot/feet (pressure center constraint). Much of previous research on the stability analysis and stability control of bipedal locomotion has been carried out under the assumption that all the constraints are always satisfied. This assumption, though it simplifies the problem, can be misleading. Limited previous research on balance control of bipedal standing considered the constraints between the feet and the ground in control design. However, the effects of constraints on bipedal standing have not been investigated. Thus, understanding the effects of the constraints between the feet and the ground on balance control of bipedal standing still remains an open question.

Another challenge for research on balance control of bipedal standing is the lack of a single quantitative criterion and an effective tool for stability analysis. One technique available for this purpose is Lyapunov's stability analysis. Lyapunov's second method is widely used in stability analysis, but due to the lack of construction methods, it is difficult to derive a Lyapunov function for highly nonlinear systems. Alternatively, Lyapunov exponents, defined as the average exponential rates of divergence or convergence of nearby orbits in the state space, can characterize the system stability. Since it is extremely difficult to determine the Lyapunov exponents analytically for complex engineering systems, they are often calculated numerically based on a mathematical model or a time series. When mathematical models of the systems are available, the method for computation of Lyapunov exponents developed by Wolf *et al.* (1985) is one of the most commonly used for smooth systems. Smooth systems are systems where every term in the ordinary differential equations is continuous. Müller (1995) extended Wolf's method to non-smooth systems, systems where at least one term in the ordinary differential equations is non-differentiable. Straightforward calculation is the advantage of using model-based method. One limitation of using mathematical models is that the calculation of Lyapunov exponents may become unfeasible owing to the model complexity and uncertainty.

The most attractive advantage of using a time series is that the data for only one state is required, which can be measured experimentally. However, the methods for calculating Lyapunov exponents based on a time series have been developed for chaotic systems in which the largest Lyapunov exponents is positive. They are considered not reliable for calculating zero and negative exponents. Robotic systems are of high, but known dimensions and, more than one state can often be measured.

Thus, there is a pressing need to develop a method based on a time series to determine the zero and negative Lyapunov exponents for potentially stable systems.

In summary, the motivation of this research is to (1) gain a better understanding of mechanics of bipedal locomotion such as (a) the effects of constraints on bipedal standing and (b) stability control mechanisms, and (2) develop an effective method for stability analysis of nonlinear systems.

The outcome of this research can have significant impact on (1) developing bipedal robots, (2) providing a solid basis for applications in diagnosing human gait disorders and preventing falls of humans and bipedal robots, (3) broaden robotic research and other engineering fields.

## 1.2 Literature Survey

Recent studies on biped robots focus on dynamic modeling, controller design and stability analysis. The following sections give the detailed literature survey of these topics.

### 1.2.1 Dynamic modeling of bipedal locomotion

Dynamic modeling is a complicated problem that requires knowledge of classic mechanics, nonlinear dynamics and advanced mathematics. Modeling of physical systems can be divided into two categories. Physical modeling is a process in which one constructs tangible scaled models that appear like the real systems. However, scaled models require a great deal of time and resources to develop, and there are limits to what can be learned from them. A mathematical model is an abstract system used for studying research problem that does not necessarily lend itself to physical model. In the modern era, this means that researchers construct a set of equations and solve them using a computer. In these models, the system is simplified by limiting the

number of components so that they represent the net effect of many parts. Therefore, the first task to study biped is to select a mechanical model with few degrees-of-freedom to keep the equations of motion at a manageable level and yet reasonably describe the motion of interest.

Multi-link planar models are used to study bipedal locomotion and the related properties. Miura and Shimoyama (1984) developed their three-link biped robots to walk sideways, backward and forward and studied in both the sagittal and frontal planes. The results served as a basis for choosing the appropriate feedback control gains. Hemami (1977) and Hurmuzlu's (1987a) three-link biped models have upright trunk and two lower limbs. Miura's model (1984) has two lower limbs and a link located at the pitch axis. Hurmuzlu's four-link biped model (1987b) put one link above Miura's model. Iqbal *et al.* (1993) studied the stability and control of a biped system. The model was based on a four-link planar biped that approximates gross human locomotion in the frontal plane. A general five-link biped is modeled with a torso and two legs, each leg consisting of a thigh and a shank. Study of this model can be found in Hemami *et al.* (1977), Hurmuzlu (1993), Wu and Chan (2002), Ma and Wu (2002), Mu and Wu (2002, and 2004). Hemami *et al.* (2004) studied dynamics, stability and control of stepping via a seven-link two-dimensional sagittal biped model. Furusho and Sano (1990) developed a nine-link biped which included the foot structure and was equipped with foot pressure and ankle torque sensors to provide information about the conditions of contact with the floor. Their work contributed toward the realization of smooth three-dimensional walking with the sole firmly gripping the floor. However, the constraints between the feet and the ground are rarely considered in multi-link planar models. In the above mentioned work, bipedal

feet were assumed to be fixed on the ground once they contacted the ground. The constraints between the feet and the ground are assumed to be satisfied automatically.

Inverted pendulum models have often been used to study bipedal posture. An inverted pendulum is an inherently unstable system and the studies of control and stabilization of such a system is one of the challenging problems in the field of automatic control. Studies of control and stabilization of single pendulum can be grouped into two classes. The first class deals with the benchmark problem of an inverted pendulum in which the base point is rocked to maintain the upright position of the pendulum. In the second class, the stabilization of an inverted pendulum is achieved by applying control torques at the base point. The simplest model that can present some bipedal locomotion activities is a single massive link modeled as an inverted pendulum. Investigators have reported that standing human subjects, when perturbed by translation of a moving support surface, typically respond by moving in a segittal plane. For small disturbance, they tend to keep the knees, hips, and neck fairly straight, moving about the ankle (Kuo 1995). Hemami *et al.* (2006) has shown that the effect of a horizontal disturbance at the ankle appears to be about 40 times that of the effect of the disturbance at the knees and at least a few hundred times larger than the effect of a disturbance at the hip. This means that, under translational disturbance, the ankle angle is subjected to the largest excursion. The knee and the hip angle excursions are relatively minor. Consequently, the biped as a whole, appears to move as a single inverted pendulum. Thus, it is reasonable to simplify a biped as a simple inverted pendulum moving in the sagittal plane. The single inverted pendulum model is simple and suitable for solving problems of posture stability of a biped system, especially when several constraints between the feet and the ground are concerned (Pai and Patton 1997). Hemami and his colleagues used a massive inverted

pendulum with the base joint fixed to the supporting ground to study the behavior of a body in standing position when no muscle dynamics was involved (Hemami *et al.* 1973, Golliday and Hemami 1976, Hemami and Camana 1976, Hemami and Golliday 1977). Torques applied at the base joint were equivalent to the ankle joint in human body to maintain the upright posture. Chow and Jacobson (1972), on the other hand, consider the posture stability of the upper body and the control of human locomotion with the use of an inverted pendulum. The upper body was modeled as a single link inverted pendulum with the prescribed base point moved only in the vertical direction. It was an important step in the development of a mathematical model of the human body. Wu (1996) and Wu *et al.* (1998) utilized the general single inverted pendulum problem to model the human upper body during gait. Their mathematical model developed with a base excited inverted pendulum can be used to predict major features of the upper body dynamics and to synthesize the mechanism of walking. Pai and his colleagues studied disturbed standing stability using a single inverted pendulum model (Pai and Patton 1997, Pai and Iqbal 1999, Iqbal and Pai 2000). The work mentioned above show that inverted pendulum models are adequate for studying various fundamental theoretic problems related to human locomotion.

### 1.2.2 Effects of constraints on bipedal balance control and motion regulation

Control of balance is an essential component of bipedal movements. The balance control of disturbed bipedal standing is important for preventing falls of humans and bipedal robots. Stabilization of bipedal models has attracted much attention in the past two decades. Various control strategies such as adaptive control (Chew and Pratt 2001), sliding mode control (Mu and Wu 2004), neural network control (Kuperstein and Wang 1990, Narendra and Parthasarathy 1990, and Bersini and Gorrini 1997),

and fuzzy control (Liu and Li 2003) have been developed. In much of the previous work, bipedal feet were assumed to be fixed on the ground once they contacted the ground, *i.e.*, all the constraints between the feet and the ground were assumed to be always satisfied automatically, and the controllers were designed only for motion regulation. Such an assumption, though simplifies the problem, can mislead research and make the outcome irrelevant to practical bipedal robots.

Bipedal locomotion (standing, walking and running) is always subjected to constraints. The constraints between the feet and the ground include: the ground reaction force being upward (gravity constraint), friction between the foot and the ground being lower than the maximum friction (friction constraint), no tipping over about the toe and heel (tip-over constraint) and pressure center being within the foot/feet (pressure center constraint).

However, research on the effects of constraints on bipedal locomotion is sparse. One distinguished work is from Pai and Patton (1997), where gravity constraint, friction constraint and center of pressure constraint during bipedal standing have been considered. In their work, they showed that the constraints impose bounds to control torque and determined numerically the control bounds. Such bounds make the control design challenging. However, they did not investigate the effects of constraints on balance control of bipedal standing.

### 1.2.3 Stability analysis

Stability is a basic requirement for the bipedal locomotion including standing, walking and running. Two different stability concepts are widely used in bipedal locomotion. One is understood as that the biped does not collapse during locomotion. In this work, this kind of stability is named tip-over stability defined by Vukobratović

(Vukobratović 1970), and the other stability concept is defined based on Lyapunov's stability theory.

### 1.2.3.1 Tip-over stability

To ensure the tip-over stability and to prevent the tipping over of a biped, several measures for the evaluation and control of the system are raised. For example, center of pressure (COP) (Marchese *et al.* 2001, Silva and Machado 2001), foot rotation indicator (FRI) (Goswami 1999), force-angle stability measure (Paradopoulos and Rey 1996), and zero moment point (ZMP) (Vukobratovic *et al.* 1970). The COP is a point on the foot/ground surface where the net ground reaction force actually acts. The FRI point is a point on the foot/ground surface, inside or outside the base of support, where the net ground reaction force would have to act to keep the foot stationary. The ZMP is defined as the point on the ground about which the sum of all the moments of the active forces equals zero (Vukobratovic *et al.* 1970). ZMP is popularly used in the study of biped dynamic walking. Methods have been proposed for synthesizing walking patterns based on the concept of ZMP. In the work of Shih (1990) and Hirai (1998), the ZMP trajectory was first designed and the hip motion and joint angle profiles are then derived. In Huang's (2001) work, however, the constraints of parameters, which can produce different types of foot motion to adapt to the ground situations, were first formulated, and then methods were introduced to generate biped trajectories with the largest ZMP stability margin. ZMP plays an important role in the analysis and design of biped dynamic locomotion, and it has also been used in biped controller design and in gait synthesis. A comprehensive survey of ZMP and its application to bipedal locomotion has been given in reference (Vokobratovic and Borovac 2004).

Pai and Patton (1997) defined the stability based on the clinical observations on balance control of human subjects and they intended to develop a clinical tool to assess a person's ability to maintain standing posture. Their stability regions are determined using an optimal algorithm. They considered constraints as conditions when they numerically calculate the ankle control torque. From a initial state, (with initial angular displacement and initial angular velocity), if the center of mass of the biped can be moved by the ankle torque determined using optimal algorithm into a region between the heel and the toe within a short time period (1s) and with a zero angular velocity, this initial state is included in stability region they defined. The whole stability region is formed by all initial states satisfying above conditions. The limitation, from a viewpoint of stability, comes from their definition of the stability. Such a definition only concerns the system performance within a short time period.

### 1.2.3.2 Summary of Lyapunov stability theory

The stability concept based on the Lyapunov's stability theory is about the system performance with respect to the disturbance in the initial states. Lyapunov not only introduced the basic definition of stability for nonlinear systems, but also proved many of the fundamental theorems. Since Lyapunov published his theory (Lyapunov 1892), a great deal of work has been done on stability of nonlinear systems based on Lyapunov's stability theory.

The key requirement to prove the system stability using Lyapunov's stability theory is to construct a Lyapunov function. Since no constructive rules or suggestions were given in his theory, the construction of a Lyapunov function for a nonlinear system remains a great challenge, which restricts the applications of this theory. In the past forty years, numerous techniques have been proposed to construct Lyapunov functions for special nonlinear systems. Amongst these techniques are: the method of

analogy with linear systems by Barbasin (1960), the method of integration by parts by Ponzo (1965), and Huaux (1967), the method of system energy by Marino and Nicosia (1983), the integral methods, the scalar-Lyapunov-function method and the intrinsic method by Chin (1986, 1987, 1988, and 1989), the extended integral method by Wu (Wu 1996 and references cited in). It is important to point out that Lyapunov's stability theory is based on conventional solution theory, *i.e.*, the dynamical systems must be smooth. For the stability analysis of non-smooth systems, Lyapunov's second method needs to be extended. Paden and Sastry (1987) first generalized Lyapunov's second method by imposing a non-zero upper bound of the derivative of the Lyapunov function with respect to time. They proved that the states of the system (solution in the sense of Filippov) converge to the equilibrium point in a finite time. Another extension of Lyapunov's stability theory based on Filippov's solution theory was done by Southwood *et al.* (1990) where the derivative of Lyapunov functions on the discontinuity surfaces were replaced with Dini-derivate. The most recent and systematic extension of Lyapunov's second method for non-smooth dynamical systems was developed by Shevitz and Paden (1994) in which a non-smooth Lyapunov function is constructed. Their result is a theory applicable to systems with switches, for which Lyapunov functions are only piecewise smooth. The above extensions of Lyapunov's stability theory to non-smooth systems were based on the belief that non-smooth Lyapunov functions are natural for non-smooth dynamical systems. However, the main challenge in construction of non-smooth Lyapunov functions is the evaluation of the derivatives of Lyapunov functions when the solution trajectories approach the discontinuity surfaces. Wu (1996) proved that if the existence and uniqueness of Filippov's solution are guaranteed, Lyapunov's second method can be applied directly to non-smooth dynamical systems. Furthermore, in

reference (Wu *et al.*, 1998b, Wu and Sepehri, 2001), a method is developed to construct smooth Lyapunov functions for non-smooth systems and it is shown that the construction of smooth Lyapunov functions is much easier for some engineering systems as compared to its non-smooth counterpart. Wu's work provided a solid framework in the study of posture stability and control of biped movement.

#### 1.2.3.3 Biped posture stability analysis using Lyapunov stability theory

Lyapunov stability theory has been used to analyze the biped posture stability. Early work on stability of biped models was restricted to small deviations about vertical stance (Vukobratović *et al.* 1970, Golliday and Hemami 1976, Hemami and Golliday 1977, Hemami and Cvetkovic 1977). Hemami and Wyman (1979) proposed a modeling and control method to constrained dynamical systems with application to a three-link biped based on Lyapunov's linearization method. Feedback linearization and pole-assignment techniques were used for the control of such nonlinear systems. Iqbal *et al.* (1993) studied the human postural and movement stability for simple voluntary movements by means of a frontal four-link mathematical biped model. Hemami and Utkin (2002) studied Lyapunov stability of constrained and embedded rigid bodies. They presented a systematic method of stabilizing the systems and a procedure for constructing Lyapunov functions. Hemami *et al.* (2006) developed a quantitative framework to study the biomechanics and neural basis of the ankle strategy for maintaining posture stability. In their work, the stability of the biped was determined near the vertical stance by computing the poles, while the biped equations were linearized about the erect posture.

### 1.2.3.4 Stability analysis using the concept of Lyapunov exponents

Although Lyapunov's second method is a powerful method, due to the lack of construction methods, it is difficult to derive a Lyapunov function for highly nonlinear systems. The alterative method is to use the concept of Lyapunov exponents. The concept of invariant exponents in the study of the stability of nonlinear differential equations was first introduced in 1889 by a Russian mathematician, Sonya Kovalevskaya, who was a professor at the University of Stockholm, and developed fully in 1892 by another Russian mathematician, Alexandr Mikhailovich Lyapunov (Kinsner 2006). The Lyapunov exponents have many important characteristics such as invariance to transformations, simple relationship to a fractal dimension, and computability directly from data, without solving the differential or difference equations describing the corresponding dynamical systems (Kinsner 2003).

### 1.2.3.4a Calculation of Lyapunov exponents from mathematical models

A Lyapunov exponent is a number that reflects the rate of divergence or convergence, averaged over the entire attractor, of two neighboring phase space trajectories. The calculation of the Lyapunov exponents can be grouped into two classes. One method for calculating Lyapunov exponents is based on mathematical models. Oseledec (1968) gave the theory of Lyapunov exponents in a form adapted to the needs of the theory of dynamical systems and of ergodic theory. Benettin *et al.* (1980) presented the theoretical results, which are necessary for the numerical computation of all Lyapunov exponents. Wright (1984) presented a new method for calculating the leading Lyapunov exponent directly from experimental data for

systems having a strange attractor with dimensionality near two. The method was exact for one-dimensional maps and gave good results for systems that have approximate one-dimensional maps associated with them even in the presence of some noise. Wolf and collaborators (Wolf *et al.* 1985) described algorithms for calculating the spectrum of Lyapunov exponents for systems in which the equations are known. This model based algorithm has been successfully applied to many smooth dynamical systems. Müller (1995) extended Wolf's method into non-smooth dynamical systems, *i.e.*, the ordinary differential equations contain non-differentiable terms. He pointed out that the required linearized equations have to be supplemented by certain transition conditions at the instants of discontinuities. The challenges in determining Lyapunov exponents are related to numerical stability and computational efficiency. Since Lyapunov exponents are calculated numerically over a long period of time, nonstandard finite difference techniques developed by Mickens (1994, 2002), and Mickens and Gumel (2002), can be combined to improve the numerical stability and the computational efficiency (Sekhavat 2005). The advantage of using mathematical model is that there is a very straightforward technique for computing a complete Lyapunov spectrum. The limitations of using mathematical models are that the mathematical models are not always available. Even if they are available, due to the model complexity and uncertainties, calculation of Lyapunov exponents can become unfeasible.

### 1.2.3.4b Calculation of Lyapunov exponents from a time series

Another method for calculating Lyapunov exponents is based on a time series, which can be measured. The theory of nonlinear dynamical systems provides new ways and methods for the characterization of irregular time series data. The basis of the new technique is based on the important Takens' Embedding Theorem (Takens

1981) which allows reconstruction of the attraction of the attractor in the time delayed embedded space and preserving its topological characteristics. The reconstruction of the attractor is done from a finite time series observation of a single variable. Most observational data reflect just a few of the many physical variables of a system and measurements of all variables are rarely possible. However, this difficulty can be overcome if the variables are nonlinearly coupled, in which case the time delay embedding technique can be used to reconstruct the phase space from the time series data. In this technique a multi-dimensional embedding space is constructed from the time series data, and a point in this embedding space represents the states of the system at a given time.

In calculation of Lyapunov exponents from a time series data directly, several methods are developed. The basic idea behind these methods is to follow sets of trajectories over short time-spans and compute their rates of separation, then average those rates over the attractor. Wolf *et al.* (1985) described a computational method for approximating the largest Lyapunov exponents directly from the rate of separation of neighboring points. Sano and Sawada (1985) proposed a method to determine the spectrum of several Lyapunov exponents (including positive, zero, and even negative ones) from the observed time series of a single variable. Zeng *et al.* (1992) computed Lyapunov exponents from limited experimental data and applied their algorithm to the daily-averaged data of surface temperature observed at two locations in the United States to quantitatively evaluate atmospheric predictability. Brown *et al.* (1991) examined the question of accurately determining, from an observed time series, the Lyapunov exponents for the dynamical system generating the data. They showed that even with very large data sets, it is clearly advantageous to use local neighborhood-to-neighborhood mapping with higher-order Taylor series, rather than just local linear

maps as has been done previously. They demonstrated the procedure using several chaotic systems. Abarbanel *et al.* (1993) reviewed research on the calculation of Lyapunov exponents based on time series for chaotic systems. Huang *et al.* (1994) presented an algorithm to obtain a reliable estimation of a full Lyapunov exponents' spectrum from a time series signal of plasma chaos. Sauer and Yorke (1999) investigated the computational artifacts due to observational noise in the experimental time series data, and gave the formulas for the expected values of the reconstructed Jacobian in some simple cases. Carretero-Gonzlez *et al.* (2000) described methods of estimating the entire Lyapunov spectrum of a spatially extended system from multivariate time series observations. Porcher and Thomas (2001) used nonlinear autoregressive stochastic modeling to estimate the dominant Lyapunov exponent in an EEG (electro-encephalogram) series and computed confidence intervals from surrogate data. Kinsner (2003) described how to measure and analyze chaos using Lyapunov metrics. Sakai *et al.* (2003) analyzed effect of extra reconstructed dimensions on Lyapunov spectrum, which includes spurious Lyapunov exponents of unknown dynamical systems. However, all the work mentioned above is meant for chaotic systems, and is considered to be not reliable for potentially stable engineering systems.

The most attractive advantage of using a time series is that the data for only one state is required, and these data can often be measured experimentally. However, the methods mentioned above are much better at calculating positive exponents than negative ones, as the methods for calculating Lyapunov exponents based on a time series were developed primarily to analyze chaotic systems. The procedures are not reliable for calculating zero and negative exponents (Wolf *et al.* 1985). Thus, there is a pressing need to develop a method based on a time series to determine the zero and

negative Lyapunov exponents. The difficulty in determining the negative exponents from time series comes from the fact that the distances become closer and closer at many locations in the directions associated with certain negative exponents. Even when there is a reasonably large and accurate data set, this will often make curvature effects within a given neighborhood become significant. A linear analysis becomes totally inaccurate when the displacement due to local data-set curvature is comparable to the thickness of the data set. Going to a higher-order approximation of the mapping should correct this.

Overall, Lyapunov stability theories have provided solid background for stability analysis of nonlinear systems. The methodologies are well-developed, but due to the lack of construction methods, it remains difficult to derive Lyapunov functions for highly nonlinear systems. The method of Lyapunov exponents is a powerful tool for chaotic systems, yet has rarely been used in the analysis of potentially stable engineering systems.

## 1.3 Objectives of this Research

There are two objectives in this research. The first objective is to study balancing control of a constrained biped during standing, which includes two parts. The first part is to investigate the effects of the constraints between the foot-link and the ground on the bounds of control torque of a bipedal system. The second part is to develop a balancing control law, which satisfy all the above constraints. The concept of Lyapunov exponents is used to analyze the stability of a biped subjected to the constraints during disturbed standing. Then the stability regions are determined based on the sign of the largest Lyapunov exponent calculated from the mathematical model. The stability region is then compared with previous work based on a different stability criterion. It is believed this is one of the first researches on balancing and

stability analysis of bipedal system with the full consideration of the constraints between the foot-link and the ground.

The second objective is to develop a method for calculating negative Lyapunov exponents using a time series. Higher-order Taylor series are used instead of linear expressions for generating local-neighbour to local-neighbour mapping in order to construct the more accurate Jacobian matrix for calculating Lyapunov exponents from time series. The constrained balancing bipedal system is used as an example to demonstrate the efficacy of this method. The results show that this method is constructive and effective, which allows the stability analysis of general robotic control systems, which could not be carried out before.

## 1.4 Thesis Organization

The remainder of this thesis is organized as follows. Chapter 2 contains the theoretical preliminaries which include the concept of Lyapunov exponents; calculation of Lyapunov exponents based on mathematical models and a time series; the non-standard finite difference scheme, and sampling theorem.

In Chapter 3, dynamical model of a biped standing subjected to three constraints between the feet and the ground and the mathematical expression for three constraints are derived. Effects of individual constraints and effects of gravity and friction constraints on bipedal balance control are carried out analytically. Effects of all three constraints on bipedal balance control are discussed from a numerical perspective. The regions on the phase plane with valid and invalid control bounds, named controllable regions and uncontrollable regions, respectively, are classified, and specific constraints, which cause the non-controllability, are identified. Three sets of parameters, namely the friction coefficient, length of the foot-link, and the location of

the mass center, are analyzed systematically with two objectives. The first one is to identify the controllable regions and uncontrollable regions. In the controllable regions, it is possible to design a balance control, while in the uncontrollable regions, regardless of the control torque, constraints will be violated, and balance control is impossible. Secondly, the ranges of required control torque are determined. The larger the control bounds, the more flexible is the balance control design.

In Chapter 4, a balancing control of a biped during standing subject to the constraints between the foot-link and the ground is investigated through controller design and stability analysis. A PD-based switching state feedback controller, which can stabilize the biped from certain initial states to the upright position while satisfying all constraints is designed for balance control. The control torque obtained from switching controller is compared with control torque from a PD controller. The purpose of this comparison is to demonstrate the importance in considering the constraints between the foot-link and the ground when the balance control law is designed. Stability of the above control system is analyzed via the concept of Lyapunov exponents. Two Lyapunov exponents are calculated based on the mathematical model subjected to three constraints. The results are used to obtain the stability region in phase plane, which is compared with previous work based on a different stability criterion (Pai and Patton 1997).

In Chapter 5, a method for stability analysis based on Lyapunov exponents calculated from a time series for potentially stable engineering systems is presented. Instead of linear expressions, higher-order Taylor expansion for generating local neighbour-to-neighbour mapping in order to construct the more accurate mapping matrix for calculating Lyapunov exponents from a time series is used. The conclusions and recommended future work are outlined in Chapter 6.

# Chapter 2

# Theoretical Preliminaries

In this chapter, the concept of Lyapunov exponents, the calculation of Lyapunov exponents based on mathematical models and a time series, the action of mapping matrices on the calculation of Lyapunov exponents, nonstandard finite difference scheme, and signal sampling theorem are reviewed.

## 2.1 The Concept of Lyapunov Exponents

Lyapunov exponents (or characteristic numbers) were first introduced by Lyapunov (Lyapunov 1892) in order to study the stability of non-stationary solutions of ordinary differential equations (ODEs) and have since been extensively studied in the literature (Dieci *et al.* 1997). As described in the work of Oseledec (1968), the concept of Lyapunov exponents provides a meaningful way to characterize the asymptotic behavior of a nonlinear dynamical system. Wolf *et al.* (1985) defined the spectrum of Lyapunov exponents in the manner most relevant to spectral calculations.

Given a smooth dynamical system in an $n$-dimensional phase space as shown below:

$$\dot{x} = f(x,t),\ x(0) = x_0,\ x \in R^n \tag{2.1}$$

where $x = \{x_1,...,x_n\}^T$ is the state vector, and $f(x,t)$ is a continuously differentiable vector function, *i.e.*, $f(x,t) \in C^1$. When monitoring the long-term evolution of an infinitestimal $n$-sphere of initial conditions, the sphere will become an $n$-ellipsoid due

to the locally deforming nature of the flow. The $i$ th one-dimensional Lyapunov exponent is then defined in terms of the length of the ellipsoidal principal axis $\|\delta x_i(t)\|$:

$$\lambda_i = \lim_{t\to\infty} \frac{1}{t} \ln \frac{\|\delta x_i(t)\|}{\|\delta x_i(t_0)\|} \quad (i = 1,...,n) \tag{2.2}$$

where the $\lambda_i$ are ordered from largest to smallest. $\|\delta x_i(t)\|$ and $\|\delta x_i(t_0)\|$ denote the lengths of the $i^{th}$ principal axis of the infinitesimal $n$-dimensional hyper-ellipsoid at final and initial times, $t$ and $t_0$, respectively.

The above definition of Lyapunov exponents indicates that Lyapunov exponents, $\lambda_i$ $(i = 1,...,n)$, are the average exponential rates of divergence or convergence of nearby orbits in the state space where $n$ is the number of Lyapunov exponents, which is equal to the dimension of the state space model of the system. The Lyapunov exponents are related to the expanding or contracting nature of different directions in phase space. Since the orientation of the ellipsoid changes continuously as it evolves, the directions associated with a given exponent vary in a complicated way through the attractor. Therefore, one cannot speak of a well-defined direction associated with a given exponent.

The concept of Lyapunov exponents provides a generalization of the linear stability analysis for perturbations of steady state solutions to time-dependent solutions. Lyapunov exponents are global properties and independent of the trajectory chosen to measure them (the fiducial trajectory). This independence is a consequence of a theorem of Oseledec (Oseledec 1968), which applies in the limit of infinite time. However, in practical application, we are usually dealing with finite-time Lyapunov exponents, which are defined as:

$$\lambda_i = \frac{1}{T} \ln \frac{\|\delta x_i(t)\|}{\|\delta x_i(t_0)\|} \quad (i = 1,...,n) \tag{2.3}$$

In the limit as $t \to \infty$, the finite-time Lyapunov exponents converge to the true Lyapunov exponents (Thiffeault and Boozer 2001).

The concept of Lyapunov exponents is an important tool in categorizing steady-state behaviour of dynamical systems, determining instability of the system, classifying invariant sets, and approximating the dimension of strange attractors or other nontrivial invariant sets (Wolf *et al.* 1985, Müller 1995, Williams 1997). A negative Lyapunov exponent indicates an average convergence of trajectories; a positive exponent indicates an average divergence. Convergence and hence negative Lyapunov exponents typify nonchaotic attractors. Divergence (and hence at least one positive Lyapunov exponent) usually happens only on chaotic attractors.

A common approach in visualizing state space motion is to imagine how a small length, area, volume or higher-dimensional element might evolve in time. Examples of such elements are a square or circle (in two-dimensional state space) and a cube or sphere (in three dimensions). The center of such an element is an observed datum point. Originating at every measured datum point, and making up the associated element's skeletal framework, is one or more equal-length orthogonal axes, called principal axes. Each axis ends at another state space point. Because those axes start at a common center point (a datum point) and each axis ends at some other point in state space, chaologists call each axis a vector, axis vector, or perturbation vector. The number of principal axes corresponds to the dimension of the state space. The two end-points of each principal axis are considered to be neighboring points in state space. We measure the growth or shrinkage of each principal axis over the entire attractor, according to whether its endpoints get closer or farther apart. That means

that we get a Lyapunov exponent for each principal axis. The largest Lyapunov exponent measures the rate of expansion of the first principal axis - the one that shows the largest amount of growth (or the slowest rate of shrinkage) over the attractor. The second Lyapunov exponent measures the rate of change of the second principal axis, and so on down to the smallest Lyapunov exponent (Williams 1997).

In dissipative systems, an attractor with one or more positive Lyapunov exponents is generally said to be strange or chaotic. Based on the fact that *(i)* one Lyapunov exponent of any limit set other than an equilibrium point must be zero, and *(ii)* the sum of the Lyapunov exponents of dissipative systems must be negative, the hyperbolic attractors can be classified as follows (Williams 1997):

- For an exponentially stable equilibrium point, $\lambda_i < 0 \ (i = 1,...,n)$
- For an exponentially stable limit cycle, $\lambda_1 = 0$ and $\lambda_i < 0 \ (i = 2,...,n)$
- For an exponentially stable k-torus, $\lambda_i = ... = \lambda_k = 0$ and $\lambda_i < 0 \ (i = k+1,...,n)$
- For a chaotic attractor, $\lambda_1 > 0$ and $\sum \lambda_i < 0 \ (i = 1,...,n)$

In any dissipative systems, whether chaotic or not, a length, area, volume or higher-dimensional element shrinks over time in state space. Conservative systems, in contrast, do not lose energy with time. The overall total area remains constant over time, even though there may be some change in shape (Williams 1997).

## 2.2 Calculation of Lyapunov Exponents Based on Mathematical Models

Since, in general, it is almost impossible to determine the Lyapunov exponents analytically for complicated systems, they are often calculated numerically (Kunze

2000). The calculation of Lyapunov exponents can be carried out in two ways. One is based on mathematical models. The other is based on a time series which can be measured experimentally.

This section includes two parts. The first part is the calculation of Lyapunov exponents for smooth systems. Second part is the calculation of Lyapunov exponents for non-smooth systems (which was defined as systems with non-differentiable points in this thesis).

### 2.2.1 Calculation of Lyapunov exponents for smooth systems

Since Lyapunov exponents are defined by the long-term evolution of the axes of an infinitesimal sphere of states. Wolf *et al.,* (1985) developed algorithms for calculating the spectrum of Lyapunov exponents from systems in which the equations are known. The procedure of calculating Lyapunov exponents from differential equations can be implemented by defining the principal axes with initial conditions whose separations are as small as the computer limitation allows and evolving such principal axes with the nonlinear equations of motion. A "fiducial" trajectory (the center of the sphere) is defined by the action of the nonlinear equations of motion on some initial conditions. The trajectories of points on the surface of the sphere are defined by the action of the linearized equations of motion on points infinitesimally separated from the fiducial trajectory. In particular, the principal axes are defined by the evolution via the linearized equations of an initially orthonormal vector frame anchored to the fiducial trajectory. This leads to the following set of equations (Wolf *et al.* 1985):

$$\begin{Bmatrix} \dot{x} \\ \dot{\psi}_{x(t)} \end{Bmatrix} = \begin{Bmatrix} f(x) \\ F(x(t))\psi_{x(t)} \end{Bmatrix} \tag{2.4}$$

where $\psi_{x(t)}$ is called the state transition matrix of the linearized system $\delta x(t) = \psi_{x(t)}\delta x_0$ and the variation equation, $\dot{\psi}_{x(t)} = F(x(t))\psi_{x(t)}$, is a matrix-valued time-varying linear differential equation. It is derived by linearization of the vector field along the trajectory $x(t)$. The Jacobian $F(x(t))$ is defined as

$$F(x(t)) = \frac{\partial f(x)}{\partial x^T}\Big|_{x=x(t)} \tag{2.5}$$

The initial conditions for numerical integrations are $\begin{Bmatrix} x(t_0) \\ \psi_{x(t)}(t_0) \end{Bmatrix} = \begin{Bmatrix} x_0 \\ I \end{Bmatrix}$ where $I$ is the identify matrix.

Lyapunov exponents are calculated by following the evolution of the area of the hyper-ellipsoid spanned by $\{\delta x_1,...,\delta x_n\}$ via separately following the evolution of $\delta x_1$, $\delta x_2$,..., $\delta x_n$ using an integration method. However, the $\delta x_1(t)$, $\delta x_2(t)$,..., $\delta x_n(t)$ may tend to align as $t \to \infty$. This alignment makes the calculations unreliable. To solve the problem, $\delta x_1(t)$, $\delta x_2(t)$,..., $\delta x_n(t)$ are reorthonormalized at each integration step. This is done by including the Gram-Schmidt Reorthonormalization (GSR) scheme in the calculation procedure. Gram-Schmidt reorthonormalization generates an orthonormal set $\{u_1,...,u_n\}$ of $n$ vectors with the property that $\{u_1,...,u_n\}$ spans the same subspace as $\{\delta x_1,...,\delta x_n\}$.

Figure 2.1 shows the geometrical interpretation of the orthonormalization for $\delta x_1^{(k)}$ and $\delta x_2^{(k)}$ ($k = 1,...,K$ and $K$ is the number of integration steps). They are orthogonalized into $v_1^{(k)}$ and $v_2^{(k)}$, then normalized into $u_1^{(k)}$ and $u_2^{(k)}$.

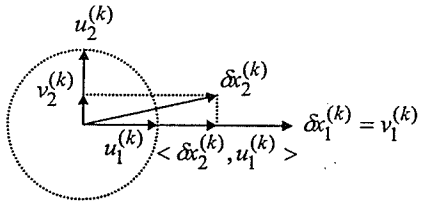


Figure 2.1 Orthonormalization of two vectors $\delta x_1^{(k)}$ and $\delta x_2^{(k)}$

Let the linearized equations of motion act on the initial frame of orthonormal vectors to give a set of vectors $\{\delta x_1, \delta x_2, ..., \delta x_n\}$. The orientation-preserving properties of GSR mean that the initial labeling of the vectors may be done arbitrarily. Then GSR provides the following orthonormal set $\{u_1, u_2, ..., u_n\}$ as defined below:

$$
\begin{aligned}
u_1 &= \frac{\delta x_1}{\|\delta x_1\|}, \\
u_2 &= \frac{\delta x_2 - \langle \delta x_2, u_1 \rangle u_1}{\|\delta x_2 - \langle \delta x_2, u_1 \rangle u_1\|}, \\
&\cdots \\
u_n &= \frac{\delta x_n - \langle \delta x_n, u_{n-1} \rangle u_{n-1} - \ldots - \langle \delta x_n, u_1 \rangle u_1}{\|\delta x_n - \langle \delta x_n, u_{n-1} \rangle u_{n-1} - \ldots - \langle \delta x_n, u_1 \rangle u_1\|},
\end{aligned}
\tag{2.6}
$$

where $\langle \ , \ \rangle$ signifies the inner product. GSR procedure allows the integration of the vector frame for as long as required for Lyapunov spectrum convergence. At the $K^{th}$ stage, the GSR procedure produces orthonormal vector frame $\{u_1, u_2, ..., u_n\}$, and for the $K$ chosen large enough, the Lyapunov exponents are:

$$
\begin{cases}
\lambda_1 \approx \dfrac{1}{Kh} \sum\limits_{k=1}^{K} \ln \left\| u_1^{(k)} \right\| \\
\lambda_2 \approx \dfrac{1}{Kh} \sum\limits_{k=1}^{K} \ln \left\| u_2^{(k)} \right\| \\
\cdots \\
\lambda_n \approx \dfrac{1}{Kh} \sum\limits_{k=1}^{K} \ln \left\| u_n^{(k)} \right\|
\end{cases}
\tag{2.7}
$$

where h is the time-step size.

This model-based algorithm described by Wolf and his collaborators (Wolf *et al.* 1985) has been successfully applied to many smooth dynamical systems. Sekhavat (Sekhavat 2004) demonstrated the above procedure of calculating Lyapunov exponents in smooth systems on the simple three-dimensional Lorenz system.

### 2.2.2 Calculation of Lyapunov exponents for non-smooth systems

Variational equation, shown in Equation (2.4), is important for calculating Lyapunov exponents, which requires that the nonlinear system is linearizable. This introduces a major problem in the calculation of Lyapunov exponents for non-smooth (non-differentiable) systems. Müller (1995) who has extended the calculation procedure to systems with non-differentiable points has addressed the problem. The extension is based on normal linearization of dynamic equations in smooth (*i.e.*, continuous and differentiable) regions of motion supplemented by transition conditions at the instant non-differentiable points.

Müller (1995) considered a nonlinear system with non-differentiable points in the neighbourhood of the action of a non-differentiable instant. The system is assumed to have reached the non-differentiable instant at $t = t_1$, and the system equations can be expressed as follows:

$$t_{initial} \le t < t_1: \qquad \dot{x} = f_1(x),\ x(t_{initial}) = x_0 \qquad f_1 \in C^1 \tag{2.8}$$

$$t = t_1: \qquad 0 = h(x(t_1)), \qquad h \in C^1 \tag{2.9}$$

$$x(t_1^+) = g(x(t_1^-)), \qquad g \in C^1 \tag{2.10}$$

$$t_1 < t: \qquad \dot{x} = f_2(x),\ x(t_1) = x(t_1^+), \qquad f_2 \in C^1 \tag{2.11}$$

It is assumed that in each interval between non-differentiable instants the system behaves "smoothly". Before the non-differentiable instant, the motion is described by

Equation (2.8). An indicator function $h(x)$ defines according to Equation (2.9) the instant of non-differentiable point: the function may be scalar, *e.g.* in the case of an impact, or it may be a vector function, *e.g.* in the case of sliding motion. The transition condition of the nonlinear system at $t = t_1$ is given by Equation (2.10), *e.g.* by impact laws. Here the plus and the minus characterize the right- and left-sided limits, *i.e.* the values of the quantity just after or just before the non-differentiable ponit. For $t > t_1$ the system is governed by Equation (2.11), and in general it is $f_2 \neq f_1$ , such that structurally variable systems are considered. Throughout it is assumed that $f_1, f_2, g, h$ are at least one-time continuously differentiable vector functions.

Before the non-differentiable instant, the linearized equation of motion follows directly from Equation (2.8) as:

$$(t_{initial} < t < t_1): \quad \delta\dot{x} = F_1(t)\delta x, \ \delta x(t_{initial}) = \delta x_0 \tag{2.12}$$

$$F_1(t) = \frac{\partial f_1(x)}{\partial x^T}\Big|_{x=x(t)} \tag{2.13}$$

After the non-differentiable instant, the linearized equations follows directly from (2.11) as:

$$(t_1 < t): \quad \delta\dot{x} = F_2(t)\delta x, \ \delta x(t_1) = \delta x_1 \tag{2.14}$$

$$F_2(t) = \frac{\partial f_2(x)}{\partial x^T}\Big|_{x=x(t)} \tag{2.15}$$

Since the nonlinear equations can not be linearized at non-differentiable instant, the linearized equations are evaluated using the indicator function, $h(x)$, and the transition function, $g(x)$, both defined based on the physical behaviour of the system. The indicator function is an at least one time continuously differentiable function and is used to determine the non-differentiable instant. The transition function describes

the transition conditions at each non-differentiable instant. The linearized equations of motion at the non-differentiable instant $(t = t_1)$ are derived as (Müller 1995):

$$\delta x^+ = G_1(x^-)\delta x^- - \left[G_1(x^-)f_1(x^-) - f_2(x^+)\right]\frac{H_1(x^-)\delta x^-}{H_1(x^-)f_1(x^-)} \tag{2.16}$$

where $x^+ = x(t_1^+)$, $x^- = x(t_1^-)$, $\delta x^+ = \delta x(t_1^+)$, and $\delta x^- = \delta x(t_1^-)$. $H_1(x^-) = \left.\frac{\partial h_1(x)}{\partial x^T}\right|_{x=x(t_1^-)}$ is the Jacobian of the indicator function, $h_1(x)$, and $G_1(x^-) = \left.\frac{\partial g_1(x)}{\partial x^T}\right|_{x=x(t_1^-)}$ is the Jacobian of the transition function, $g_1(x)$. If the system trajectory returns to the original region at the non-differentiable instant $(t = t_2)$, the transition condition of the linearized equations is:

$$\delta x^+ = G_2(x^-)\delta x^- - [G_2(x^-)f_2(x^-) - f_1(x^+)]\frac{H_2(x^-)\delta x^-}{H_2(x^-)f_2(x^-)} \tag{2.17}$$

where $x^+ = x(t_2^+)$, $x^- = x(t_2^-)$, $\delta x^+ = \delta x(t_2^+)$, and $\delta x^- = \delta x(t_2^-)$. The Jacobian matrices $H_2$ and $G_2$ are similarly derived using the indicator and transition functions $h_2(x)$ and $g_2(x)$, respectively. The above equations represent the generalized linearization required in the calculation of Lyapunov exponents and are employed in Chapter 4 to calculate the Lyapunov exponents.

Overall, the procedure for calculating of Lyapunov exponents based on mathematical model is described as follows:

*Step 1:* Choose initial condition for nonlinear system and linear system (orthonormal frame) as shown in Equation (2.4);

*Step 2:* Integrating nonlinear and linear equations simultaneously, obtaining

next step initial conditions;

*Step 3:* Using GSR procedure to obtain the reorthonormal frame using Equation (2.6);

*Step 4:* Calculating Lyapunov exponents by Equation (2.7);

*Step 5:* Repeating Step 2 to Step 4, until convergent values of Lyapunov exponents are achieved.

## 2.3 Calculation of Lyapunov Exponents Based on a Time Series Using Linear Mapping

It is very difficult to directly observe all aspects of the evolution of a high dimensional dynamical system such as a turbulent flow. Out of necessity, it is frequently the case that experimentalists study such systems by measuring a relatively low number of different quantities (We assume that all measurements have infinite precision). Since not in all experiments we could have access to all of the variables, the worst case is only a single time series is obtainable. A single experimental time series is affected by all of the relevant dynamical variables, and therefore it contains a relatively complete historical record of the dynamics. It is possible to glean the dynamics from a single time series without reference to other physical variables. This concept was first illustrated by Paclard *et al.* (1980) and given a rigorous mathematical basis by Takens (1981) and Mané (1981).

Reconstruction of the attractor from a single time series requires the generation of additional variables. For some experimental systems, the effective number of degrees

of freedom is relatively small. Consequently, it is possible to define a low-dimensional phase space that captures the dynamics in a geometric structure embedded in that space. The embedded geometric set is called the reconstructed attractor and it is usually topologically equivalent to the attractor, which would be produced by the numerical solution of the dynamical system equations if they were known.

A time series is a sequence of observations, which are ordered in time (or space). If observations are made on some phenomenon throughout time, it is most sensible to display the data in the order in which they arose, particularly since successive observations will probably be dependent. A time series is best displayed in a scatter plot. The series value X is plotted on the vertical axis and time $t$ on the horizontal axis. Time is called the independent variable. There are two kinds of time series data:

1. Continuous, where we have an observation at every instant of time, *e.g.* lie detectors, electrocardiograms. We denote this using observation $X$ at time $t$, $X(t)$.

2. Discrete, where we have an observation at (usually regularly) spaced intervals. We denote this as $X_t$.

There are some reliable and practical methods for the calculation of Lyapunov exponents if the differential equations of the systems are known (Wolf *et al.* 1985, Williams 1997, Müller 1995). Unfortunately, in most cases, we do not know the differential equations of the systems under study. We only possess one (or more) observable time series from the systems. Therefore, developing methods for calculating the Lyapunov exponents from a time series became important to assess the existence of deterministic chaos in a system. Wolf *et al.* (1985) presented an

algorithm allowing one to estimate the largest non-negative Lyapunov exponent of a time series by tracking the evolution of a set of vectors in the embedding phase space. Sano and Sawada (1985) and Eckmann *et al.* (1986) proposed a Jacobian algorithm which estimates a local flow operator from the evolution of spatially neighboring points to quantify the mean divergence of nearby orbits of the attractor.

Since all of the relevant dynamical variables affect a single experimental time series, the time series contains a relatively complete historical record of the dynamics. The procedure of calculating Lyapunov exponents from a time series is described as follows.

*Step 1:* Reconstructing the phase space from a time series

*Step 2:* Generating local neighborhood-to-neighborhood mapping

*Step 3:* Constructing the Jacobian matrix

*Step 4:* Calculating Lyapunov exponents

*Step 5:* Repeating Step 2 to Step 4

These different steps are described in detail as follows.

### 2.3.1 Reconstruction of the phase space

Two methods are widely used in reconstructing phase space from a time series. One method is time delay method; the other one is derivative method. Here the first one is reviewed.

- ***Time-Delay Method (Delay coordinate method)***

To classify a time series with nonlinear tools (*e.g.* Lyapunov exponents), we must first appropriately reconstruct the phase space where the behavior of the system is

embedded. In other words, we must describe the geometric structure of the dynamical system by calculating the $d_E$ dimensional phase space.

Suppose a time series $x_1, x_2, ..., x_N$, $N$ is the number of the data available. It will be easier to work with $x_i, (i = 1, ..., N)$ and the set of variables obtained from it by shifting its value by a fixed lag $T_{lag}$. It suffices to choose $T_{lag}$ in such a way that the following $n$ variables remain linearly independent:

$$\{X_1\} = \begin{Bmatrix} x_1 \\ x_{1+T_{lag}} \\ \cdots \\ x_{1+(d_E-1)T_{lag}} \end{Bmatrix},$$

$$\{X_2\} = \begin{Bmatrix} x_2 \\ x_{2+T_{lag}} \\ \cdots \\ x_{2+(d_E-1)T_{lag}} \end{Bmatrix},$$

$$\cdots,$$

$$\{X_n\} = \begin{Bmatrix} x_n \\ x_{n+T_{lag}} \\ \cdots \\ x_{n+(d_E-1)T_{lag}} \end{Bmatrix} \tag{2.18}$$

where $n = N - d_E \cdot T_{lag} - T_{evol}$ is the useful size of dataset.

The above variables will be used to define a dynamical system, and their evolution will be embedded in an abstract space spanned by these variables, the phase space. The set $\{X_i\}$ $(i = 1,2,...,n)$ will define the phase space trajectories.

When reconstructing phase space, two parameters $T_{lag}$ and $d_E$ are very important. $T_{lag}$ is the time-delay, which determines how many of the data points are used in the

analysis. If $T_{lag}$ is too small, the successive points in the phase space may be too close together to be sufficiently independent. If $T_{lag}$ is too large, the successive points may be so independent as to be essentially random. $d_E$ is the embedding dimension, which describes the number of variables in phase space from a given time series. If $d_E$ is too small, too many false nearest neighbors will arise when the point $\{X_i\}$ is considered as a point in the $d_E$ dimensional phase space. If $d_E$ is too large, the points become so distant in the $d_E$ dimensional space that again they are essentially random. Determining the embedding dimension $d_E$ of a nonlinear time series plays an important role in the reconstruction of nonlinear dynamics.

### 2.3.2 Generation of the local neighbour-to-neighbour using linear mapping

When dealing with the data which are generated from the unknown dynamical system, the initial problem for calculating its Lyapunov exponents is to estimate the Jacobian matrices. In order to obtain the Jacobian matrices, the local-neighbour to local-neighbour mapping has to be determined first.

Let $v(t)$ be a point in the $d_E$-dimensional reconstructed phase space; there are other nearby points in $R^{dE}$. "Nearby" is measured by some norm in $R^{dE}$. Let $v^i(t)$ be the $d_E$ nearest neighbors to $v(t)$. Then the small vectors $\Delta v^i(t) \in R^{dE}$ between $v(t), (i = 1,2,...,d_E)$ and $v^i(t)$ are

$$\Delta v^i(t) = v^i(t) - v(t) \in R^{dE} \tag{2.19}$$

After evolving forward to time $t+\Delta t$, $v(t)$ and $v^i(t)$ move to $v(t+\Delta t)$ and $v^i(t+\Delta t)$, respectively, thus small vectors $\Delta z^i(t) \in R^{dE}$ between $v^i(t+\Delta t)$ and $v(t+\Delta t)$ are

$$\Delta z^i(t) = v^i(t+\Delta t) - v(t+\Delta t) \in R^{dE} \tag{2.20}$$

Assuming the norm $\Delta v^i$ and the time interval $\Delta t$ are small enough, the Jacobian matrix can be approximated by using the local linear neighbour-to-neighbour map $F$ from $\Delta v^i(t)$ to $\Delta z^i(t)$. This $d_E \times d_E$ matrix $J$ is determined by the least-square method, which minimizes the following distance,

$$\Pi = \sum_{i=1}^{N} \left\| \Delta z^i - J \Delta v^i \right\|^2 \tag{2.21}$$

which lead to the following results:

$$J = CV^{-1}, \tag{2.22a}$$

$$C_{kl} = \sum_{i=1}^{N} \Delta z_k^i \Delta v_l^i, \tag{2.22b}$$

$$V_{kl} = \sum_{i=1}^{N} \Delta v_k^i \Delta v_l^i, \; k,l = 1,2,...,n \tag{2.22c}$$

### 2.3.3 Construction of Jacobian matrix

The Jacobian is the linear part of the dynamics in a local approximation. Once the local neighbour-to-neighbour mapping is obtained, Jacobian matrix can be constructed. In the linear case, the last step gives a sequence of matrices $J_1$, $J_2$,...., $J_K$. The vectors in matrix $J_i$ can be orthonormalized using GSR procedure,

Householder QR decomposition, or singular-value decomposition. Householder QR decomposition is used in Zeng *et al.* (1992).

$$\begin{aligned} J_1 Q_{(0)} &= Q_{(1)} R_{(1)}, \\ J_2 Q_{(1)} &= Q_{(2)} R_{(2)}, \\ &\cdots \\ J_{(j+1)} Q_{(j)} &= Q_{(j+1)} R_{(j+1)}, \\ &\cdots \end{aligned} \tag{2.23}$$

Where $Q_{(j)}$ are orthonormal matrices, $R_{(j)}$ are upper triangular matrices with positive diagonal elements such that $Q_{(0)}$ is the unit matrix.

### 2.3.4 Calculation of Lyapunov exponents

Properly defined, the calculation of Lyapunov exponents requires computation of the local Jacobian matrix along a trajectory (one trajectory is enough if the system is ergodic). After obtaining the Jacobian matrix, multiplying these Jacobians together and then calculating the eigenvalues. Then, (up to some constant related to the sampling time) the Lyapunov exponents can be computed as the logarithm of these eigenvalues.

$$\lambda_i = \frac{1}{n\Delta t K} \ln \prod_{j=1}^{K} (R_j)_{ii} = \frac{1}{n\Delta t K} \sum_{j=1}^{K} \ln (R_j)_{ii}, \qquad i = 1,2,...,d_E \tag{2.24}$$

where $K$ is the number of matrices. The entire procedure is described in reference (Abarbanel 1996).

## 2.4 The Action of Matrices on the Calculation of Lyapunov Exponents

This section was heavily borrowed from Sauer's book (Sauer 2006) on singular value decomposition. This visional idea is excellent to help better understand the actions of mapping matrices on the calculation of Lyapunov exponents.

The image of the unit sphere in $R^m$ under a $m \times m$ matrix is an ellipsoid. This interesting fact underlies the singular value decomposition, which has many applications in matrix analysis in general and especially for compression purposes. Figure 2.2 is an illustration of the ellipse that corresponds to the matrix

$$A = \begin{bmatrix} 3 & 0 \\ 0 & \frac{1}{2} \end{bmatrix} \tag{2.25}$$

Imagine taking the vector $v$ corresponding to each point on the unit circle, multiplying by $A$, and then plotting the endpoint of the resulting vector $Av$. The result is the ellipse shown. In order to describe the ellipse, it helps to use an orthonormal set of vectors to define the basis of a coordinate system, as shown in Figure 2.2.

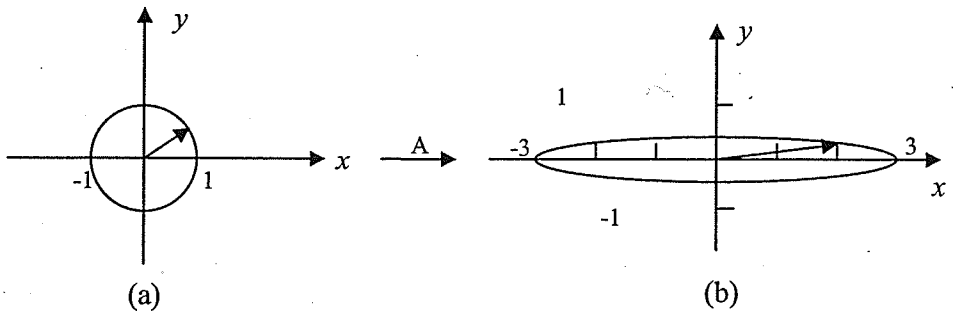


Figure 2.2 the image of the unit circle under a $2 \times 2$ matrix.
(a) The unit circle in $R^2$
(b) The ellipse with semi major axes (3, 0) and (0, ½)

**Theorem 2.1**

Let $A$ be a $m \times n$ matrix. Then there are exist two orthonormal bases $\{v_1,...,v_n\}$ of $R^n$, and $\{u_1,...,u_m\}$ of $R^m$, and real numbers $s_1 \geq \cdots \geq s_n \geq 0$ such that $Av_i = s_i u_i$ for $1 \leq i \leq \min\{m,n\}$. The columns of $V = [v_1|\cdots|v_n]$, the right singular vectors, are the set of orthonormal eigenvectors of $A^T A$; and the columns of $U = [u_1|\cdots|u_m]$, the left singular vectors, are the set of orthonormal eigenvectors of $AA^T$.

Based on Theorem 2.1 that for every $m \times n$ matrix $A$, there are orthonormal sets $\{u_1,...,u_m\}$ and $\{v_1,...,v_n\}$, together with nonnegative numbers $s_1 \geq \cdots \geq s_n \geq 0$, satisfying

$$\begin{aligned} Av_1 &= s_1 u_1 \\ Av_2 &= s_2 u_2 \\ &\vdots \\ Av_n &= s_{n1} u_n \end{aligned} \tag{2.26}$$

The vectors are visualized in Figure 2.2. Vector $v_i$ are called the right singular vectors of the matrix $A$, vector $u_i$ are called the left singular vectors of the matrix $A$, and the $s_i$ are called the singular values of the matrix $A$.

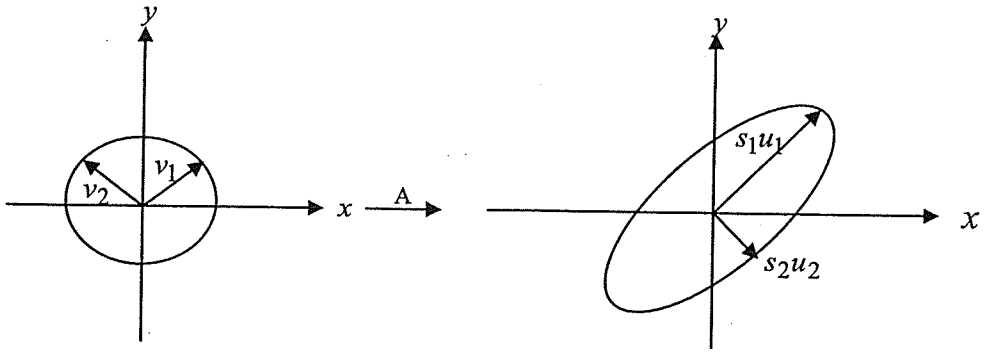


Figure 2.3 The ellipse associated to a matrix. Every $2\times2$ matrix $A$ can be viewed in the following simple way: There is a coordinate system $\{v_1, v_2\}$ for which $A$ sends $v_1 \to s_1u_1$ and $v_2 \to s_2u_2$, where $\{u_1, u_2\}$ is another coordinate system and $s_1, s_2$ are nonnegative numbers. This picture extends to $R^m$ for a $m\times n$ matrix.

This useful fact immediately explains how a $2\times2$ matrix maps the unit circle into an ellipse. The vectors $v_i$ are the basis of a rectangular coordinate system on which $A$ acts in a simple way: they produce the basis vectors of a new coordinate system, the vectors $u_i$, with some stretching quantified by the scalars $s_i$. The stretched basis vectors $s_iu_i$ are the semi-major axes of the ellipse, as shown in Figure 2.3.

**Example**

Find the singular values and singular vectors for the matrix A shown in Equation (2.25) represented in Figure 2.2

Clearly, the matrix stretches by 3 in the x direction and shrinks by a factor of $1/2$ in the y direction. The singular vectors and singular values of $A$ are

$$A\begin{bmatrix}1\\0\end{bmatrix} = 3\begin{bmatrix}1\\0\end{bmatrix}$$
$$A\begin{bmatrix}0\\1\end{bmatrix} = \frac{1}{2}\begin{bmatrix}0\\1\end{bmatrix} \qquad (2.27)$$

The vectors $3(1,0)$ and $\frac{1}{2}(0,1)$ form the semi-major axes of the ellipse. The right singular vectors are [1,0], [0,1], and the left singular vectors are [1,0], [0,1]. The singular values are 3 and $1/2$.

There is a standard way to keep track of this information, in a matrix factorization of the $m \times n$ matrix $A$ - Form a $m \times m$ matrix $U$ whose columns are the left singular vectors $u_i$, an $n \times n$ matrix $V$ whose columns are the right singular vectors $v_i$, and a diagonal $m \times n$ matrix $S$ whose diagonal entries are the singular values $s_i$. Then the singular value decomposition (SVD) of the $m \times n$ matrix $A$ is

$$A = USV^T \tag{2.28}$$

The following lemma shows that the SVD exists for a general matrix $A$:

**Lemma 2.1** Let $A$ be an $m \times n$ matrix. The eigenvalues of $A^T A$ are nonnegative.

## 2.5 Mickens' Non-Standard Finite Difference Scheme

In order to reduce numerical instabilities while calculating numerical solutions of dynamical systems, Mickens (2002) introduced a framework for non-standard finite difference discretization of nonlinear differential equations, which is essentially the discrete representation of the system constructed according to the following rules:

*Rule 1.* The orders of the discretized derivatives should be equal to the orders of the corresponding derivatives of the differential equations. If the orders of the discretized derivatives are larger than those of the differential equation, spurious solutions (convergence to false steady-state) and scheme-dependent numerical instabilities would occur.

*Rule 2.* Discrete representations for derivatives must, in general, have nontrivial denominator functions. For example, the discrete first derivative of the continuous equation $\frac{dx}{dt} = f(x)$,

in nonstandard scheme takes the form:

$$\frac{dx}{dt} \to \frac{x^{(k+1)} - x^{(k)}}{\phi(h, R^*)} \tag{2.29}$$

where

$$\phi(h, R^*) = \frac{1 - e^{-R^* h}}{R^*} \tag{2.30}$$

The value of $R^*$ is determined as the maximum value of $R_i$:

$$R^* \equiv \max\left\{|R_i|; i = 1,2,...,I\right\} \tag{2.31}$$

where $R_i$ is defined as

$$R_i \equiv \left.\frac{df}{dx}\right|_{x=\bar{x}^{(i)}} \tag{2.32}$$

and $\bar{x}^{(i)}; i = 1,2,...,I$ is the set of the system's fixed points.

Thus, $0 < \phi(h, R^*) < \frac{1}{R^*}$ and the function $\phi$ can be interpreted as a "renormalized" or "rescaled" time step-size such that its value is never larger than the smallest time scale of the system $T^* = \frac{1}{R^*}$.

*Rule 3.* Nonlinear terms should, in general, be replaced by non-local discrete representations.

For example, the term $x^2$ can be represented by $x^{(k+1)}x^{(k)}$ or even $2(x^{(k)})^2 - x^{(k+1)}x^{(k)}$.

*Rule 4.* Special conditions that hold for the solutions of the differential equations should also hold for the solution of the finite difference scheme. For

example, for many dynamical systems a condition of positivity holds for the dependent variable. If the numerical scheme leads to solutions that can violate this condition, then numerical instabilities will eliminate any possibility of obtaining meaningful results.

## 2.6 Some Basic Concepts and Sampling Theorem

Although this research on calculation of Lyapunov exponents from a time series is based on the assumption that the time series data are accurate and no information loss during sampling, the proper analog-to-digital conversion is an important issue when calculating Lyapunov exponents using a time series. Thus, it is necessary to review some basic concepts and the sampling theorem (in detail refer to Shenoi 2006, Cover and Thomas 1991, Kinsner 2007).

### 2.6.1 Some basic concepts

**a. Continuous-time signal (analog signal)**

A continuous-time signal (analog signal) is a function whose amplitude and time have infinite resolution. A one-dimensional continuous-time signal $f(t)$ is expressed as a function of time that varies continuously from $-\infty$ to $\infty$.

**b. Discrete-time signal**

A discrete-time signal is a function whose amplitude has infinite resolution, but is defined only at discrete intervals of time, and undefined at all other values of time. Although a discrete-time function may be defined at arbitrary values of time in the interval $-\infty$ to $\infty$, only a function defined at equal intervals of time is considered and defined at $t = nT$, where $T$ is a fixed interval in seconds known as the sampling period and $n$ is an integer variable defined over $-\infty$ to $\infty$.

If one chooses to sample $f(t)$ at equal intervals of $T$ seconds, one generates $f(nT) = f(t)\big|_{t=nT}$ as a sequence of numbers (samples). Since $T$ is fixed, $f(nT)$ is a function of only the integer variable $n$ and hence can be considered as a function of $n$ or expressed as $f(n)$. The sampling process is done by measuring the continuous/analog signal's value every $T$ seconds, (in practice, the sampling interval is typically quite small, approximately milliseconds or even microseconds).

**c. Digital signal**

A digital signal has finite resolution in both amplitude and time. This thesis deals with digital signals exclusively.

**d. Signal-to-noise ratio**

Signal-to-noise ratio (often abbreviated SNR or S/N) is an electrical engineering concept defined as the ratio of a signal power to the noise power corrupting the signal.

In less technical terms, signal-to-noise ratio compares the level of a desired signal (such as music) to the level of background noise. The higher the ratio, the less obtrusive the background noise is.

When using digital storage the number of bits of each value determines the maximum signal-to-noise ratio. In this case the noise is the error signal caused by the quantization of the signal, taking place in the analog-to-digital conversion. The noise level is non-linear and signal-dependent; different calculations exist for different signal models. The noise is modeled as an analog error signal being summed with the signal before quantization ("additive noise").

### 2.6.2 The Nyquist-Shannon sampling and reconstruction theorem

An analog signal cannot be represented on a computer whose resolution is always finite. Thus, it is necessary to convert such signals to a sequence digital values. It is, therefore, required to define the rate at which new digital values are sampled from the analog signal. The rate of new values is called the *sampling rate* or *sampling frequency* of the converter. The Nyquist-Shannon sampling and reconstruction theorem asserts that, given a bandlimited continuous-time signal, $x(t)$, that is uniformly sampled at a sufficient rate, even if all of the information in the signal between samples is discarded, there remains sufficient information in the samples so that the original continuous-time signal can be mathematically reconstructed from only those samples. The sampling theorem states that a signal can be exactly reproduced if it is sampled at a frequency $f_s$, where $f_s$ is greater than twice the maximum frequency in the signal. This relationship defines the minimum theoretical sample rate, which is sufficient to reconstruct the signal exactly. If the highest frequency of the signal is known, the theorem gives us the lowest possible sampling frequency to assure perfect reconstruction. If the sampling frequency is known, the theorem gives us an upper bound for the frequencies of the signal to assure perfect reconstruction.

Most mechanical signals have frequencies limited to below 100 kHz. Therefore, using a 200 kHz sampling rate should satisfy most mechanical engineering applications. The price for such a high sampling rate will be the larger number of sample data to be stored and processed. Note that this limit should not be applied to electrical engineering, where signals can contain much higher frequencies.

# Chapter 3

# Effects of Constraints on Balance Control of Bipedal Standing

## 3.1 Introduction

In this chapter, the effects of the constraints between the foot-link and the ground on bipedal standing are systematically studied. The constraints include: the gravity constraint, *i.e.*, the foot-link does not lift from the ground; the friction constraint, *i.e.*, the foot-link does not slide, the center of pressure (COP) constraint, *i.e.*, the center of the pressure is within the contact surface between the foot-link and the ground, and the tip-over constraint, *i.e.,* the bipedal foot-link does not rotate about either the toes or the heels. The tip-over constraint can be characterized by the zero moment point (ZMP) when both feet are on the same level ground, and it has been proven that COP and ZMP coincide for this case (Vukobratović and Borovac 2004). Thus, the tip-over constraint is equivalent to the COP constraint and the latter is studied here. The bipedal model is simplified as an inverted pendulum with one rigid foot-link on the level ground. It has been reported that standing human subjects, when perturbed by translation of a moving support surface for small disturbance, typically respond by moving in the segittal plane, and they tend to keep the knees, hips, and neck fairly straight, moving about the ankle (Kuo 1995). Thus, it is reasonable to simplify a biped as a simple inverted pendulum moving in the sagittal

plane, and inverted pendulum models have often been used to study bipedal posture (Hemami *et al.* 1978, Hemami and Stokes 1983, Wu *et al.* 1998).

The first objective is to determine the bounds imposed on the control torque satisfying the constraints. The second objective is to explore the effects of the constraints on the bipedal standing. Questions to be answered are: What are the physical indications of the control bounds? Are there any other conditions imposed on the biped during balance control of standing? How do three constraints interact? Which constraints are more dominant?

## 3.2 Dynamic Equations of the Bipedal Model

In this work, the bipedal model is simplified to include a rigid foot-link, which provides a base of support on the ground and an inverted pendulum, representing the legs, trunk, arms and head as shown in Figure 3.1a. The free body diagrams for the pendulum and the foot-link are shown in Figure 3.1b and Figure 3.1c.

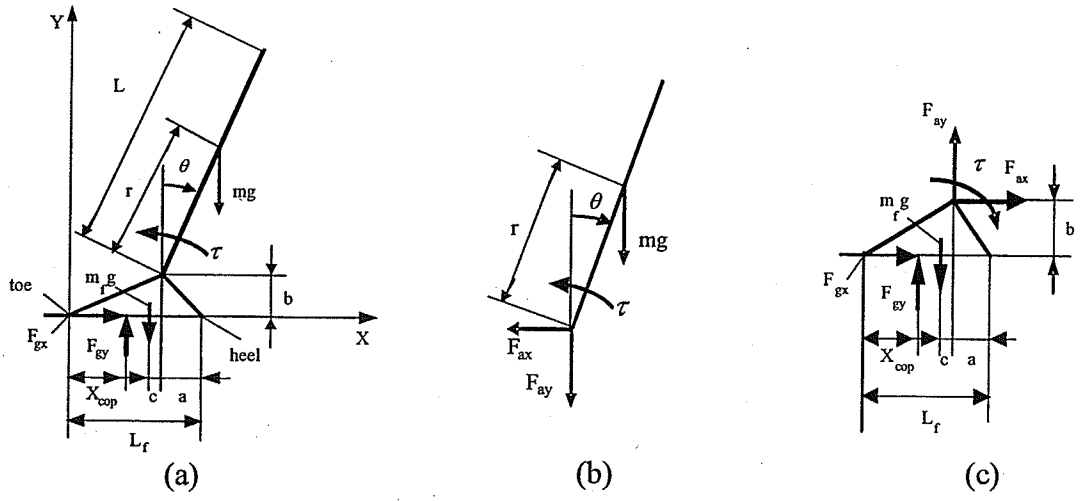


Figure 3.1 (a) Simplified bipedal model, (b) free body diagram of the inverted pendulum, and (c) free body diagram of the foot-link

The feet position is assumed to be bilaterally symmetric and stationary, and the biped moves in the sagittal plane. Three dynamic equations of the inverted pendulum are developed using the Euler-Lagrangian equation as:

$$\tau = mgr\sin\theta - (I + mr^2)\ddot{\theta} \tag{3.1a}$$

$$F_{ax} = mr\dot{\theta}^2 \sin\theta - mr\ddot{\theta}\cos\theta \tag{3.1b}$$

$$F_{ay} = mr\dot{\theta}^2 \cos\theta + mr\ddot{\theta}\sin\theta - mg \tag{3.1c}$$

where $F_{ax}$ and $F_{ay}$ are the horizontal and vertical force components between the foot-link and the inverted pendulum, respectively. As shown in Figure 1, $\tau, \theta$, $\dot{\theta}$ and $\ddot{\theta}$ are the ankle torque (counter clockwise as "+"), angular displacement, velocity and acceleration of the body (clockwise as "+"), respectively. Note that with a positive angle, $\theta$, the biped leans posteriorly and with a negative $\theta$, the biped leans anteriorly. The parameters $r$, $L$, $m$ and $I$ are the distance between the center of mass of the pendulum and the ankle, length of pendulum, mass of the body and the moment of inertia of the pendulum about the mass center, respectively. The origin of the fixed coordinate system is located at the toe. The x-axis is horizontal pointing from the toe to the heel, and the y-axis is upward.

Since the foot-link is static, three equilibrium equations are:

$$F_{ax} = -F_{gx} \tag{3.2a}$$

$$F_{ay} = m_f g - F_{gy} \tag{3.2b}$$

$$F_{gy}\,(L_f - a - x_{cop}) + m_f gc - F_{gx} b - \tau = 0 \tag{3.2c}$$

$F_{gx}$ and $F_{gy}$ are the horizontal and vertical ground reaction forces, respectively. The parameters $a$, $c$, $b$, $x_{cop}$, $L_f$, $m_f$ and $m$ are the horizontal distance between the ankle

and the heel, between the mass center of the foot-link and the ankle, ankle height, distance between the pressure center and the toe, the length of the foot-link, mass of the foot-link and mass of the body, respectively.

By eliminating the ankle forces, $F_{ax}$ and $F_{ay}$ from Equations (3.1) and (3.2), the dynamic equations for the bipedal system are

$$\tau = mgr\sin\theta - (I + mr^2)\ddot{\theta} \tag{3.3a}$$

$$F_{gx} = mr\ddot{\theta}\cos\theta - mr\dot{\theta}^2\sin\theta \tag{3.3b}$$

$$F_{gy} = (m_f + m)g - mr\ddot{\theta}\sin\theta - mr\dot{\theta}^2\cos\theta \tag{3.3c}$$

## 3.3 Constraints and their Mathematical Expressions

Unlike many of the previous papers, in this research, the foot-link is not fixed on the ground, but is required to be stationary. There are four constraints between the foot-link and the ground during bipedal standing, namely the gravity constraint, *i.e.*, the foot-link do not lift from the ground; the friction constraint, *i.e.*, the foot-link do not slide; the Center of Pressure (COP) constraint, *i.e.*, the center of the pressure is within the contact surface between the foot-link and the ground, and the tip-over constraint, *i.e.*, the biped does not rotate around the toes or the heels. The tip-over constraint can be characterized by the zero moment point (ZMP) when both feet are on the same level ground. For this case, it has been proven that COP and ZMP coincide (Vukobratović and Borovac 2004). Thus, the tip-over constraint is equivalent to the COP constraint as both feet are on the same level ground. So, three constraints are considered in this research. The gravity constraint requires that the vertical ground force ($F_{gy}$) be upward. The friction constraint

requires that the horizontal ground force ($F_{gx}$) be lower than the maximum static friction. The COP constraint requires that the pressure center ($x_{COP}$) be between the toe and the heel indicating that tip-over does not occur. The three constraints are written as (Pai and Patton 1997):

$$F_{gy} \geq 0 \tag{3.4a}$$

$$\left|F_{gx}\right| \leq \mu F_{gy} \tag{3.4b}$$

$$0 \leq x_{cop} \leq L_f \tag{3.4c}$$

From Equation (3.2c), the pressure center ($x_{cop}$) is

$$x_{cop} = L_f - a - \frac{bF_{gx} - \tau + cm_f g}{F_{gy}} \tag{3.4d}$$

## 3.4 Effects of Each Individual Constraint

In this section, the ranges of the control torque satisfying each constraint as shown in Inequality (3.4) are determined analytically. Their effects on bipedal standing are also discussed.

### 3.4.1 Effects of gravity constraint

The range of the control torque satisfying the gravity constraint is determined. The angular acceleration, $\ddot{\theta}$, is first solved from Equation (3.1a) in terms of the control torque $\tau$, angle $\theta$, and physical parameters. The results are then substituted into Equation (3.3c) to solve for the vertical ground reaction force, $F_{gy}$. Considering Inequality (3.4a), one has

$$\frac{\Delta_1}{I + mr^2}(\tau - mgr\sin\theta) \geq mr\dot{\theta}^2\cos\theta - (m_f + m)g \tag{3.5a}$$

where

$$\Delta_I = mr\sin\theta \tag{3.5b}$$

To solve the torque, $\tau$, both sides of Inequality (3.5a) are divided by $\frac{\Delta_I}{I+mr^2}$, which leads to two cases:

**Case 1.** $\theta = 0$ $(\Delta_I = 0)$:

As $\theta = 0$, Inequality (3.5a) imposes that

$$(m_f + m)g - mr\dot{\theta}^2 \geq 0$$

which leads to

$$\dot{\theta}^2 \leq \frac{(m_f + m)g}{mr} \tag{3.6}$$

Inequality (3.6) is the condition on the angular velocity satisfying the gravity constraint at the upright position. The angular velocity must be lower than $\sqrt{\frac{(m_f + m)g}{mr}}$ and the restriction on the control torque is covered by angular velocity. Otherwise, regardless of the torque, the gravity constraint will be violated, *i.e.*, the foot-link will be lifted from the ground.

**Case 2.** $\theta \neq 0$ $(\Delta_I \neq 0)$**:**

As $\theta \neq 0$, from Inequality (3.5a), one has

$$\tau \geq \tau_{lift} \qquad \text{when} \qquad \theta > 0 \ (\Delta_I > 0) \tag{3.7a}$$

$$\tau \leq \tau_{lift} \qquad \text{when} \qquad \theta < 0 \ (\Delta_I < 0) \tag{3.7b}$$

where

$$\tau_{lift} = mgr\sin\theta + \frac{I + mr^2}{\Delta_I}\left[mr\dot{\theta}^2\cos\theta - (m_f + m)g\right] \tag{3.7c}$$

Inequalities (3.7a) and (3.7b) show the ranges of the control torque satisfying the gravity constraint when the biped is not at the upright position. No restriction is imposed on the angular velocity.

### 3.4.2 Effects of friction constraint

The range of the control torque satisfying the friction constraint shown in Inequality (3.4b), is determined as detailed below:

$$F_{gx} \geq -\mu F_{gy} \tag{3.8a}$$

$$F_{gx} \leq \mu F_{gy} \tag{3.8b}$$

The satisfaction of Inequality (3.8a) indicates that slipping posteriorly of the foot-link (slipping along the positive x-axis as shown in Figure 3.1a) is prevented. Similarly, the satisfaction of Inequality (3.8b) indicates that slipping anteriorly (slipping along the negative x-axis) is prevented. To find the bounds of the control torque without slipping, the angular acceleration, $\ddot{\theta}$, is solved from Equation (3.1a), and is substituted into Equations (3.3b) and (3.3c). With inequalities (3.8a) and (3.8b), one has:

$$\frac{\Delta_2}{I+mr^2}(\tau - mgr\sin\theta) \leq \mu(m_f + m)g - mr\dot{\theta}^2(\sin\theta + \mu\cos\theta) \tag{3.9a}$$

$$\frac{\Delta_3}{I+mr^2}(\tau - mgr\sin\theta) \geq mr\dot{\theta}^2(\mu\cos\theta - \sin\theta) - \mu(m_f + m)g \tag{3.9b}$$

where

$$\Delta_2 = mr(\cos\theta - \mu\sin\theta) \tag{3.9c}$$

$$\Delta_3 = mr(\cos\theta + \mu\sin\theta) \tag{3.9d}$$

To solve the control torque, $\tau$, Inequality (3.9a) is divided by $\frac{\Delta_2}{I+mr^2}$ and Inequality (3.9b) by $\frac{\Delta_3}{I+mr^2}$, which lead to two critical angles:

$$\theta_{cr1} = \theta^* = tan^{-1}(\frac{1}{\mu}) \qquad \text{when} \quad \Delta_2 = 0 \tag{3.10a}$$

$$\theta_{cr2} = -\theta^* = -tan^{-1}(\frac{1}{\mu}) \qquad \text{when} \quad \Delta_3 = 0 \tag{3.10b}$$

As the biped is at the critical angle, $\pm\theta^*$, inequalities (3.9a) and (3.9b) lead to

$$\left|\dot{\theta}\right| \le \dot{\theta}_{cr1}(\theta^*) \qquad \text{when} \quad \theta = \theta^* \tag{3.11a}$$

$$\left|\dot{\theta}\right| \le \dot{\theta}_{cr1}(-\theta^*) \qquad \text{when} \quad \theta = -\theta^* \tag{3.11b}$$

where the critical angular velocity, $\dot{\theta}_{cr1}(\theta)$, is

$$\dot{\theta}_{cr1}(\theta) = \sqrt{\frac{(m_f + m)g}{mr}\cos\theta} \tag{3.11c}$$

It is interesting to note that both critical angles are symmetric about the upright position, and are determined by the friction coefficient, $\mu$. Only the magnitudes of critical angular velocities, not the direction, affect the satisfaction of the friction constraint.

The critical angles $\pm\theta^*$ divide the region $-90^o \le \theta \le 90^o$ into three sub-regions, and the range of the control torque satisfying the friction constraint is determined in each sub-region.

**Region 1:** $-90^o \le \theta < -\theta^*$

In this region, the biped leans anteriorly. From Equations (3.9c) and (3.9d), $\Delta_2 > 0$ and $\Delta_3 < 0$. From inequalities (3.9a) and (3.9b), one has

$$\tau \le min\left(\tau_{slip-posterior}, \tau_{slip-anterior}\right) \tag{3.12a}$$

where $\tau_{slip-posterior}$ and $\tau_{slip-anterior}$ are the ankle torques at the onset that the foot-link is to

slip posteriorly and anteriorly, respectively. They are defined as:

$$\tau_{slip-posterior} = mgr\sin\theta + \frac{I+mr^2}{\Delta_2}[\mu(m_f+m)g - mr\dot{\theta}^2(\sin\theta+\mu\cos\theta)] \quad (3.12b)$$

$$\tau_{slip-anterior} = mgr\sin\theta + \frac{I+mr^2}{\Delta_3}[mr\dot{\theta}^2(\mu\cos\theta-\sin\theta) - \mu(m_f+m)g] \quad (3.12c)$$

Next, the minimum between $\tau_{slip-posterior}$ and $\tau_{slip-anterior}$ is determined by examining $\tau_{slip-posterior} - \tau_{slip-anterior}$,

$$\tau_{slip-posterior} - \tau_{slip-anterior} = \frac{2M\mu mr}{\Delta_2\Delta_3}[(m_f+m)g\cos\theta - mr\dot{\theta}^2]\begin{cases}\geq 0 & |\dot{\theta}| \geq \dot{\theta}_{cr1}(\theta) \\ \leq 0 & |\dot{\theta}| \leq \dot{\theta}_{cr1}(\theta)\end{cases} \quad (3.13)$$

where $\dot{\theta}_{cr1}(\theta)$ is defined in Equation (3.11c). Thus, Inequality (3.12a) becomes

$$\tau \leq \tau_{slip-posterior} \quad \text{when} \quad |\dot{\theta}| \leq \dot{\theta}_{cr1}(\theta) \quad (3.14a)$$

$$\tau \leq \tau_{slip-anterior} \quad \text{when} \quad |\dot{\theta}| \geq \dot{\theta}_{cr1}(\theta) \quad (3.14b)$$

Inequality (3.14) reveals some interesting insights into the effects of the angular velocity on the satisfaction of the friction constraint. As the angular velocity changes, the control bounds are dictated by different friction conditions. Inequality (3.14) can be used to identify the specific friction constraint to be violated, and therefore to predict the movement of the foot-link. For example, with a low magnitude of angular velocity ($|\dot{\theta}| \leq \dot{\theta}_{cr1}$), a high control torque ($\tau > \tau_{slip-posterior}$) causes the foot-link to slip posteriorly. On the other hand, with a high angular velocity ($|\dot{\theta}| \geq \dot{\theta}_{cr1}$), a high control torque ($\tau > \tau_{slip-anterior}$) causes the foot-link to slip anteriorly.

**Region 2:** $-\theta^* < \theta < \theta^*$

From Equations (3.9c) and (3.9d), $\Delta_2 > 0$ and $\Delta_3 > 0$. From inequalities (3.9a) and (3.9b), one has

$$\tau_{slip-anterior} \leq \tau \leq \tau_{slip-posterior} \tag{3.15}$$

Inequality (3.15) requires that $\tau_{slip-posterior} \geq \tau_{slip-anterior}$. By examining $\tau_{slip-posterior} - \tau_{slip-anterior}$, in order to ensure that $\tau_{slip-posterior} - \tau_{slip-anterior} > 0$, the following condition must be satisfied:

$$|\dot{\theta}| \leq \dot{\theta}_{cr1}(\theta) \tag{3.16}$$

where $\dot{\theta}_{cr1}$ is given in Equation (3.11c). Inequality (3.16) shows that as the biped is around the upright position within $\pm\theta^*$, the angular velocity must be below $\dot{\theta}_{cr1}$. Otherwise, regardless of the control torque, the friction constraint will be violated. As $|\dot{\theta}| \leq \dot{\theta}_{cr1}(\theta)$, the bounds for the control torque, shown in Inequality (3.15), can be used to identify the specific friction constraint to be violated and to predict the potential movement of the foot-link once the constraint is violated. For example, with a high control torque ($\tau > \tau_{slip-posterior}$), the biped is to slip posteriorly, while, with a low control torque ($\tau < \tau_{slip-anterior}$), the biped is to slip anteriorly.

**Region 3:** $\theta^* < \theta \leq 90^o$

In this region, the biped leans posteriorly. From Equations (3.9c) and (3.9d), $\Delta_2 < 0$ and $\Delta_3 > 0$. From inequalities (3.9a) and (3.9b), one has

$$\tau \geq max\left(\tau_{slip-posterior}, \tau_{slip-anterior}\right) \tag{3.17}$$

Next determine the maximum between $\tau_{slip-posterior}$ and $\tau_{slip-anterior}$ by examining $\tau_{slip-posterior} - \tau_{slip-anterior}$. From Equation (3.13), the lower bound of the control torque is

$$\tau \geq \tau_{slip-anterior} \quad \text{when} \quad |\dot{\theta}| \leq \dot{\theta}_{cr1}(\theta) \tag{3.18a}$$

$$\tau \geq \tau_{slip-posterior} \quad \text{when} \quad |\dot{\theta}| \geq \dot{\theta}_{cr1}(\theta) \tag{3.18b}$$

The control torque must satisfy Inequality (3.18) to prevent the foot-link from slipping. It is interesting to note that as the biped leans posteriorly, with a high angular velocity ($|\dot{\theta}| \geq \dot{\theta}_{cr1}$), a low control torque ($\tau < \tau_{slip-posterior}$) causes the foot-link to slip posteriorly, and with a low angular velocity ($|\dot{\theta}| \leq \dot{\theta}_{cr1}$), a low torque ($\tau < \tau_{slip-anterior}$) causes the foot-link to slip anteriorly.

Inequalities (3.14), (3.16) and (3.18) not only show the bounds of the control torque, but also indicate the specific constraint causing the control bounds. Thus, they can be used to identify the constraint to be violated and to predict the movement of the foot-link once the constraint is violated. Inequalities (3.14), (3.16) and (3.18) further show that the angular velocity dictates the constraint resulting in the control bounds, thus it plays a crucial role in satisfying the friction constraint.

### 3.4.3 Effects of center of pressure (COP) constraint

The COP constraint, shown in Inequality (3.4c), requires that the COP reside within the boundary of support. Inequality (3.4c) can be divided into two parts (referring to Figure 3.1a):

$$x_{cop} \le L_f \tag{3.19a}$$

$$x_{cop} \ge 0 \tag{3.19b}$$

Substituting Equation (3.4d) into Inequality (3.19), and considering that $F_{gy} \ge 0$, one has

$$aF_{gy} + bF_{gx} - \tau + cm_f g \ge 0 \tag{3.20a}$$

$$(L_f - a)F_{gy} - bF_{gx} + \tau - cm_f g \ge 0 \tag{3.20b}$$

Substituting Equations (3.3b) and (3.3c) into Inequality (3.20) and combining with (3.1a),

$$\frac{\Delta_4}{I + mr^2}\tau \ge \frac{mr(a\sin\theta - b\cos\theta)}{I + mr^2} mgr\sin\theta + mr\dot{\theta}^2(a\cos\theta + b\sin\theta) - a(m_f + m)g - cm_f g \tag{3.21a}$$

$$\frac{\Delta_5}{I + mr^2}\tau \ge \frac{mr\left[(L_f - a)\sin\theta + b\cos\theta\right]}{I + mr^2} mgr\sin\theta + mr\dot{\theta}^2\left[(L_f - a)\cos\theta - b\sin\theta\right] - (L_f - a)(m_f + m)g + cm_f g \tag{3.21b}$$

where

$$\Delta_4 = mr(a\sin\theta - b\cos\theta) - M \tag{3.21c}$$

$$\Delta_5 = M + mr\left[(L_f - a)\sin\theta + b\cos\theta\right] \tag{3.21d}$$

For a general bipedal model, it is not unreasonable to assume that the distance between the ankle and the mass center of the body is greater than the length of the foot-link, *i.e.*, $r > L_f$, thus $r > a$. As $-90^\circ \le \theta \le 90^\circ$, $mrb\cos\theta \ge 0$, $mra\sin\theta < mr^2$ and $mr(L_f - a)\sin\theta \le mr(L_f - a) \le mr^2$. Thus $\Delta_4 < 0$ and $\Delta_5 > 0$.

From inequalities (3.21a) and (3.21b), the bounds of control torque

$$\tau_{cop-toe} \le \tau \le \tau_{cop-heel} \tag{3.22a}$$

where

$$\tau_{cop-heel} = \frac{1}{\Delta_4}\{m^2 r^2 g \sin\theta(a\sin\theta - b\cos\theta) + (I + mr^2)[mr\dot{\theta}^2(a\cos\theta + b\sin\theta) - (\frac{L_f m_f}{2} + am)g]\} \quad (3.22b)$$

$$\tau_{cop-toe} = \frac{1}{\Delta_5}\{m^2 r^2 g \sin\theta[(L_f - a)\sin\theta + b\cos\theta] + (I + mr^2)mr\dot{\theta}^2[((L_f - a)\cos\theta - b\sin\theta] - (I + mr^2)[\frac{L_f m_f}{2} + (L_f - a)m]g\} \quad (3.22c)$$

Inequality (3.22a) requires that $\tau_{cop-heel} \geq \tau_{cop-toe}$. Next $\tau_{cop-heel} - \tau_{cop-toe}$ is examined:

$$\tau_{cop-heel} - \tau_{cop-toe} = \frac{1}{\Delta_4\Delta_5}\{\Delta_5\{m^2r^2g\sin\theta(a\sin\theta - b\cos\theta) + (I+mr^2)[mr\dot{\theta}^2(a\cos\theta + b\sin\theta) - (\frac{L_f m_f}{2} + am)g]\} - \Delta_4\{m^2r^2g\sin\theta[(L_f - a)\sin\theta + b\cos\theta] + (I+mr^2)mr\dot{\theta}^2[(L_f - a)\cos\theta - b\sin\theta] - (I+mr^2)[\frac{L_f m_f}{2} + (L_f - a)m]g\}\}$$

Since $\Delta_4\Delta_5 < 0$, to ensure that $\tau_{cop-heel} - \tau_{cop-toe} > 0$, the following inequality must be satisfied:

$$\Delta_5\{m^2r^2g\sin\theta(a\sin\theta - b\cos\theta) + (I+mr^2)[mr\dot{\theta}^2(a\cos\theta + b\sin\theta) - (\frac{L_f m_f}{2} + am)g]\} - \Delta_4\{m^2r^2g\sin\theta[(L_f - a)\sin\theta + b\cos\theta] + (I+mr^2)mr\dot{\theta}^2[(L_f - a)\cos\theta - b\sin\theta] - (I+mr^2)[\frac{L_f m_f}{2} + (L_f - a)m]g\} < 0$$

Let $M = I + mr^2$, and the condition ensuring that $\tau_{cop-heel} - \tau_{cop-toe} > 0$ is

$$|\dot{\theta}| \leq \dot{\theta}_{cr2} \quad (3.23a)$$

where

$$\dot{\theta}_{cr2} = \sqrt{\frac{g}{mr(M\cos\theta + mrb)}\left\{mrb(m_f + m)\cos\theta + mrcm_f \sin\theta + M(m_f + m) - m^2 r^2 \sin^2\theta\right\}} \tag{3.23b}$$

Inequalities (3.22a) and (3.23a) indicate that the angular velocity of the biped plays an important role in keeping the COP within the base of support. If the angular velocity is higher than the critical value, $\dot{\theta}_{cr2}$, regardless of the control torque, the COP constraint will be violated. If the angular velocity is below the critical value of $\dot{\theta}_{cr2}$, Inequality (3.22a) further indicates that if the control torque is too high ($\tau > \tau_{cop-heel}$), the COP will be behind the heel, *i.e.*, the foot-link will rotate about the heel. If the control torque is too low ($\tau < \tau_{cop-toe}$), the COP will be ahead of the toe, *i.e.*, the foot-link will rotate about the toe. For both cases, the pressure center constraint is violated indicating that tip-over will occur, but in a different manner.

## 3.5 Effects of Multiple Constraints

### 3.5.1 Effects of gravity and friction constraints

In this section, the bounds of the control torque satisfying the gravity and friction constraints will be determined analytically, and their effects on the bipedal standing will be investigated. Based on the results from Section 3.3, the region for the angle, $\theta$, from $-90^0$ to $90^0$, is divided into four sub-regions by three singular points. In each sub-region, the signs of $\Delta_1, \Delta_2$ and $\Delta_3$ are shown in Table 3.1.

Table 3.1 Signs of $\Delta_1, \Delta_2$ and $\Delta_3$ in each sub-region

| $\theta$ | $-90^o \le \theta < -\theta^*$ | $-\theta^*$ | $-\theta^* < \theta \le 0^0$ | $0^0$ | $0^0 \le \theta < \theta^*$ | $\theta^*$ | $\theta^* < \theta \le 90^o$ |
|---|---|---|---|---|---|---|---|
| $\Delta_1$ | − | | | 0 | + | | |
| $\Delta_2$ | + | | | | | 0 | − |
| $\Delta_3$ | − | 0 | + | | | | |

where $\Delta_1, \Delta_2, \Delta_3$ and $\pm\theta^*$ are defined in Equations (3.5b), (3.9c), (3.9d) and (3.10).

The procedure of determining the control bounds, satisfying the gravity constraint and the friction constraint, are detailed here. The control bounds are determined in each of the regions:

**Region 1.** $-90^o \le \theta < -\theta^*$ $(\Delta_1 < 0, \Delta_2 > 0, \Delta_3 < 0)$

From inequalities (3.7b) and (3.12), the satisfaction of the gravity constraint and the friction constraint requires that

$$\tau \le min(\tau_{lift}, \tau_{slip-posterior}, \tau_{slip-anterior}) \tag{3.24}$$

Based on Inequality (3.14), minimum between $\tau_{slip-anterior}$ and $\tau_{lift}$ when $|\dot{\theta}| \ge \dot{\theta}_{cr}$, and the minimum between $\tau_{slip-posterior}$ and $\tau_{lift}$ when $|\dot{\theta}| \le \dot{\theta}_{cr}$ will now be found. Thus, one has:

$$\tau_{slip-anterior} - \tau_{lift} = \frac{Mmr}{\Delta_1 \Delta_3}\left[(m_f + m)g\cos\theta - mr\dot{\theta}^2\right] \le 0 \qquad |\dot{\theta}| \ge \dot{\theta}_{cr}(\theta)$$

$$\tau_{slip-posterior} - \tau_{lift} = \frac{Mmr}{\Delta_1 \Delta_2}\left[(m_f + m)g\cos\theta - mr\dot{\theta}^2\right] \le 0 \qquad |\dot{\theta}| \le \dot{\theta}_{cr}(\theta)$$

Thus,

$$\tau \le \tau_{slip-anterior} \qquad |\dot{\theta}| \ge \dot{\theta}_{cr}(\theta) \tag{3.25a}$$

$$\tau \le \tau_{slip-posterior} \qquad |\dot{\theta}| \le \dot{\theta}_{cr}(\theta) \tag{3.25b}$$

**Region 2.** $-\theta^* < \theta < 0^0$, $(\Delta_1 < 0, \Delta_2 > 0, \Delta_3 > 0)$

From inequalities (3.7b) and (3.15) under the condition shown in Inequality (3.16), one has

$$\tau_{slip-anterior} \le \tau \le min(\tau_{lift}, \tau_{slip-posterior}) \tag{3.26}$$

Comparing $\tau_{lift}$ and $\tau_{slip-posterior}$, and considering Inequality (3.16), one has

$$\tau_{slip-posterior} - \tau_{lift} = \frac{Mmr}{\Delta_1 \Delta_2}\left[(m_f + m)g\cos\theta - mr\dot{\theta}^2\right] \le 0$$

Thus, the control torque should be:

$$\tau_{slip-anterior} \le \tau \le \tau_{slip-posterior} \qquad |\dot{\theta}| \le \dot{\theta}_{cr}(\theta) \tag{3.27}$$

**Region 3.** $0^0 < \theta < \theta^*$ $(\Delta_1 > 0, \Delta_2 > 0, \Delta_3 > 0)$

Considering the conditions for both the gravity constraint and the friction constraint shown in inequalities (3.7a), (3.15) and (3.16), one has

$$max(\tau_{lift}, \tau_{slip-anterior}) \le \tau \le \tau_{slip-posterior} \tag{3.28}$$

Comparing $\tau_{lift}$ and $\tau_{slip-anterior}$, and considering Inequality (3.16), one has

$$\tau_{slip-anterior} - \tau_{lift} = \frac{Mmr}{\Delta_1 \Delta_3}\left[(m_f + m)g\cos\theta - mr\dot{\theta}^2\right] \ge 0 \tag{3.29}$$

Thus, the control torque should be:

$$\tau_{slip-anterior} \le \tau \le \tau_{slip-posterior} \qquad |\dot{\theta}| \le \dot{\theta}_{cr}(\theta) \tag{3.30}$$

**Region 4.** $\theta^* < \theta \le 90^o \quad (\Delta_1 > 0, \Delta_2 < 0, \Delta_3 > 0)$

From inequalities (3.7a) and (3.17), one has

$$\tau \ge max(\tau_{lift}, \tau_{slip-posterior}, \tau_{slip-anterior}) \tag{3.31}$$

Since $\tau_{slip-posterior} > \tau_{slip-anterior}$ as $|\dot{\theta}| \ge \dot{\theta}_{cr}$ based on Inequality (3.13), the maximum between $\tau_{slip-posterior}$ and $\tau_{lift}$ should be found. Similarly, since when $|\dot{\theta}| \le \dot{\theta}_{cr}$ $\tau_{slip-anterior} > \tau_{slip-posterior}$, the maximum between $\tau_{slip-anterior}$ and $\tau_{lift}$ is needed. Thus, the following relations hold:

$$\tau_{slip-posterior} - \tau_{lift} = \frac{Mmr}{\Delta_1 \Delta_2}\left[(m_f + m)g\cos\theta - mr\dot{\theta}^2\right] \ge 0 \qquad |\dot{\theta}| \ge \dot{\theta}_{cr}(\theta)$$

$$\tau_{slip-anterior} - \tau_{lift} = \frac{Mmr}{\Delta_1 \Delta_3}\left[(m_f + m)g\cos\theta - mr\dot{\theta}^2\right] \ge 0 \qquad |\dot{\theta}| \le \dot{\theta}_{cr}(\theta)$$

The overall bounds for the control torque in the region of $\theta^* < \theta \le 90^o$ is

$$\tau \ge \tau_{slip-posterior} \qquad |\dot{\theta}| \ge \dot{\theta}_{cr}(\theta) \tag{3.32a}$$

$$\tau \ge \tau_{slip-anterior} \qquad |\dot{\theta}| \le \dot{\theta}_{cr}(\theta) \tag{3.32b}$$

There exist three particular positions $\theta = \pm|\theta^*|$ and $\theta = 0$, at which some special conditions should be considered.

1. $\theta = -\theta^* \ (\Delta_1 < 0, \Delta_2 > 0, \Delta_3 = 0)$

From Inequalities (3.7b), (3.10b) and (3.11b), the following conditions must be satisfied to maintain the gravity and friction constraints:

$$\tau \le \tau_{slip-posterior} \qquad \text{and} \qquad |\dot{\theta}| \le \dot{\theta}_{cr}(-\theta^*) \tag{3.33}$$

2. $\theta = 0^0$ $(\Delta_1 = 0, \Delta_2 > 0, \Delta_3 > 0)$

Based on the results shown in Inequality (3.6), (3.15) and (3.16), the gravity constraint and the friction constraint will both be satisfied under the following conditions:

$$\tau_{slip-anterior} \le \tau \le \tau_{slip-posterior} \quad \text{and} \quad |\dot{\theta}| \le \dot{\theta}_{cr}(0) \tag{3.34}$$

3. $\theta = \theta^*$ $(\Delta_1 > 0, \Delta_2 = 0, \Delta_3 > 0)$

From Inequalities (3.7a), (3.10a) and (3.11a), the following conditions must be satisfied to maintain the gravity and friction constraints:

$$\tau \ge \tau_{slip-anteriort} \quad \text{and} \quad |\dot{\theta}| \le \dot{\theta}_{cr}(\theta^*) \tag{3.35}$$

Overall, the control bounds are summarized in Table 3.2.

Table 3.2 Control bounds satisfying the gravity and the friction constraints

<table>
<tr><td></td><td>$-90^o \le \theta < -\theta^*$</td><td>$\theta = -\theta^*$</td><td>$-\theta^* < \theta < \theta^*$</td><td>$\theta = \theta^*$</td><td>$\theta^* < \theta \le 90^o$</td></tr>
<tr><td>$|\dot{\theta}| \le \dot{\theta}_{cr}$</td><td colspan="2">$\tau \le \tau_{slip-posterior}$<br>High $\tau$ causes posterior slipping</td><td>$\tau_{slip-anterior} \le \tau \le \tau_{slip-posteric}$<br>High $\tau$ causes posterior slipping<br>Low $\tau$ causes anterior slipping</td><td colspan="2">$\tau \ge \tau_{slip-anterior}$<br>Low $\tau$ causes anterior slipping</td></tr>
<tr><td>$|\dot{\theta}| > \dot{\theta}_{cr}$</td><td>$\tau \le \tau_{slip-anterior}$<br>High $\tau$ causes anterior slipping</td><td colspan="3">Regardless of the control torque, the friction constraint is violated.</td><td>$\tau \ge \tau_{slip-posterior}$<br>Low $\tau$ causes posterior slipping</td></tr>
</table>

Table 3.2 shows that in all the regions, the bounds of the control torque are determined by the friction constraint only. This indicates that the friction constraint is more dominant as compared with the gravity constraint. Thus the gravity constraint is not needed to be

considered since it is always satisfied if the friction constraint is satisfied. Table 3.2 also shows that keeping angular velocity below the critical value is very important when biped is around upright position (within two critical angles). To the best of this author's knowledge, it is shown here for the first time that the angular velocity plays a important role in balancing control. If this condition is violated, regardless of the control torque, the friction constraint is violated, slipping will occur.

### 3.5.2 Effects of all constraints

In this section, the bounds of the control torque satisfying all three constraints will be determined and their effects on bipedal standing will be investigated. For simplicity, the angle of the biped is restricted to $-\theta^* < \theta < \theta^*$. The gravity constraint and the tip-over constraint are not in effect since the former is always satisfied when the friction constraint is satisfied and the latter is equivalent to the COP constraint. The control bounds and the conditions satisfying the friction and COP constraint are considered simultaneously, and the results are:

$$max(\tau_{slip-anterior}, \tau_{cop-toe}) \le \tau \le min(\tau_{slip-posterior}, \tau_{cop-heel}) \tag{3.36a}$$

and $$\left|\dot{\theta}\right| \le \min(\dot{\theta}_{cr1}, \dot{\theta}_{cr2}) \tag{3.36b}$$

Where $\tau_{slip-anterior}$, $\tau_{slip-posterior}$, $\tau_{cop-heel}$ and $\tau_{cop-toe}$ are defined in Equations (3.11d), (3.11e), (3.22b) and (3.22c). $\dot{\theta}_{cr1}$ and $\dot{\theta}_{cr2}$ are defined in Equations (3.11c) and (3.23b). First comparing $\dot{\theta}_{cr1}$ and $\dot{\theta}_{cr2}$ as detailed in the APPENDIX A, it is found that in most of the region within $\pm\theta^*$, the minimum critical angular velocity is determined by the friction constraint. However, there is a small range between $-\left|\tilde{\theta}\right|$, shown in Equation

(A5), and the upright position, the minimum angular velocity is determined by the COP constraint.

Inequality (3.36) is valid under the condition that the upper bound of the control torque is higher than the lower bound. Due to the complexity of the mathematical forms of the torques, the numerical results are explored and a parametric analysis is conducted to obtain an overall understanding of the effects of the constraint on balancing of bipedal standing. Three sets of parameters, namely the friction coefficient, $\mu$ (which has significant influence on the friction force between the foot-link and the ground); length of the foot-link, $L_f$ (which can provide important information for choosing proper feet length during bipedal robots design); and the location of the mass center, $r$ (which indicates the mass distribution of designed bipedal robots), were analyzed systematically. There are two objectives. One is to identify the regions in the phase plane with valid and invalid control bounds, named controllable regions and uncontrollable regions, respectively. In the controllable regions, it is possible to design a balancing control, while in the uncontrollable regions, regardless of the control torque, constraints will be violated, and balancing is impossible. Another objective is to determine the range of the control torque. A large range of control torque is desirable for balancing control design. This parametric analysis will help us to gain a comprehensive understanding of the effects of the constraints on biped standing. The parameters from previous literature (Pai *et al.* 1997) are used as basic parameters here and are listed in Table 3.3.

Table 3.3 Physical parameters

| | |
|---|---|
| Body height | H = 1.78 m |
| Body mass | mass = 80 kg |
| Foot-link mass | $m_f$ = 2*0.0145*mass = 2.32 kg |
| Pendulum mass | m = mass - $m_f$ = 77.68 kg |
| Length of ankle-to-center of mass | r = 0.575*H = 1.02 m |
| Horizontal ankle-to-heel distance | a = 0.19*$L_f$ = 0.05 m |
| Vertical ankle height | b = 0.039*H = 0.07 m |
| Foot-link length | $L_f$ = 0.152*H = 0.27 m |
| Pendulum length | L = H – b = 1.71 m |
| Coefficient of friction | $\mu$ = 0.5 |
| Gravity acceleration | g = 9.80 m/s$^2$ |
| Horizontal ankle-to-center of foot | c = 0.5*$L_f$ – a = 0.085 m |

A computer program is developed to determine the minimum between $\tau_{slip-posterior}$ and $\tau_{cop-heel}$, and the maximum between $\tau_{slip-anterior}$ and $\tau_{cop-toe}$ as shown in Inequality (3.36). Next $min(\tau_{slip-posterior}, \tau_{cop-heel})$ and $max(\tau_{slip-anterior}, \tau_{cop-toe})$ are compared to assure the validity of the control bounds.

Two sets of Figures are presented. In Figures 3.2, 3.4 and 3.6, the regions with valid control bounds are shown as regions 1-3 in white color, while the regions with invalid control bounds are shown in gray color. Regions 1-3 are defined by different control bounds, which are determined from different constraints as shown in Table 3.4. The horizontal axis is the angular displacement, and the vertical axis is the angular velocity of the biped. Curves are separators of regions that satisfy and violate a constraint. For example, in Figures 3.2, 3.4 and 3.6, curves a, b are separators of regions that satisfy COP constraint and friction constraint, respectively. The regions below these curves are good

regions. Figures 3.3, 3.5 and 3.7 show the ranges of the control torque determined by the upper(grid surfaces) and lower control bounds. The smooth gray surfaces are the lower bounds and the grid surfaces are the upper bounds (smooth surfaces), where x-axis is the angular displacement, y-axis is the angular velocity of the biped, and z-axis is the control torque.

Validity of the bounds, *i.e.*, the upper control bound is higher than the lower control bound indicates the satisfaction of the constraints, and the possibility of designing a control law to satisfy the constraints.

Table 3.4 Summary of the control bounds satisfying all three constraints

| State space region | Control bounds |
|---|---|
| Region1 | $\tau_{cop-toe} < \tau < \tau_{slip-posterior}$ |
| Region2 | $\tau_{cop-toe} < \tau < \tau_{cop-heel}$ |
| Region3 | $\tau_{slip-anterior} < \tau < \tau_{cop-heel}$ |

### 3.5.2a Effects of friction coefficient

This section examines how friction coefficients affect the controllable regions, the control bounds imposed on the control torque and the critical angular velocity. Friction coefficient affects the friction force and the friction constraint. Investigating the effects of friction coefficient on controllable regions, control bounds and critical angular velocity will help us prevent biped slipping on the ground. The friction coefficient, $\mu$, varies from 0.15 to 1, and all other parameters are shown in Table 3.3. Since the results are

consistent, for the sake of brevity, the results for the friction coefficients of 0.15, 0.5 and 1 are presented.

Figure 3.2 shows the controllable regions (in white) and non-controllable regions (in gray) in the phase plane. The horizontal axis is the angular displacement within the critical angles $\pm\theta^*$, which depend on the friction coefficient. As shown in Equation (3.11c), the critical angular velocity is independent of the friction coefficient. Thus, changes in the friction coefficient have no effects on the critical angular velocity. It was first found that as the friction coefficient is greater than 0.15, regardless of the changes in the friction coefficient, the constraints, determining each region as shown in Table 3.4, remain the same. Region 2 is determined by the COP constraints, while regions 1 and 3 are determined by both friction and COP constraints as shown in Table 3.4. Figure 3.2a shows that with a low friction coefficient, friction constraint is dominant since a large portion of the controllable region is determined by the friction constraint (regions 1 and 3). From Figure 3.2b and 3.2c, it can be seen that as the friction coefficient increases, the controllable regions, especially region 2, enlarge significantly, while the uncontrollable regions I and II reduce significantly. A large region 2 indicates that with modest and high friction coefficient, the COP constraint becomes dominant, *i.e.*, tipping over is the main concern. Note that the region around the upright position, such as region 2, is of special interests for the following two reasons: (1) with small disturbance during standing, bipeds, *e.g.* humans, respond as an inverted pendulum by keeping knees and the hip straight (Kuo 1995), and (2) the biped will ultimately reside in such a region. Thus in the following sections, results related to the states in a region around the upright position will be presented and discussed in detail.

The bounds of the control torque as the friction coefficient varies from 0.15 to 1 are shown in Figure 3.3. The control bounds for region 2 are determined by the COP constraint, as shown in Table 3.4, which are independent of the friction coefficient. Thus, changes in the friction coefficient have no effects on the control bounds in region 2. Figure 3.3 shows that the control bound determined by the COP constraint, are not sensitive to the angle and angular velocity at the ankle joint, and the range is large, which makes the control design feasible. However, the control bounds determined by the friction constraint (*e.g.* region 1 and 3) are sensitive to the changes in the angle and angular velocity, and the range of the control torque decreases significantly, which makes the design of balancing control difficult.

Overall, it was found that in most part of the controllable region, the critical angular velocity is determined by the friction constraint, and keeping the angular velocity below the critical value is important. Otherwise, regardless of the control torque, the friction constraints will be violated and balance control is out of the question. Although the friction constraint determines the critical angular velocity in most of the regions, the friction coefficient has no effects on the critical angular velocity as shown in Equation (3.11c). With a low friction coefficient, the controllable region is small and the control bounds are mainly determined by the friction constraint, indicating that the friction constraint is a main concern. As the friction coefficient increases, the controllable region enlarges significantly, especially the region determined by the COP constraint (region 2). The range of the control torque in region 2 is independent from the friction coefficient, and is much higher as compared with the range associated with the friction constraint.

Thus, as the friction coefficient is modest or reasonably high, the friction coefficient has little effects on balance control of bipedal standing.

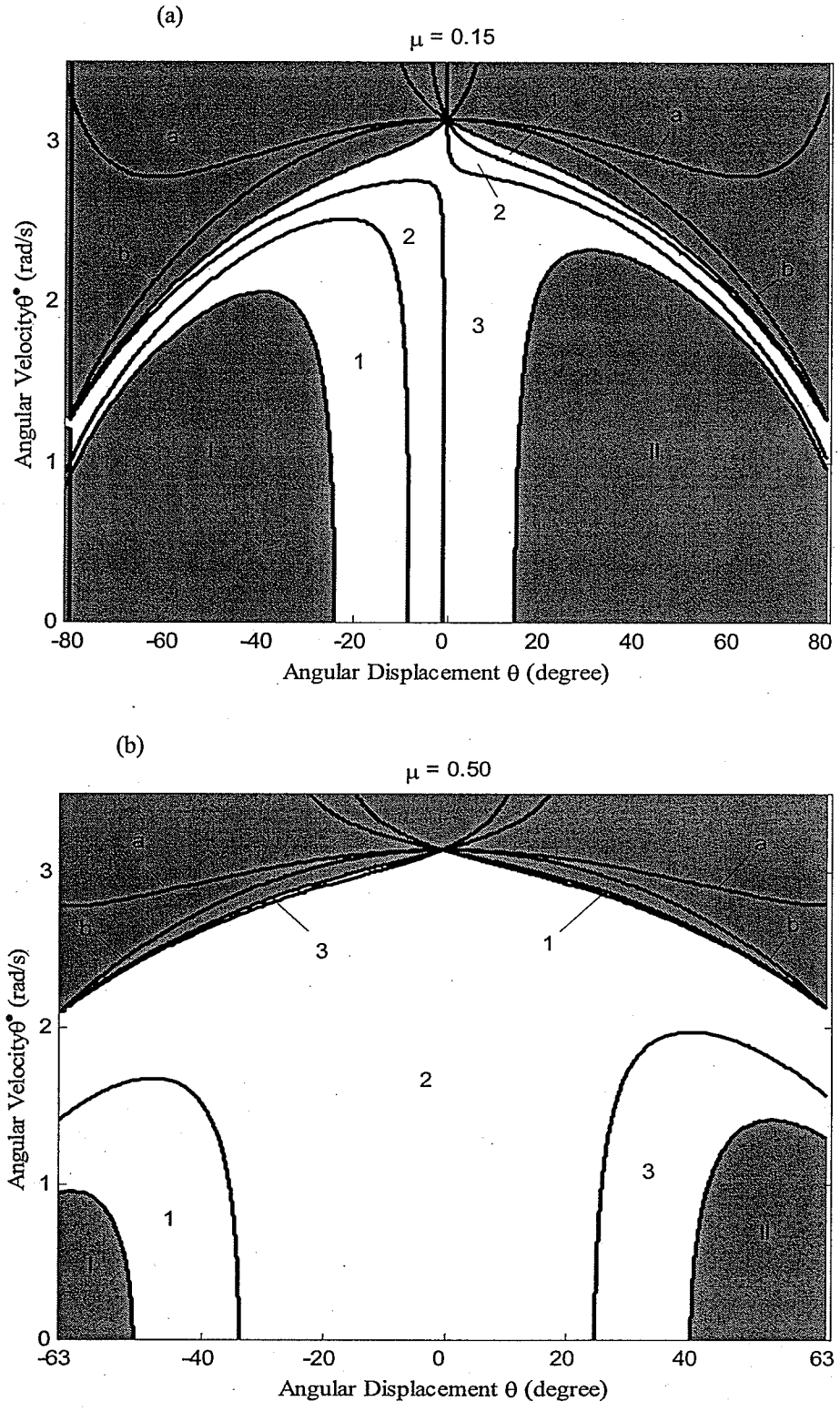

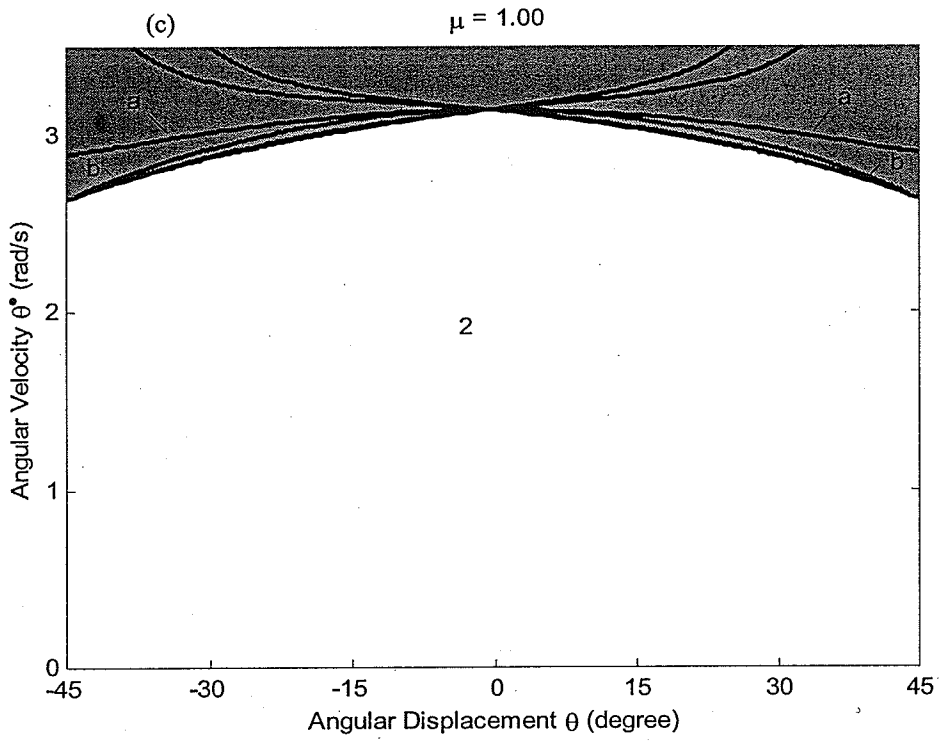


Figure 3.2 Effects of friction coefficient on controllable and uncontrollable regions

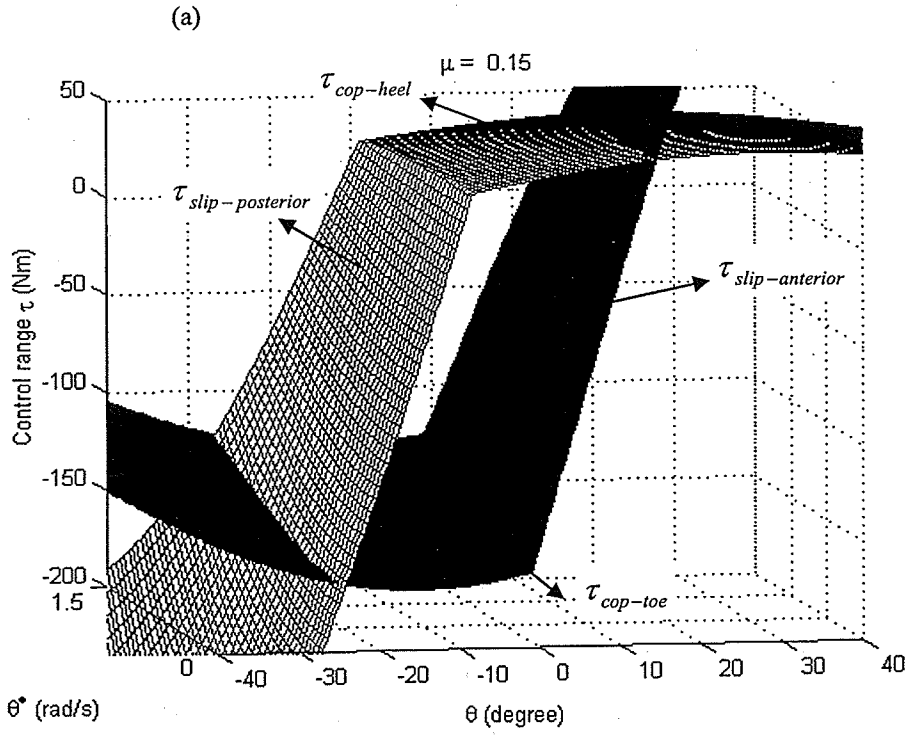

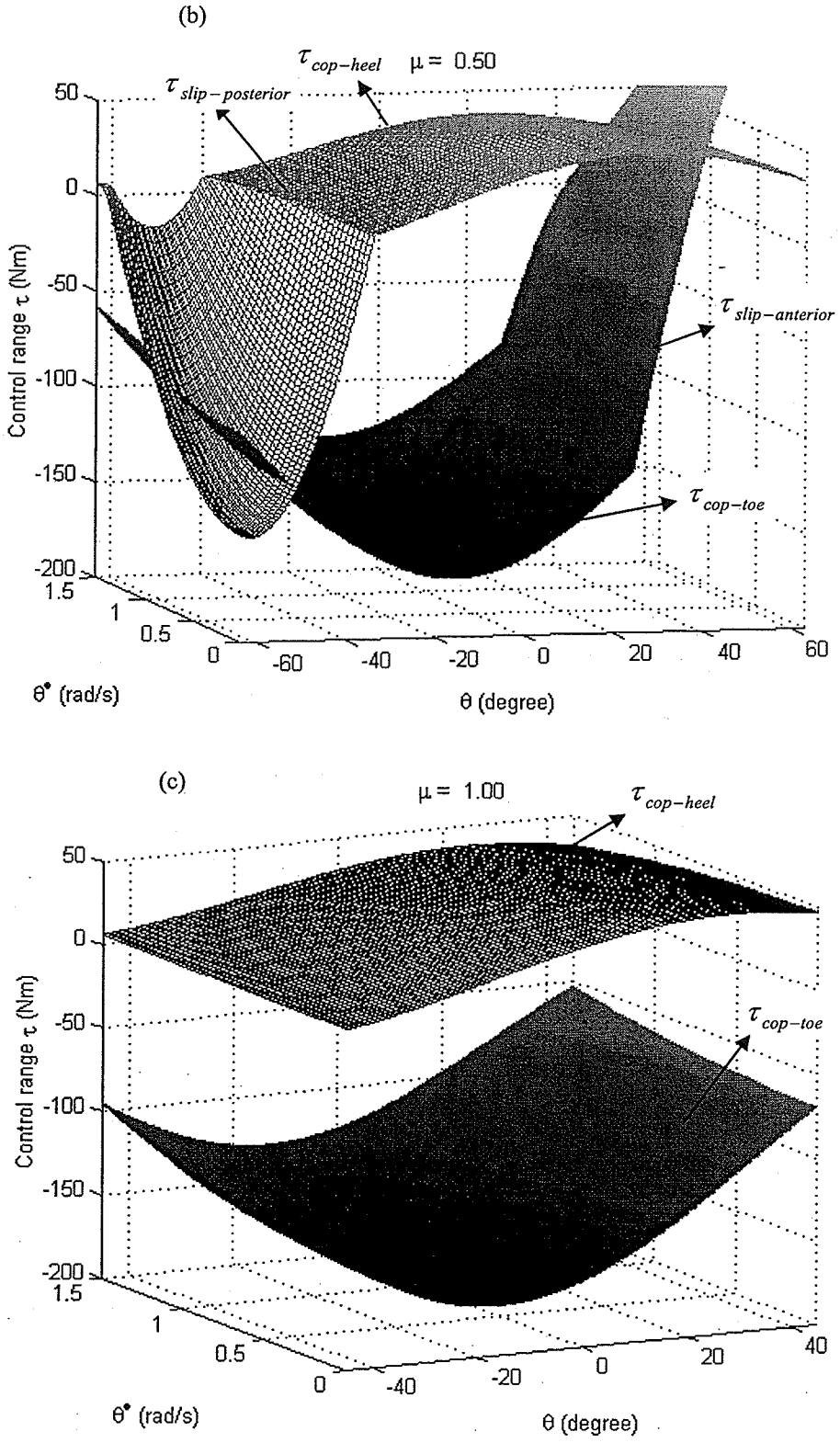


Figure 3.3 Effects of friction coefficient on range of control torques

### 3.5.2b Effects of the length of the foot-link

This section examines how the length of the foot-link affects the controllable regions, control bounds and critical angular velocity. As the length of the foot-link ($L_f$) varies with respect to height of the biped (H) from 0 to 0.380, all other parameters remain the same and are shown in Table 3.3, the controllable and non-controllable regions are shown in Figure 3.4, and the bounds of the control torque are shown in Figure 3.5.

Figure 3.4 shows that, as proven in the appendix, the critical angular velocity in most of the controllable regions is determined by the friction constraint, which is independent of the length of the foot-link. The constraints determining each controllable region as shown in Table 3.4 remain unchanged in spite of the changes in the length of the foot-link. The overall controllable regions enlarge marginally with the increase in the length of the foot-link. Note that region 2 decreases while regions 1 and 3 enlarge significantly with the increase in the length of the foot-link. Referring to Table 3.4, the control bounds of regions 1 and 3 are determined by the friction and COP constraints, respectively, indicating that as the length of the foot-link increases, the friction constraint plays a more important role in determining the control bounds. This is not surprising. For example in region 3, the lower control bound is determined by the maximum between the friction constraint ($\tau_{slip-anterior}$) and the COP constraint ($\tau_{cop-toe}$). As shown in Equation (3.22c), $\tau_{cop-toe}$, with negative values, decreases with the increase in the length of the foot-link ($L_f$). Thus, $\tau_{slip-anterior}$ becomes the maximum in a larger region 3.

Figure 3.5 shows that the positive upper control bound determined by the COP constraint increases marginally, but the negative lower bound by the COP constraint

decreases significantly with the increase in the length of the foot-link. Thus, the range of the control torque increases significantly in region 2, which makes the control design feasible. Since the control bounds determined by the friction constraint is independent of the length of the foot-link, the changes in the length of the foot-link has no effects on the friction-related control bounds. The control bounds from the friction constraint are sensitive to the angular displacement and angular velocity of the biped. Thus, as the biped deviates from the upright position, the range of the control torque decreases significantly making the control design challenging. Although Figure 3.4a shows a large controllable region as the length of the foot-link is zero, Figure 3.5a shows that the range of the control torque is zero, *i.e.*, the control torque is predetermined by the constraints, which, in general, can not stabilize the biped at the upright position since it is not meant for balance control.

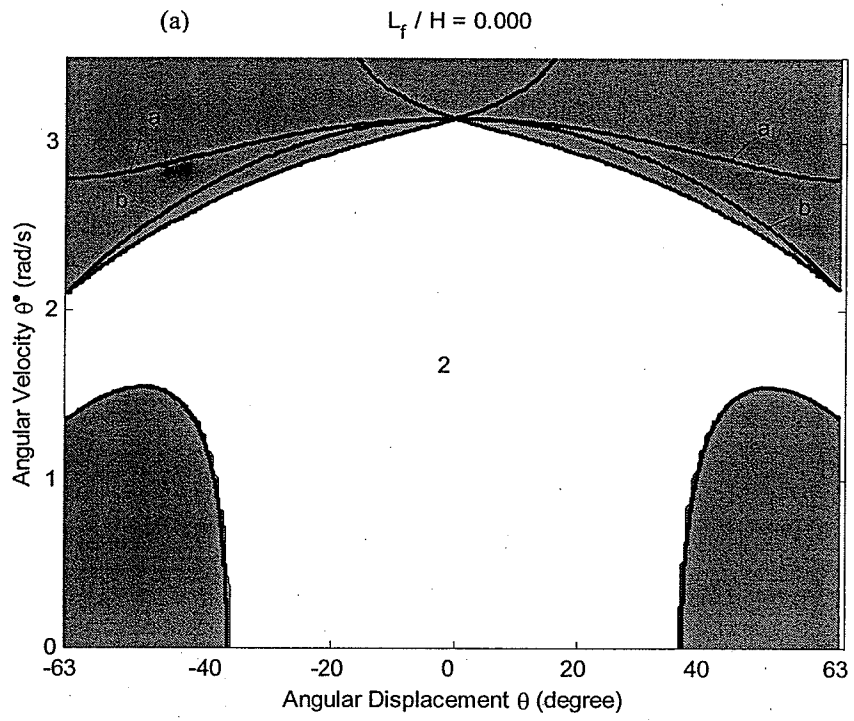
(a)
$L_f$ / H = 0.000
a
a
b
b
2
3
2
1
0
-63
-40
-20
0
20
40
63
Angular Velocity θ̇ (rad/s)
Angular Displacement θ (degree)

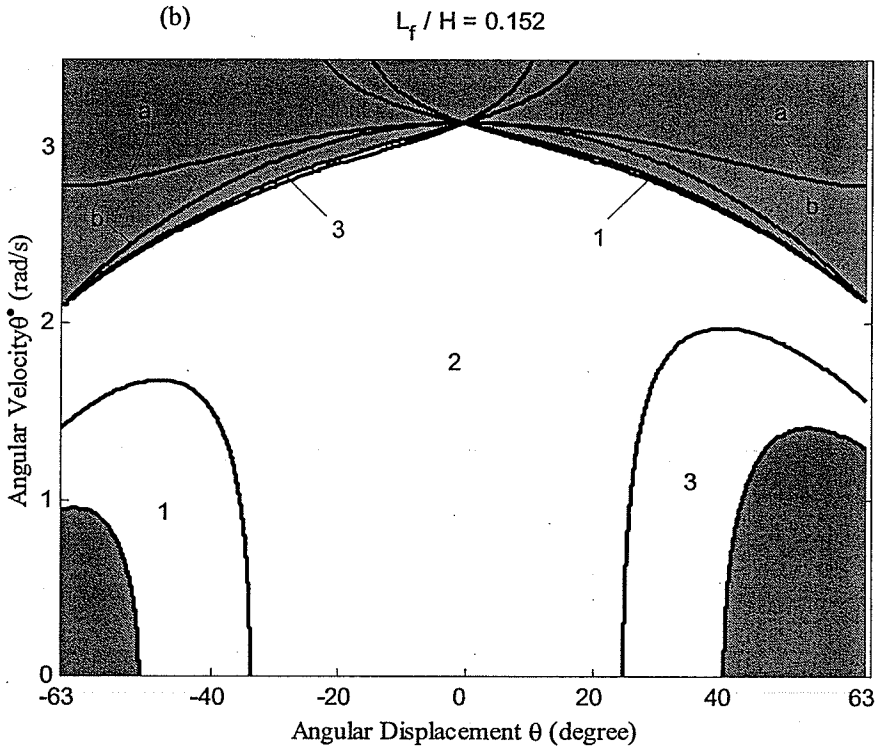
(b)
$L_f$ / H = 0.152
a
a
b
b
3
1
2
1
3
3
2
1
0
-63
-40
-20
0
20
40
63
Angular Velocity θ̇ (rad/s)
Angular Displacement θ (degree)

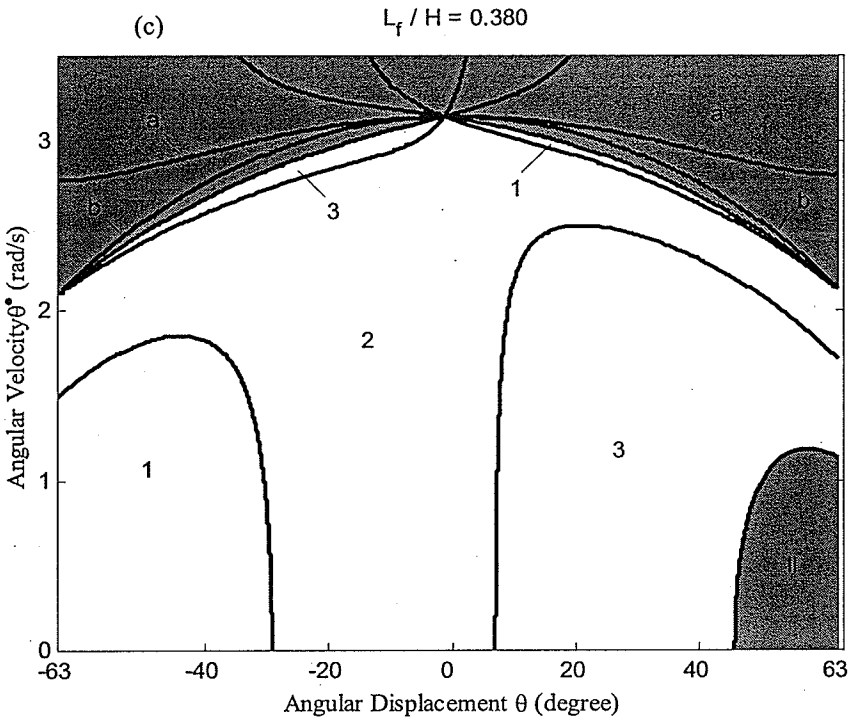


Figure 3.4 Effects of length of foot-link on controllable and uncontrollable regions

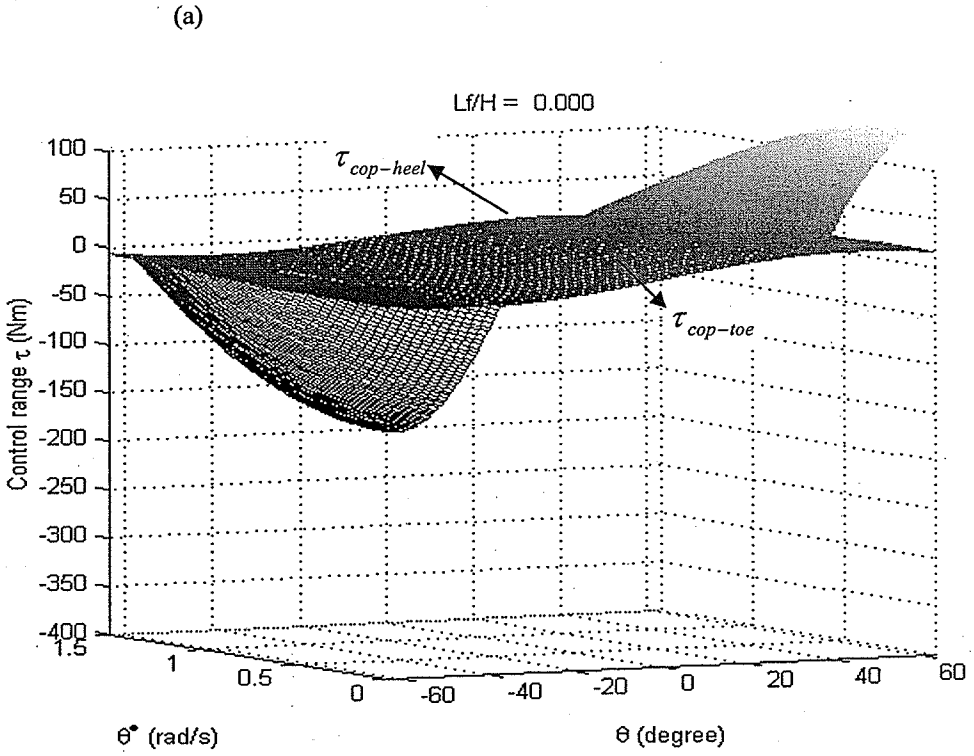

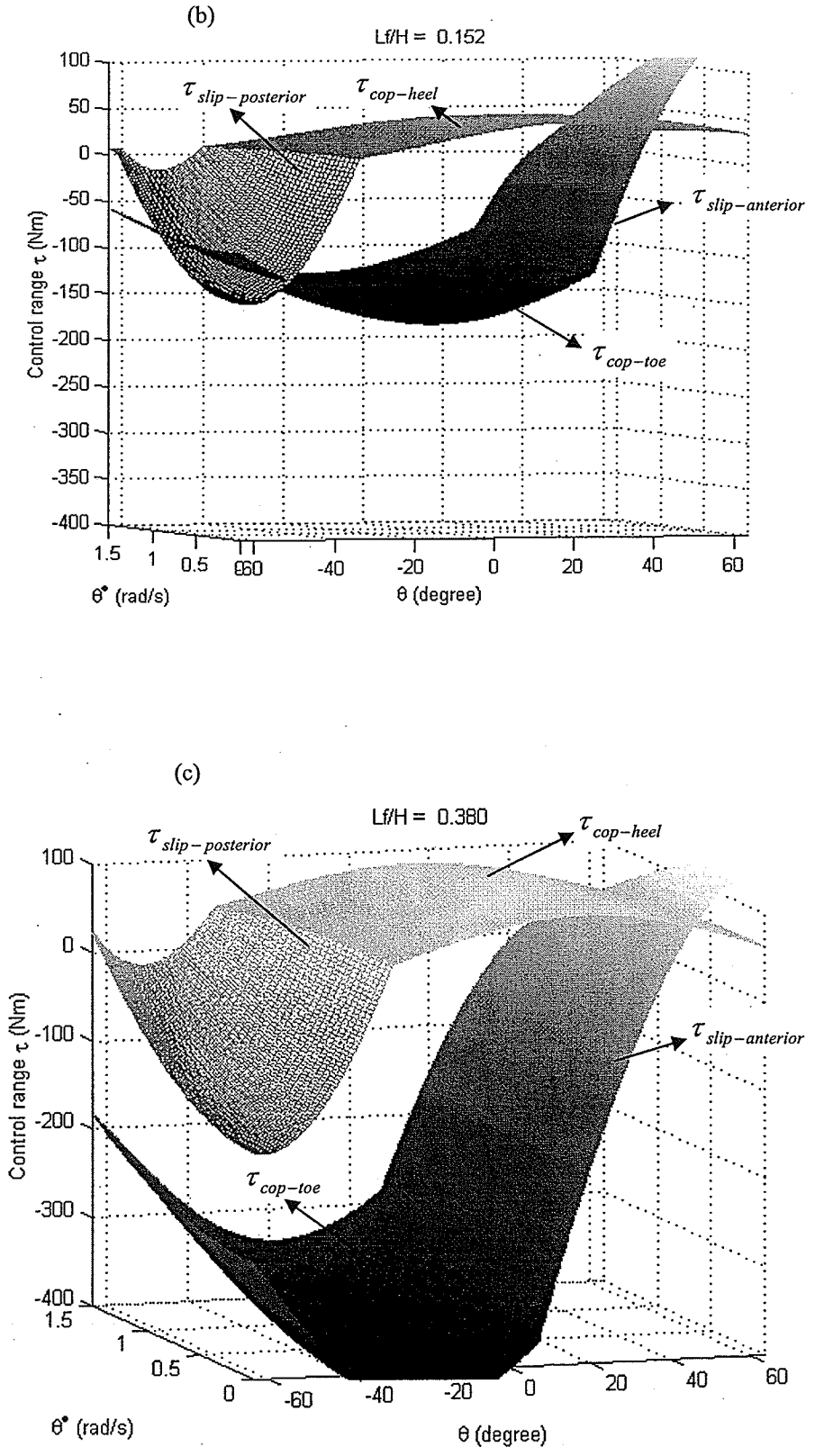


Figure 3.5 Effects of the length of the foot-link on range of control torques

### 3.5.2c Effects of the location of the mass center

This section examines the effects of the location of the mass center on the controllable regions, control bounds and critical angular velocity. As the location of the masse center $r$ varies with respect to the height of the biped (H) from 0 to 0.958, all other parameters remain the same as shown in Table 3.3. The controllable regions and the critical angular velocity are shown in Figure 3.6, and the bounds of the control torque are shown in Figure 3.7.

Figure 3.6a shows that as the mass center is close to the ankle, the critical angular velocity is high and the controllable regions are large. As the mass center moves up on the biped, the critical angular velocities decrease significantly, so do the controllable regions as shown in Figures 3.6b and 3.6c. However, comparing Figures 3.6b and 3.6c, it can be seen that the controllable regions decrease only marginally. Figure 3.7 shows that the ranges of the control torque in regions 1, 2 and 3 are not sensitive to the location of the mass center and, the constraints determining the control bounds as shown in Table 3.4 remain the same regardless of the location of the mass center. The results indicate that as r/H is above 0.5 and in a region around the up right position within $\pm 20^o$, the location of the mass center has little effects on the controllable region and the control bounds.

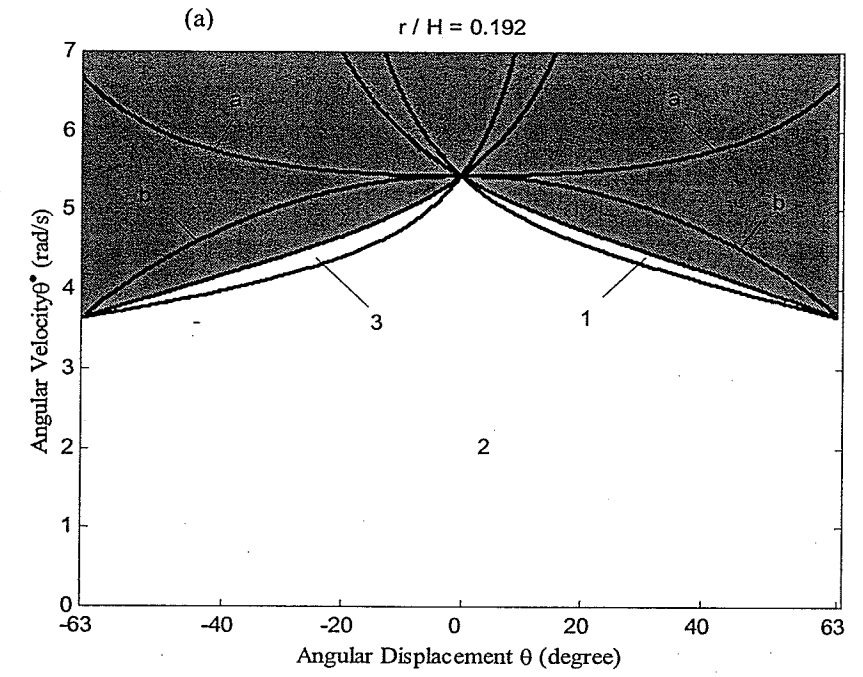
(a)
r / H = 0.192
Angular Velocityθ• (rad/s)
Angular Displacement θ (degree)
a
b
1
2
3

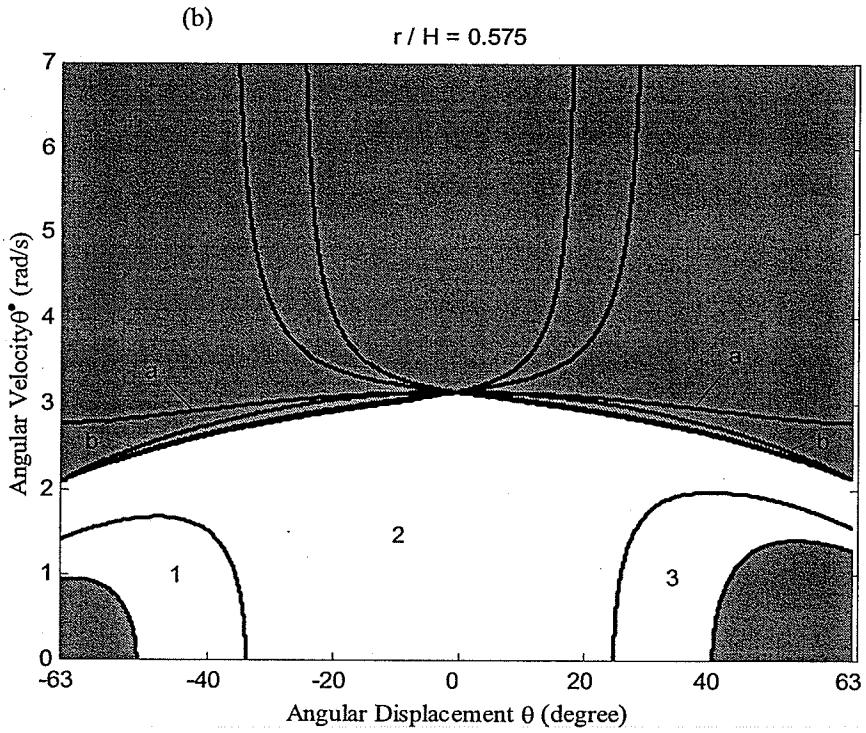
(b)
r / H = 0.575
Angular Velocityθ• (rad/s)
Angular Displacement θ (degree)
a
b
1
2
3

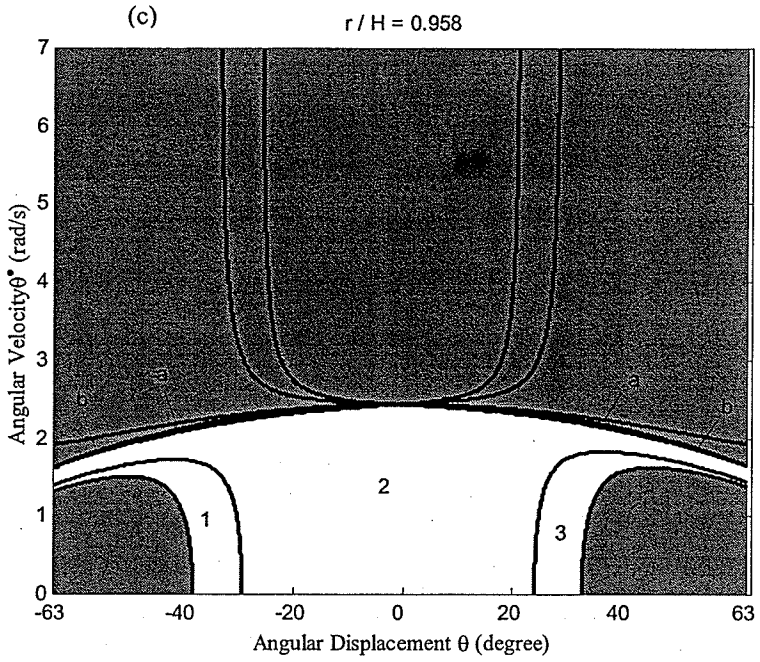


Figure 3.6 Effects of center of mass position on controllable and uncontrollable regions

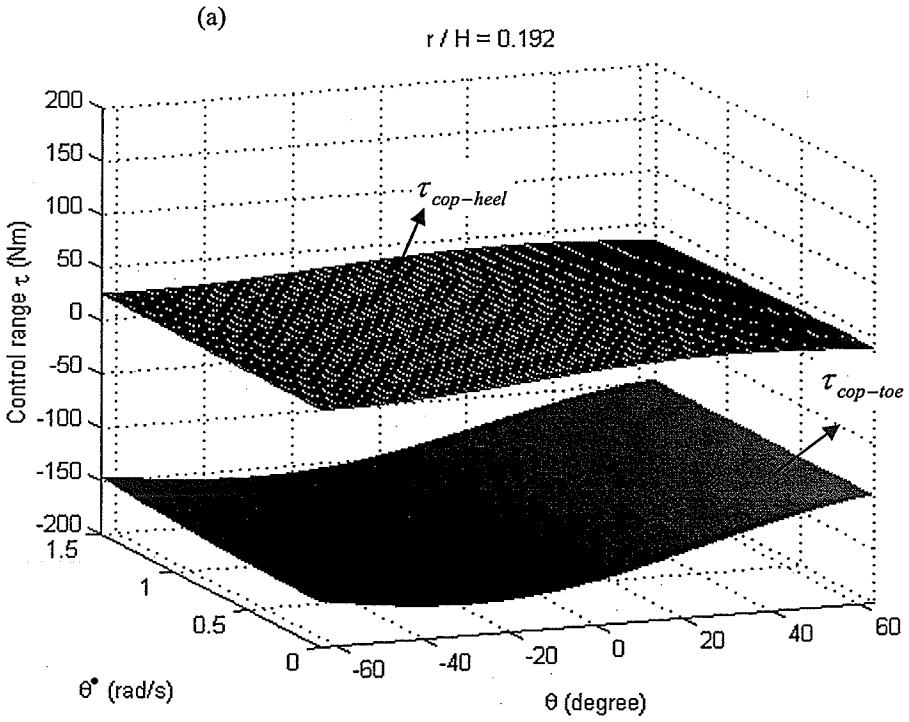

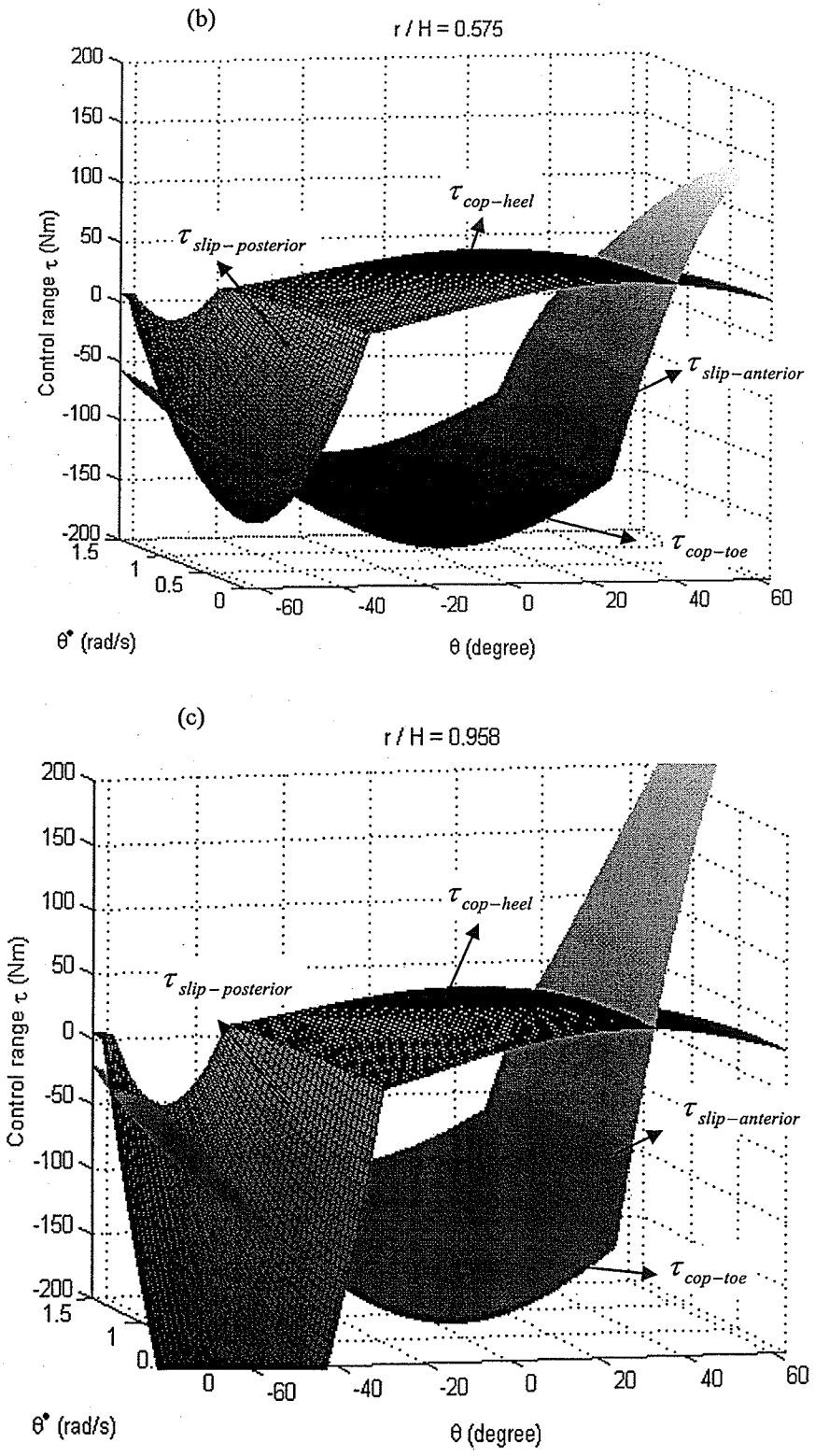


Figure 3.7 Effects of center of mass position on range of control torques

## 3.6 Discussions

During balance control of bipedal standing, all constraints between the foot-link and the ground must be maintained as demonstrated in the previous work (Pai and Patton 1997). The satisfaction of these constraints imposes bounds on the control torque, which is crucial for designing balance control laws. In addition, understanding the interactions among the constraints enable us to gain an understanding of the mechanics of bipedal balancing, which is important to the development of bipedal robots. Since the COP constraint and the tip-over constraint are equivalent as both feet are assumed to be on the level ground, in this work, the effects of the three constraints, namely the gravity constraint, friction constraint and COP constraint, on balance control of a planar biped during standing are investigated.

Analytical solutions to the bounds of the controlled ankle torque satisfying each individual constraint, and satisfying both the gravity and friction constraints simultaneously are determined. The control bounds satisfying all three constraints are also obtained using a numerical method. Such control bounds are presented versus the angle and the angular velocity. A large range of the control torque is desirable since it makes the control design feasible. Furthermore, the results of control bounds show explicitly the specific constraint causing such bounds, which, in turn, predicts the specific constraint to be violated and the corresponding potential movement of the foot-link. For example, in region 2 of Figures 3.2, 3.4 and 3.6, the control bounds are determined by the COP constraint, *i.e.* tip-over constraint. If the ankle torque is too high, above $\tau_{cop-heel}$, the COP will move behind the heel, *i.e.*, the foot-link will rotate about the heel. Otherwise the foot-

link will rotate about the toe. Either way the COP (tip-over) constraint is violated, but the foot-link will move in a very different way. Thus, the solutions to the control bounds are not only important for designing balance control laws, but also helpful for preparing protective measures for bipedal robots.

Regions in the phase plane satisfying all the constraints are determined. More importantly, regions within which the constraints cannot be satisfied are also identified. If the states of the biped fall in such regions, regardless of the control torque, the constraints will be violated and stabilization cannot be achieved. The effects of the friction coefficient, the length of the foot-link and location of the mass center of the pendulum on the above regions have also been investigated.

Through this work, it was found that the satisfaction of the constraints imposes not only the bounds to the control torque, but also conditions on the angular velocity of the biped. The critical angular velocity has also been determined analytically. It is further found that in a region around the upright position, if the angular velocity is above the critical value, regardless of the control torque, the constraints cannot be satisfied. This region is extremely important since the biped will reside in it ultimately. Thus, keeping the angular velocity below the critical value is crucial in balance control.

Comparing the gravity constraint and the friction constraint, the friction constraint is more important in that, once the friction constraint is satisfied, the gravity constraint is automatically satisfied. Comparing the friction constraint and the COP constraint in the region 2, the critical angular velocity for the biped under study is determined by the friction constraint in most of the region, indicating the importance of the friction

constraint. However, as the angular velocity is below the critical value and with a modest and high friction coefficient, the bounds of the control torque are determined only by the COP constraint. Since the COP constraint is equivalent to the tip-over constraint, the (COP) tip-over constraint is the most dominant among three constraints. This finding shows the importance of the foot design in satisfying the COP constraint, and consequently all three constraints in balance control of bipedal standing.

The work, presented in this chapter, is a comprehensive investigation of the effects of all constraints between the foot-link and the ground on the balancing of biped standing while the friction coefficient, the length of the foot-link and the location of the mass center are varied. Two sets of results have been presented, controllable / uncontrollable regions and ranges of the control torque.

Overall, it was found that in most of the controllable region, the critical angular velocity is determined by the friction constraint, and keeping the angular velocity below the critical value is important. Otherwise, regardless of the control torque, the friction constraints will be violated and balance control is out of the question. Although the friction constraint determines the critical angular velocity in most of the regions, the friction coefficient has no effects on the critical angular velocity as shown in Equation (A10). With a low value of friction coefficient, the controllable region is very small and the control bounds are mainly determined by the friction constraint, indicating that the friction constraint is a main concern. As the friction coefficient increases, the controllable region enlarges significantly, especially the region determined by the COP constraint (region 2). The range of the control torque in region 2 is independent from the friction

coefficient, and is much higher as compared with the range associated with the friction constraint. Thus, as long as the friction coefficient is modest or reasonably high, the friction coefficient has little effects on balance control of bipedal standing. The overall controllable regions enlarge marginally with the increase in the length of the foot-link. As the length of the foot-link increases, the friction constraint plays a more important role in determining the control bounds. As the mass center is close to the ankle, the critical angular velocity is high and the controllable regions are large. The location of the mass center has little effects on the controllable region and the control bounds as long as r/H is above 0.5.

This work is a comprehensive investigation of the effects of constraints on balancing of bipedal standing and is believed important to the development of bipedal walking robots. The work has significant impact on balance control of bipedal standing, since satisfaction of constraints between the foot-link and the ground is imperative in control design. Furthermore, these results also reveal interesting physical insights into the effects of constraints on bipedal standing, the interactions among the constraints and between the biped and the environment. Such insights allow us to understand the mechanics of bipedal balancing, which has positive impact on developing better bipedal robots. In next chapter, the importance of considering constraints during control law design will be demonstrated. A stability region will be determined based on the concept of Lyapunov exponent from a mathematical model and will be compared with previous work.

# Chapter 4

# Stability Analysis of Bipedal Standing Using the Concept of Lyapunov Exponents Based on a Mathematical Model

## 4.1 Introduction

The balance control of disturbed bipedal standing is important for preventing falls of humans and bipedal robots. Stabilization of bipedal models has attracted much attention in the past two decades. Various control strategies such as adaptive control (Chew and Pratt 2001), sliding mode control (Mu and Wu 2004), neural network (Kuperstein and Wang 1990, Narendra and Parthasarathy 1990, and Bersini and Gorrini 1997), and fuzzy control (Zhi and Chunwen 2003) have been developed. In much of the previous work, bipedal foot-link were assumed to be fixed on the ground once they contacted the ground, *i.e.*, the constraints between the foot-link and the ground were assumed to be satisfied automatically, and the controllers were designed only for motion regulation. There exist several constraints between the foot-link and the ground. In Chapter 3, the effects of constraints on balance control of a simplified two-dimensional biped during standing were investigated, and the bounds imposed on the control torque due to the constraints

were determined. Such control bounds have significant effects on designing balance control laws. Furthermore, it is found that the angular velocity of the biped plays a crucial role in satisfying the constraints, *i.e.*, the angular velocity must be kept below the critical value. Thus, a balance control law of bipedal standing should be designed for motion regulation while satisfying the control bounds and meeting the requirement of the angular velocity. Such a design task is extremely challenging.

Another challenge for balancing bipedal standing is the lack of a single quantitative criterion and an effective tool for stability analysis. Wu *et al.* (1998a, 1998b) developed mathematical models to study the control mechanisms of human trunk movement during walking. The control laws were designed based on Lyapunov's stability theory. The limitation of the Lyapunov's stability control is due to the difficulties in deriving a Lyapunov function, which, in turn, restricts the control design. Pai and Patton (1997) investigated balance control of human standing with the consideration of the constraints between the foot-link and the ground. They determined the feasible stability boundaries using the computer simulations of movement termination with the aid of an optimization routine. The limitation, from a viewpoint of stability, comes from their definition of the stability, *i.e.*, the center of mass of the biped can be moved into a region between the heel and the toe within a short time period (1s) and with a zero angular velocity. However, the bipeds satisfying their criteria may still fall away from the upright position. Thus, the long-term behaviours of dynamical systems should be considered.

Lyapunov's stability analysis of a biped during standing is a challenging task. Due to the lack of constructive methods for deriving Lyapunov functions, Lyapunov's second

method is difficult to use in highly nonlinear systems. Sekhavat *et al.* (2004) employed the concept of Lyapunov exponents to analyze the stability of nonlinear dynamical systems and showed that the method is constructive and powerful.

The goal of the work is to investigate the balance control and to analyze the stability of a biped during disturbed standing while satisfying the constraints between the foot-link and the ground. The biped model is simplified as an inverted pendulum with one rigid foot-link on the level ground. It has been reported that standing human subjects, when perturbed by small disturbance, typically respond by moving in a segittal plane (which is the vertical anterior to posterior plane), and they tend to keep the knees, hips, and neck straight, moving about the ankle (Kuo 1995). Thus, it is reasonable to simplify a biped as a simple inverted pendulum moving in the sagittal plane. The foot-link is in contact with the ground, but is not fixed. Three constraints are considered, *i.e.*, no lifting, no slippage, and the center of pressure (COP) remaining within the contact region between the foot-link and the ground. A PD-based state switching feedback control law is designed to stabilize the biped to the upright position while satisfying all constraints. The stability of the constrained control system is analyzed using the concept of Lyapunov exponents and a stability region is determined. Techniques developed by Wolf *et al.* (1985) for smooth systems, and extended by Müller (1995) to non-smooth systems, together with non-standard finite difference scheme developed by Mickens (1994), are combined to improve the numerical stability and the computational efficiency. In this chapter, the systematic mathematical derivations will not be included, but will summarize the major dynamic equations and mathematical form of the constraints. Please refer to Sections 3.2 and 3.3 in Chapter 3 for detailed derivations and explanations.

The dynamic equations for the bipedal system are:

$$\tau = mgr\sin\theta - (I + mr^2)\ddot{\theta} \tag{3.3a}$$

$$F_{gx} = mr\ddot{\theta}\cos\theta - mr\dot{\theta}^2\sin\theta \tag{3.3b}$$

$$F_{gy} = (m_f + m)g - mr\ddot{\theta}\sin\theta - mr\dot{\theta}^2\cos\theta \tag{3.3c}$$

The three constraints are written as (Pai and Patton 1997):

$$F_{gy} \geq 0 \tag{3.4a}$$

$$\left|F_{gx}\right| \leq \mu F_{gy} \tag{3.4b}$$

$$0 \leq x_{cop} \leq L_f \tag{3.4c}$$

From Equation (3.2c), the pressure center ($x_{cop}$) is

$$x_{cop} = L_f - a - \frac{bF_{gx} - \tau + cm_f g}{F_{gy}} \tag{3.4d}$$

## 4.2 Controller Design

A PD-based switching state feedback control law is designed to stabilize the biped at the upright posture while keeping the foot-link stationary. The controller considers each constraint, shown in Equation (3.2), and determines the maximum and minimum feasible torque necessary to satisfy the constraints between the foot-link and the ground. The controller is a simple PD control as the control torque is within the control bounds, and it takes the value of the control bounds as it approaches the bounds. The controller is shown as:

$$\tau = \begin{cases} \tau_{PD} & if \ \ \tau_{lower} \leq \tau_{PD} \leq \tau_{upper} \\ \tau_{upper} & if \ \ \tau_{PD} \geq \tau_{upper} \\ \tau_{lower} & if \ \ \tau_{PD} \leq \tau_{lower} \end{cases} \tag{4.1}$$

where $\tau_{PD} = k_p\theta + k_d\dot{\theta}$, the upper bound $\tau_{upper}$ and the lower bound $\tau_{lower}$ depend on the state space, *i.e.*, $\theta$ and $\dot{\theta}$, which have been determined in Section 3.5. The block diagram of the controller is shown in Figure 4.1.

Note that the control law is designed to satisfy only the control bounds. The condition imposed on the angular velocity is not considered in the control design, but it is used as a criterion to terminate the controller and the simulations if it is violated.

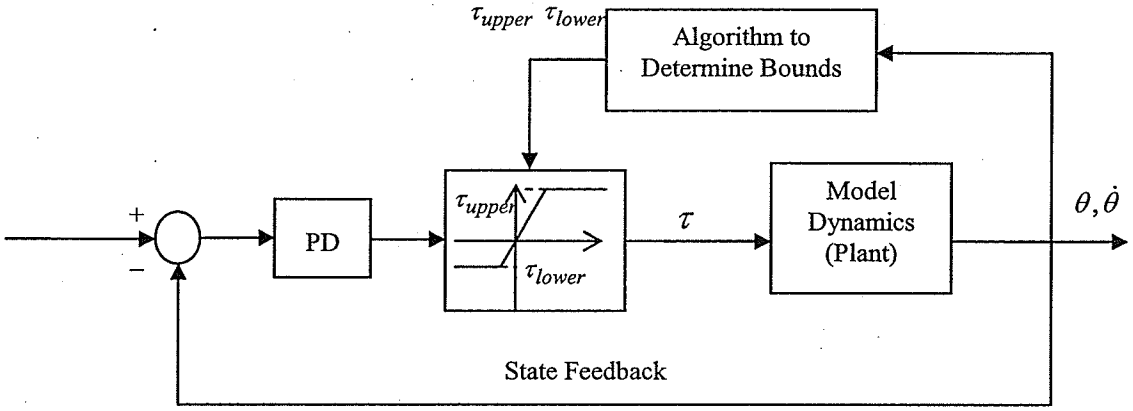


Figure 4.1. Block diagram of the control system subjected to $|\dot{\theta}| < \dot{\theta}_{critical}$.

## 4.3 Stability Analysis

Stability analysis investigates the long-term behavior of motion under the influence of a disturbance in the initial states. For stable motion, the effects of the disturbance are insignificant, *i.e.*, the disturbed motion stays close to the undisturbed one. In the unstable case, an infinitesimal disturbance causes a considerable change in the motion (Most *et al.* 2004). In this work, stability is defined based on Lyapunov's stability theory, and is analyzed using the concept of Lyapunov exponents. If the largest Lyapunov exponent converges to a constant negative value, the dynamical system is exponentially stable about the equilibrium point, which is the upright posture. Since it is almost impossible to

get the theoretical expression of Lyapunov exponents for our highly nonlinear bipedal system, the numerical method based on Wolf's work (Wolf *et al.* 1985) is developed.

The state space model of the system is derived by defining the state vector $x = \{\theta, \dot{\theta}\}^T = \{x_1, x_2\}^T$ and combining Equation (4.1) with Equation (3.1a):

$$\dot{x} = f(x) = \begin{cases} f_1(x) = \begin{cases} x_2 \\ \dfrac{mgr\sin x_1 - \tau_{PD}}{M} \end{cases} & if \quad \tau_{lower} \le \tau_{PD} \le \tau_{upper} \quad (\text{Re}gion1) \\ f_2(x) = \begin{cases} x_2 \\ \dfrac{mgr\sin x_1 - \tau_{upper}}{M} \end{cases} & if \quad \tau_{PD} \ge \tau_{upper} \quad (\text{Re}gion2) \\ f_3(x) = \begin{cases} x_2 \\ \dfrac{mgr\sin x_1 - \tau_{lower}}{M} \end{cases} & if \quad \tau_{PD} \le \tau_{lower} \quad (\text{Re}gion3) \end{cases} \tag{4.2}$$

The above 2-dimensional state-space model leads to two Lyapunov exponents. The signs of the Lyapunov exponents provide qualitative information about the system stability. Note that within each region, the control torque $\tau$ is smooth. The controller is overall continuous, but the non-differentiable points occur at the instants of switching, where the derivative of the right-hand side of the state space model shown in Equation (4.2) do not exist. Thus, linearization of the nonlinear equations at these points, required by the calculation of Lyapunov exponents, is addressed by resorting to the work of Müller (1995) in which the conventional calculation procedure (Wolf *et al.* 1985) has been extended to systems with non-differential points. Since the stability of the system is investigated based on the signs of the exponents, suppression of numerical instabilities is of significant importance. Furthermore, since the calculation of Lyapunov exponents should be carried out over a sufficiently long period of time, the computational efficiency becomes important. The nonstandard finite difference discrete scheme proposed by

Mickens (1994 and 2002) and Mickens and Gumel (2002) can solve the above two problems. The scheme is capable of providing results with step-size larger than Runge-Kutta method, and thus, enhances the efficiency of computation (Sekhavat *et al.* 2004, Abo-Shanab *et al.* 2005). The non-standard finite difference schemes developed in this research are described in Section 4.3. They are used to suppress the numerical instabilities and to improve calculation efficiency. The procedure of calculating Lyapunov exponents from mathematical model is described in Chapter 2.

It is known that although Lyapunov exponents are calculated along a single solution trajectory, they have the same values for all trajectories in the same stability region. Thus it is considered as a state space property. The stability region is defined to include initial states, from which, using our PD based switching state controller, the biped can be stabilized to the upright position with all of the largest Lyapunov exponent being convergent to the same negative value. To determine the stability region, the algorithm developed by Nusse and Yorke (1998) is adapted, where the region of interest is first divided into grid boxes. The grid box at the origin of the state-space (also called 'center box') contains the stable equilibrium point. Next, the size of neighboring grid boxes is chosen and Lyapunov exponents are calculated using the initial states from each neighboring box. If the same convergent and negative exponents are obtained, the neighboring grid box belongs to the stability region.

## 4.4 Calculation of Lyapunov Exponents for a Bipedal Model

In this section, the nonstandard finite difference schemes, which consider all cases corresponding to different control regions shown as Region 1, Region2 and Region3 in Equation (4.2), are presented. Note that within Region 1, Region2 and Region3, control

torque $\tau$ is smooth. Nonstandard finite difference schemes are developed by following Mickens' rules (Mickens 1994 and 2002). While, at the instants of switching points, due to the existence of non-differentiable points, the linearized equations are evaluated using the indicator function, $h(x)$, and the transition function, $g(x)$, both defined based on the physical behaviour of the system. The indicator function $h(x)$ is at least one time continuously differentiable function and determines the instant of the non-differentiable point. The transition function $g(x)$ describes the transition conditions at each instant of the non-differentiable point. The indicator function and Jacobian of transition condition are chosen based on Müller's method (Müller 1995).

Overall, when the nonstandard finite difference schemes were constructed, two cases should be considered. One is smooth case, *i.e.*, in region 1, 2, and 3, the other is nonsmooth (non-differentiable) case, *i.e.*, at the switching points. The reason of using nonstandard finite difference scheme is to suppress the numerical instabilities and to improve calculation efficiency. The key issue in numerical integration of our PD-based switching control system is to determine the regions and the switching points. The procedure of numerical integration using nonstandard finite difference scheme is presented as follows.

*Step 1:* For a given initial state, control torque and control bounds are calculated based on the equations developed in Section 3.5. Each integrated point is considered as a "trial" point until the switching condition shown in (4.1) is checked.

*Step 2:* Check the state points. If no switching occurs, the point remains in same regions and next state is obtained based on numerical

integration using nonstandard finite difference scheme corresponding to this region. If one switching occurs, next state is obtained based on numerical integration using nonstandard finite difference scheme corresponding to switching points. The transition condition of the linearized equations is calculated according to Müller's method (Müller 1995).

*Step 3:* Using GSR procedure to obtain the orthonormal vectors, calculating Lyapunov exponents.

*Step 4:* Continuously integrate until target is achieved or terminate by conditions obtained from constraints

### 4.4.1 Smooth cases:

***In Region1:***

The nonlinear equation is:

$$\dot{x} = f_1(x) = \begin{cases} x_2 \\ \dfrac{mgr\sin x_1 - \tau_{PD}}{M} \end{cases} \tag{4.3}$$

which can be written in a matrix form

$$\begin{bmatrix} \dot{x}_1 \\ \dot{x}_2 \end{bmatrix} = \begin{bmatrix} f_{11} \\ f_{12} \end{bmatrix} \tag{4.4}$$

where $f_{11} = x_2$

$$f_{12} = \frac{mgr\sin x_1 - kpx_1 - kvx_2}{M} \tag{4.5}$$

The linearization results in:

$$\delta\dot{x} = F_1(x)\delta x \tag{4.6}$$

where

$$F_1(x) = \begin{bmatrix} \frac{\partial f_{11}}{\partial x_1} & \frac{\partial f_{11}}{\partial x_2} \\ \frac{\partial f_{12}}{\partial x_1} & \frac{\partial f_{12}}{\partial x_2} \end{bmatrix} = \begin{bmatrix} f_{111} & f_{112} \\ f_{121} & f_{122} \end{bmatrix} \tag{4.7}$$

$$f_{111} = \frac{\partial f_{11}}{\partial x_1} = 0, \qquad f_{112} = \frac{\partial f_{11}}{\partial x_2} = 1,$$

$$f_{121} = \frac{\partial f_{12}}{\partial x_1} = \frac{mgr\cos x_1 - kp}{M}, \qquad f_{122} = \frac{\partial f_{12}}{\partial x_2} = -\frac{kv}{M},$$

$$\begin{aligned} \begin{bmatrix} \dot{x}_3 & \dot{x}_4 \\ \dot{x}_5 & \dot{x}_6 \end{bmatrix} &= \begin{bmatrix} f_{111} & f_{112} \\ f_{121} & f_{122} \end{bmatrix} \cdot \begin{bmatrix} x_3 & x_4 \\ x_5 & x_6 \end{bmatrix} \\ &= \begin{bmatrix} 0 & 1 \\ f_{121} & f_{122} \end{bmatrix} \cdot \begin{bmatrix} x_3 & x_4 \\ x_5 & x_6 \end{bmatrix} = \begin{bmatrix} x_5 & x_6 \\ f_{121}x_3 + f_{122}x_5 & f_{121}x_4 + f_{122}x_6 \end{bmatrix} \end{aligned} \tag{4.8}$$

So

$$\begin{bmatrix} \dot{x}_1 \\ \dot{x}_2 \\ \dot{x}_3 \\ \dot{x}_4 \\ \dot{x}_5 \\ \dot{x}_6 \end{bmatrix} = \begin{bmatrix} f_{11} \\ f_{12} \\ x_5 \\ x_6 \\ f_{121}x_3 + f_{122}x_5 \\ f_{121}x_4 + f_{122}x_6 \end{bmatrix} \tag{4.9}$$

Since $f_{122} < 0$, according to Mickens' Rules, one has

$$\begin{aligned} x_5 &= 2x_5^{new} - x_5 \\ x_6 &= 2x_6^{new} - x_6 \end{aligned} \tag{4.10}$$

The nonstandard finite difference scheme was constructed as:

$$
\begin{aligned}
x_1{}^{new} &= x_1 + hx_2 \\
x_2{}^{new} &= \left\{x_2 + h\frac{1}{M}\left(mgr\sin(x_1{}^{new}) - kpx_1{}^{new}\right)\right\}/\left(1 + h\frac{kv}{M}\right) \\
x_3{}^{new} &= x_3 + hx_5 \\
x_4{}^{new} &= x_4 + hx_6 \\
x_5{}^{new} &= \left\{(1 - hf_{122})x_5 + hf_{121}x_3{}^{new}\right\}/(1 - 2hf_{122}) \\
x_6{}^{new} &= \left\{(1 - hf_{122})x_6 + hf_{121}x_4{}^{new}\right\}/(1 - 2hf_{122})
\end{aligned}
\tag{4.11}
$$

Using this nonstandard finite difference scheme, both nonlinear differential equations of motion and linearized differential equations of motion are integrated one step simultaneously, the new states and new principal vectors are obtained. Then using GSR procedure, orthonormal vectors are generated. Following the procedure described in Section 2.2 in Chapter 2, the whole spectra of the Lyapunov exponents is calculated. The same discussion holds for Region 2, Region 3 and for every switching point.

***In Region2:***

The nonlinear equation is:

$$
\dot{x} = f_2(x) = \begin{cases} x_2 = f_{21} \\ \dfrac{mgr\sin x_1 - \tau_{upper}}{M} = f_{22} \end{cases}
\tag{4.12}
$$

Where

$$
f_{22} = \frac{mgr\sin x_1}{M} - \frac{1}{M[mr(a\sin x_1 - b\cos x_1) - M]}\{m^2r^2g\sin x_1(a\sin x_1 - b\cos x_1)
$$

$$
+ M[mrx_2^2(a\cos x_1 + b\sin x_1) - (\frac{L_f m_f}{2} + am)g]\}
$$

which can be written in a matrix form

$$\begin{bmatrix} \dot{x}_1 \\ \dot{x}_2 \end{bmatrix} = \begin{bmatrix} f_{21} \\ f_{22} \end{bmatrix} \tag{4.13}$$

The linearization results in:

$$\delta\dot{x} = F_2(x)\delta x \tag{4.14}$$

where,

$$F_2(x) = \begin{bmatrix} \frac{\partial f_{21}}{\partial x_1} & \frac{\partial f_{21}}{\partial x_2} \\ \frac{\partial f_{22}}{\partial x_1} & \frac{\partial f_{22}}{\partial x_2} \end{bmatrix} = \begin{bmatrix} f_{211} & f_{212} \\ f_{221} & f_{222} \end{bmatrix} \tag{4.15}$$

$$f_{211} = \frac{\partial f_{21}}{\partial x_1} = 0, \qquad f_{212} = \frac{\partial f_{21}}{\partial x_2} = 1,$$

$$f_{221} = \frac{\partial f_{22}}{\partial x_1}$$

$$= \{mr[g\cos x_1 M - Mx_2^2(a\sin x_1 - b\cos x_1) + mrx_2^2(a^2 + b^2) + mrgb$$

$$-(a\cos x_1 + b\sin x_1)(\frac{L_f m_f}{2} + am)g\}/[mr(a\sin x_1 - b\cos x_1) - M]^2$$

$$f_{222} = \frac{\partial f_{22}}{\partial x_2} = -2\frac{mrx_2(a\cos x_1 + b\sin x_1)}{mr(a\sin x_1 - b\cos x_1) - M} \tag{4.16}$$

$$\begin{aligned} \begin{bmatrix} \dot{x}_3 & \dot{x}_4 \\ \dot{x}_5 & \dot{x}_6 \end{bmatrix} &= \begin{bmatrix} f_{211} & f_{212} \\ f_{221} & f_{222} \end{bmatrix} \cdot \begin{bmatrix} x_3 & x_4 \\ x_5 & x_6 \end{bmatrix} \\ &= \begin{bmatrix} 0 & 1 \\ f_{221} & f_{222} \end{bmatrix} \cdot \begin{bmatrix} x_3 & x_4 \\ x_5 & x_6 \end{bmatrix} \\ &= \begin{bmatrix} x_5 & x_6 \\ f_{221}x_3 + f_{222}x_5 & f_{221}x_4 + f_{222}x_6 \end{bmatrix} \end{aligned} \tag{4.17}$$

So

$$\begin{bmatrix} \dot{x}_1 \\ \dot{x}_2 \\ \dot{x}_3 \\ \dot{x}_4 \\ \dot{x}_5 \\ \dot{x}_6 \end{bmatrix} = \begin{bmatrix} f_{21} \\ f_{22} \\ x_5 \\ x_6 \\ f_{221}x_3 + f_{222}x_5 \\ f_{221}x_4 + f_{222}x_6 \end{bmatrix} \tag{4.18}$$

The nonstandard finite difference scheme is:

$$\begin{aligned} x_1{}^{new} &= x_1 + hx_2 \\ x_2{}^{new} &= \{x_2 + hf_{22}(x_1{}^{new}, x_2)\} \\ x_3{}^{new} &= x_3 + hx_5 \\ x_4{}^{new} &= x_4 + hx_6 \end{aligned} \tag{4.19}$$

when $f_{222} > 0$, let

$$\begin{aligned} x_5 &= 2x_5 - x_5{}^{new} \\ x_6 &= 2x_6 - x_6{}^{new} \end{aligned} \tag{4.20}$$

then

$$\begin{aligned} x_5{}^{new} &= \{(1 + 2hf_{222})x_5 + hf_{221}x_3{}^{new}\}/(1 + hf_{222}) \\ x_6{}^{new} &= \{(1 + 2hf_{222})x_6 + hf_{221}x_4{}^{new}\}/(1 + hf_{222}) \end{aligned} \tag{4.21}$$

when $f_{222} < 0$, let

$$\begin{aligned} x_5 &= 2x_5{}^{new} - x_5 \\ x_6 &= 2x_6{}^{new} - x_6 \end{aligned} \tag{4.22}$$

then

$$\begin{aligned} x_5{}^{new} &= \{(1 - hf_{222})x_5 + hf_{221}x_3{}^{new}\}/(1 - 2hf_{222}) \\ x_6{}^{new} &= \{(1 - hf_{222})x_6 + hf_{221}x_4{}^{new}\}/(1 - 2hf_{222}) \end{aligned} \tag{4.23}$$

Following the same procedure described in Region 1, Lyapunov exponents can be calculated.

***In Region3:***

The nonlinear equation is:

$$\dot{x} = f_3(x) = \begin{cases} x_2 = f_{31} \\ \dfrac{mgr\sin x_1 - \tau_{lower}}{M} = f_{32} \end{cases} \tag{4.24}$$

where

$$f_{32} = \frac{mgr\sin x_1}{M} - \frac{1}{M\{M + mr[(L_f - a)\sin x_1 + b\cos x_1]\}}\{m^2r^2 g\sin x_1[(L_f - a)\sin x_1 + b\cos x_1] + Mmrx_2^2[(L_f - a)\cos x_1 - b\sin x_1] - M[\frac{L_f m_f}{2} + (L_f - a)m]g\}$$

which can be written in a matrix form

$$\begin{bmatrix} \dot{x}_1 \\ \dot{x}_2 \end{bmatrix} = \begin{bmatrix} f_{31} \\ f_{32} \end{bmatrix} \tag{4.25}$$

The linearization results in:

$$\delta\dot{x} = F_3(x)\delta x \tag{4.26}$$

where

$$F_3(x) = \begin{bmatrix} \dfrac{\partial f_{31}}{\partial x_1} & \dfrac{\partial f_{31}}{\partial x_2} \\ \dfrac{\partial f_{32}}{\partial x_1} & \dfrac{\partial f_{32}}{\partial x_2} \end{bmatrix} = \begin{bmatrix} f_{311} & f_{312} \\ f_{321} & f_{322} \end{bmatrix} \tag{4.27}$$

$$f_{311} = \frac{\partial f_{31}}{\partial x_1} = 0, \quad f_{312} = \frac{\partial f_{31}}{\partial x_2} = 1$$

$$f_{321}=\frac{\partial f_{32}}{\partial x_1}=\frac{mr}{\{M+mr[(L_f-a)\sin x_1+b\cos x_1]\}^2}\{g\cos x_1 M+Mx_2^2[(L_f-a)\sin x_1$$
$$+b\cos x_1]+mrx_2^2(a^2+b^2)+mrgb-[(L_f-a)\cos x_1-b\sin x_1]\left[\frac{L_f m_f}{2}+(L_f-a)m\right]g$$
$$+mrx_2^2L_f(L_f-2a)\}$$
$$f_{322}=\frac{\partial f_{32}}{\partial x_2}=-2\frac{mrx_2[(L_f-a)\cos x_1-b\sin x_1]}{M+mr[(L_f-a)\sin x_1+b\cos x_1]} \tag{4.28}$$

$$\begin{bmatrix}\dot{x}_3 & \dot{x}_4\\ \dot{x}_5 & \dot{x}_6\end{bmatrix}=\begin{bmatrix}f_{311} & f_{312}\\ f_{321} & f_{322}\end{bmatrix}\begin{bmatrix}x_3 & x_4\\ x_5 & x_6\end{bmatrix}$$
$$=\begin{bmatrix}0 & 1\\ f_{321} & f_{322}\end{bmatrix}\begin{bmatrix}x_3 & x_4\\ x_5 & x_6\end{bmatrix}=\begin{bmatrix}x_5 & x_6\\ f_{321}x_3+f_{322}x_5 & f_{321}x_4+f_{322}x_6\end{bmatrix} \tag{4.29}$$

So

$$\begin{bmatrix}\dot{x}_1\\ \dot{x}_2\\ \dot{x}_3\\ \dot{x}_4\\ \dot{x}_5\\ \dot{x}_6\end{bmatrix}=\begin{bmatrix}f_{31}\\ f_{32}\\ x_5\\ x_6\\ f_{321}x_3+f_{322}x_5\\ f_{321}x_4+f_{322}x_6\end{bmatrix} \tag{4.30}$$

The nonstandard finite difference scheme is:

$$\begin{aligned}x_1^{new}&=x_1+hx_2\\ x_2^{new}&=\{x_2+hf_{32}(x_1^{new},x_2)\}\\ x_3^{new}&=x_3+hx_5\\ x_4^{new}&=x_4+hx_6\end{aligned} \tag{4.31}$$

when $f_{322}>0$, let

$$\begin{aligned}x_5&=2x_5-x_5^{new}\\ x_6&=2x_6-x_6^{new}\end{aligned}, \tag{4.32}$$

then

$$x_5{}^{new} = \left\{(1+2hf_{322})x_5 + hf_{321}x_3{}^{new}\right\}/(1+hf_{322})$$
$$x_6{}^{new} = \left\{(1+2hf_{322})x_6 + hf_{321}x_4{}^{new}\right\}/(1+hf_{322}) \tag{4.33}$$

when $f_{322} < 0$, let

$$x_5 = 2x_5{}^{new} - x_5$$
$$x_6 = 2x_6{}^{new} - x_6 \tag{4.34}$$

then

$$x_5{}^{new} = \left\{(1-hf_{322})x_5 + hf_{321}x_3{}^{new}\right\}/(1-2hf_{322})$$
$$x_6{}^{new} = \left\{(1-hf_{322})x_6 + hf_{321}x_4{}^{new}\right\}/(1-2hf_{322}) \tag{4.35}$$

Following the same procedure described in Region 1, Lyapunov exponents can be calculated.

### 4.4.2 Non-smooth cases:

At the instants of switching points, the linearized equations are evaluated using the indicator function, $h(x)$, and the transition function, $g(x)$, both defined based on the physical behaviour of the system.

***At $t = t_1$, Region1 Switches to Region2***

The indicator function is

$$h_1 = \tau_{PD} - \tau_{upper} = 0 \tag{4.36}$$

Jacobian of the indicator function is

$$H_1 = \left[\frac{\partial h_1}{\partial x_1} \quad \frac{\partial h_1}{\partial x_2}\right] = \left[h_{11} \quad h_{12}\right] \tag{4.37}$$

Jacobian of the transition condition is

$$G_1 = \begin{bmatrix} 1 & 0 \\ 0 & 1 \end{bmatrix} \tag{4.38}$$

The transition condition of the linearized equations is:

$$\delta x(t_1^+) = G_1(x^-)\delta x(t_1^-) - \left[G_1(x^-)f_1(x(t_1^-)) - f_2(x(t_1^+)\right]\frac{H_1(x^-)\delta x(t_1^-)}{H_1(x^-)f_1(x(t_1^-))} \tag{4.39}$$

where "+" and "–" sign denote the time just after and before switch instants $t_1$.

$$\begin{bmatrix} x_3^{new} & x_4^{new} \\ x_5^{new} & x_6^{new} \end{bmatrix}$$

$$= \begin{bmatrix} 1 & 0 \\ 0 & 1 \end{bmatrix}\begin{bmatrix} x_3 & x_4 \\ x_5 & x_6 \end{bmatrix} - \left\{\begin{bmatrix} 1 & 0 \\ 0 & 1 \end{bmatrix}\begin{bmatrix} f_{11} \\ f_{12} \end{bmatrix} - \begin{bmatrix} f_{21} \\ f_{22} \end{bmatrix}\right\}\frac{\begin{bmatrix} h_{11} & h_{12} \end{bmatrix}\begin{bmatrix} x_3 & x_4 \\ x_5 & x_6 \end{bmatrix}}{\begin{bmatrix} h_{11} & h_{12} \end{bmatrix}\begin{bmatrix} f_{11} \\ f_{12} \end{bmatrix}}$$

$$= \begin{bmatrix} x_3 & x_4 \\ x_5 & x_6 \end{bmatrix} - \left\{\begin{bmatrix} f_{11} \\ f_{12} \end{bmatrix} - \begin{bmatrix} f_{21} \\ f_{22} \end{bmatrix}\right\}\frac{\begin{bmatrix} h_{11}x_3 + h_{12}x_5 & h_{11}x_4 + h_{12}x_6 \end{bmatrix}}{h_{11}f_{11} + h_{12}f_{12}}$$

$$= \begin{bmatrix} x_3 & x_4 \\ x_5 & x_6 \end{bmatrix} - \frac{1}{h_{11}f_{11} + h_{12}f_{12}}\begin{bmatrix} f_{11} - f_{21} \\ f_{12} - f_{22} \end{bmatrix}\begin{bmatrix} h_{11}x_3 + h_{12}x_5 & h_{11}x_4 + h_{12}x_6 \end{bmatrix}$$

$$= \begin{bmatrix} x_3 & x_4 \\ x_5 & x_6 \end{bmatrix} - \frac{1}{h_{11}f_{11} + h_{12}f_{12}}\begin{bmatrix} (f_{11} - f_{21})(h_{11}x_3 + h_{12}x_5) & (f_{11} - f_{21})(h_{11}x_4 + h_{12}x_6) \\ (f_{12} - f_{22})(h_{11}x_3 + h_{12}x_5) & (f_{12} - f_{22})(h_{11}x_4 + h_{12}x_6) \end{bmatrix} \tag{4.40}$$

Let

$$\alpha_1 = \frac{f_{11} - f_{21}}{h_{11}f_{11} + h_{12}f_{12}}$$

$$\beta_1 = \frac{f_{12} - f_{22}}{h_{11}f_{11} + h_{12}f_{12}} \tag{4.41}$$

Then

$$\begin{bmatrix} x_3^{new} & x_4^{new} \\ x_5^{new} & x_6^{new} \end{bmatrix} = \begin{bmatrix} x_3 & x_4 \\ x_5 & x_6 \end{bmatrix} - \begin{bmatrix} \alpha_1 h_{11}x_3 + \alpha_1 h_{12}x_5 & \alpha_1 h_{11}x_4 + \alpha_1 h_{12}x_6 \\ \beta_1 h_{11}x_3 + \beta_1 h_{12}x_5 & \beta_1 h_{11}x_4 + \beta_1 h_{12}x_6 \end{bmatrix} \tag{4.42}$$

The nonstandard finite difference scheme is:

$$\begin{aligned} x_1{}^{new} &= x_1 + hx_2 \\ x_2{}^{new} &= \left\{x_2 + hf_{22}\left(x_1{}^{new}, x_2\right)\right\} \end{aligned} \tag{4.43}$$

when $\alpha_1 h_{11} > 0$, let

$$\begin{aligned} x_3 &= 2x_3{}^{new} - x_3 \\ x_4 &= 2x_4{}^{new} - x_4 \end{aligned} \tag{4.44}$$

then

$$\begin{aligned} x_3{}^{new} &= \{(1+\alpha_1 h_{11})x_3 - \alpha_1 h_{12} x_5\}/(1+2\alpha_1 h_{11}) \\ x_4{}^{new} &= \{(1+\alpha_1 h_{11})x_4 - \alpha_1 h_{12} x_6\}/(1+2\alpha_1 h_{11}) \end{aligned} \tag{4.45}$$

when $\alpha_1 h_{11} < 0$, let

$$\begin{aligned} x_3 &= 2x_3 - x_3{}^{new} \\ x_4 &= 2x_4 - x_4{}^{new} \end{aligned} \tag{4.46}$$

then

$$\begin{aligned} x_3{}^{new} &= \{(1-2\alpha_1 h_{11})x_3 - \alpha_1 h_{12} x_5\}/(1-\alpha_1 h_{11}) \\ x_4{}^{new} &= \{(1-2\alpha_1 h_{11})x_4 - \alpha_1 h_{12} x_6\}/(1-\alpha_1 h_{11}) \end{aligned} \tag{4.47}$$

when $\beta_1 h_{12} > 0$, let

$$\begin{aligned} x_5 &= 2x_5{}^{new} - x_5 \\ x_6 &= 2x_6{}^{new} - x_6 \end{aligned} \tag{4.48}$$

then

$$\begin{aligned} x_5{}^{new} &= \left\{(1+\beta_1 h_{12})x_5 - \beta_1 h_{11} x_3{}^{new}\right\}/(1+2\beta_1 h_{12}) \\ x_6{}^{new} &= \left\{(1+\beta_1 h_{12})x_6 - \beta_1 h_{11} x_4{}^{new}\right\}/(1+2\beta_1 h_{12}) \end{aligned} \tag{4.49}$$

when $\beta_1 h_{12} < 0$, let

$$\begin{aligned} x_5 &= 2x_5 - x_5{}^{new} \\ x_6 &= 2x_6 - x_6{}^{new} \end{aligned} \tag{4.50}$$

then

$$x_5^{new} = \left\{(1-2\beta_1 h_{12})x_5 - \beta_1 h_{11} x_3^{new}\right\}/(1-\beta_1 h_{12})$$
$$x_6^{new} = \left\{(1-2\beta_1 h_{12})x_6 - \beta_1 h_{11} x_4^{new}\right\}/(1-\beta_1 h_{12}) \quad (4.51)$$

Following the same procedure described in Region 1, Lyapunov exponents can be calculated.

***At $t = t_2$, Region2 Switches to Region1***

Indicator function is

$$h_2 = h_1 = \tau_{ctr} - \tau_{upper} = 0 \quad (4.52)$$

Jacobian of indicator function is

$$H_2 = H_1 = \left[\frac{\partial h_1}{\partial x_1} \quad \frac{\partial h_1}{\partial x_2}\right] = \begin{bmatrix} h_{11} & h_{12} \end{bmatrix} \quad (4.53)$$

Jacobian of transition condition is

$$G_2 = G_1 = \begin{bmatrix} 1 & 0 \\ 0 & 1 \end{bmatrix} \quad (4.54)$$

The transition condition of the linearized equations is:

$$\delta x(t_2^+) = G_2(x^-)\delta x(t_2^-) - \left[G_2(x^-) f_2(x(t_2^-)) - f_1(x(t_2^+)\right] \frac{H_2(x^-)\delta x(t_2^-)}{H_2(x^-) f_2(x(t_2^-))} \quad (4.55)$$

where "+" and "_" sign denote the time just after and before switch instants $t_2$.

$$\begin{bmatrix} x_3^{new} & x_4^{new} \\ x_5^{new} & x_6^{new} \end{bmatrix}$$

$$= \begin{bmatrix} 1 & 0 \\ 0 & 1 \end{bmatrix} \begin{bmatrix} x_3 & x_4 \\ x_5 & x_6 \end{bmatrix} - \left\{ \begin{bmatrix} 1 & 0 \\ 0 & 1 \end{bmatrix} \begin{bmatrix} f_{21} \\ f_{22} \end{bmatrix} - \begin{bmatrix} f_{11} \\ f_{12} \end{bmatrix} \right\} \frac{\begin{bmatrix} h_{11} & h_{12} \end{bmatrix} \begin{bmatrix} x_3 & x_4 \\ x_5 & x_6 \end{bmatrix}}{\begin{bmatrix} h_{11} & h_{12} \end{bmatrix} \begin{bmatrix} f_{21} \\ f_{22} \end{bmatrix}}$$

$$
\begin{aligned}
&= \begin{bmatrix} x_3 & x_4 \\ x_5 & x_6 \end{bmatrix} - \left\{ \begin{bmatrix} f_{21} \\ f_{22} \end{bmatrix} - \begin{bmatrix} f_{11} \\ f_{12} \end{bmatrix} \right\} \frac{\begin{bmatrix} h_{11}x_3 + h_{12}x_5 & h_{11}x_4 + h_{12}x_6 \end{bmatrix}}{h_{11}f_{21} + h_{12}f_{22}} \\
&= \begin{bmatrix} x_3 & x_4 \\ x_5 & x_6 \end{bmatrix} - \frac{1}{h_{11}f_{21} + h_{12}f_{22}} \begin{bmatrix} f_{21} - f_{11} \\ f_{22} - f_{12} \end{bmatrix} \begin{bmatrix} h_{11}x_3 + h_{12}x_5 & h_{11}x_4 + h_{12}x_6 \end{bmatrix} \\
&= \begin{bmatrix} x_3 & x_4 \\ x_5 & x_6 \end{bmatrix} - \frac{1}{h_{11}f_{21} + h_{12}f_{22}} \begin{bmatrix} (f_{21} - f_{11})(h_{11}x_3 + h_{12}x_5) & (f_{21} - f_{11})(h_{11}x_4 + h_{12}x_6) \\ (f_{22} - f_{12})(h_{11}x_3 + h_{12}x_5) & (f_{22} - f_{12})(h_{11}x_4 + h_{12}x_6) \end{bmatrix}
\end{aligned}
\tag{4.56}
$$

Let

$$
\alpha_2 = \frac{f_{21} - f_{11}}{h_{11}f_{11} + h_{12}f_{12}},
$$

$$
\beta_2 = \frac{f_{22} - f_{12}}{h_{11}f_{11} + h_{12}f_{12}} \tag{4.57}
$$

Then

$$
\begin{bmatrix} x_3^{new} & x_4^{new} \\ x_5^{new} & x_6^{new} \end{bmatrix} = \begin{bmatrix} x_3 & x_4 \\ x_5 & x_6 \end{bmatrix} - \begin{bmatrix} \alpha_2 h_{11}x_3 + \alpha_2 h_{12}x_5 & \alpha_2 h_{11}x_4 + \alpha_2 h_{12}x_6 \\ \beta_2 h_{11}x_3 + \beta_2 h_{12}x_5 & \beta_2 h_{11}x_4 + \beta_2 h_{12}x_6 \end{bmatrix} \tag{4.58}
$$

The nonstandard finite difference scheme is:

$$
\begin{aligned}
x_1^{new} &= x_1 + hx_2 \\
x_2^{new} &= \left\{ x_2 + hf_{22}\left( x_1^{new}, x_2 \right) \right\}
\end{aligned}
\tag{4.59}
$$

when $\alpha_2 h_{11} > 0$, let

$$
\begin{aligned}
x_3 &= 2x_3^{new} - x_3 \\
x_4 &= 2x_4^{new} - x_4
\end{aligned}
\tag{4.60}
$$

then

$$
\begin{aligned}
x_3^{new} &= \{(1 + \alpha_2 h_{11})x_3 - \alpha_2 h_{12}x_5\}/(1 + 2\alpha_2 h_{11}) \\
x_4^{new} &= \{(1 + \alpha_2 h_{11})x_4 - \alpha_2 h_{12}x_6\}/(1 + 2\alpha_2 h_{11})
\end{aligned}
\tag{4.61}
$$

when $\alpha_2 h_{11} < 0$, let

$$x_3 = 2x_3 - x_3^{new}$$
$$x_4 = 2x_4 - x_4^{new} \tag{4.62}$$

then

$$x_3^{new} = \{(1-2\alpha_2 h_{11})x_3 - \alpha_2 h_{12} x_5\}/(1-\alpha_2 h_{11})$$
$$x_4^{new} = \{(1-2\alpha_2 h_{11})x_4 - \alpha_2 h_{12} x_6\}/(1-\alpha_2 h_{11}) \tag{4.63}$$

when $\beta_2 h_{12} > 0$, let

$$x_5 = 2x_5^{new} - x_5$$
$$x_6 = 2x_6^{new} - x_6 \tag{4.64}$$

then

$$x_5^{new} = \{(1+\beta_2 h_{12})x_5 - \beta_2 h_{11} x_3^{new}\}/(1+2\beta_2 h_{12})$$
$$x_6^{new} = \{(1+\beta_2 h_{12})x_6 - \beta_2 h_{11} x_4^{new}\}/(1+2\beta_2 h_{12}) \tag{4.65}$$

when $\beta_2 h_{12} < 0$, let

$$x_5 = 2x_5 - x_5^{new}$$
$$x_6 = 2x_6 - x_6^{new} \tag{4.66}$$

Then

$$x_5^{new} = \{(1-2\beta_2 h_{12})x_5 - \beta_2 h_{11} x_3^{new}\}/(1-\beta_2 h_{12})$$
$$x_6^{new} = \{(1-2\beta_2 h_{12})x_6 - \beta_2 h_{11} x_4^{new}\}/(1-\beta_2 h_{12}) \tag{4.67}$$

Following the same procedure described in Region 1, Lyapunov exponents can be calculated.

***At $t = t_3$, Region1 Switches to Region3***

Indicator function is

$$h_3 = \tau_{ctr} - \tau_{lower} = 0 \tag{4.68}$$

Jacobian of indicator function is

$$H_3 = \begin{bmatrix} \frac{\partial h_3}{\partial x_1} & \frac{\partial h_3}{\partial x_2} \end{bmatrix} = \begin{bmatrix} h_{31} & h_{32} \end{bmatrix} \tag{4.69}$$

Jacobian of transition condition is

$$G_3 = \begin{bmatrix} 1 & 0 \\ 0 & 1 \end{bmatrix} \tag{4.70}$$

The transition condition of the linearized equations is:

$$\delta x(t_3^+) = G_3(x^-)\delta x(t_3^-) - \left[G_3(x^-)f_1(x(t_3^-)) - f_3(x(t_3^+)\right]\frac{H_3(x^-)\delta x(t_3^-)}{H_3(x^-)f_1(x(t_3^-))} \tag{4.71}$$

where "+" and "_" sign denote the time just after and before switch instants $t_3$.

$$\begin{bmatrix} x_3^{new} & x_4^{new} \\ x_5^{new} & x_6^{new} \end{bmatrix}$$

$$= \begin{bmatrix} 1 & 0 \\ 0 & 1 \end{bmatrix}\begin{bmatrix} x_3 & x_4 \\ x_5 & x_6 \end{bmatrix} - \left\{\begin{bmatrix} 1 & 0 \\ 0 & 1 \end{bmatrix}\begin{bmatrix} f_{11} \\ f_{12} \end{bmatrix} - \begin{bmatrix} f_{31} \\ f_{32} \end{bmatrix}\right\}\frac{\begin{bmatrix} h_{31} & h_{32} \end{bmatrix}\begin{bmatrix} x_3 & x_4 \\ x_5 & x_6 \end{bmatrix}}{\begin{bmatrix} h_{31} & h_{32} \end{bmatrix}\begin{bmatrix} f_{11} \\ f_{12} \end{bmatrix}}$$

$$= \begin{bmatrix} x_3 & x_4 \\ x_5 & x_6 \end{bmatrix} - \left\{\begin{bmatrix} f_{11} \\ f_{12} \end{bmatrix} - \begin{bmatrix} f_{31} \\ f_{32} \end{bmatrix}\right\}\frac{\begin{bmatrix} h_{31}x_3 + h_{32}x_5 & h_{31}x_4 + h_{32}x_6 \end{bmatrix}}{h_{31}f_{11} + h_{32}f_{12}}$$

$$= \begin{bmatrix} x_3 & x_4 \\ x_5 & x_6 \end{bmatrix} - \frac{1}{h_{31}f_{11} + h_{32}f_{12}}\begin{bmatrix} f_{11} - f_{31} \\ f_{12} - f_{32} \end{bmatrix}\begin{bmatrix} h_{31}x_3 + h_{32}x_5 & h_{31}x_4 + h_{32}x_6 \end{bmatrix}$$

$$= \begin{bmatrix} x_3 & x_4 \\ x_5 & x_6 \end{bmatrix} - \frac{1}{h_{31}f_{11} + h_{32}f_{12}}\begin{bmatrix} (f_{11} - f_{31})(h_{31}x_3 + h_{32}x_5) & (f_{11} - f_{31})(h_{31}x_4 + h_{32}x_6) \\ (f_{12} - f_{32})(h_{31}x_3 + h_{32}x_5) & (f_{12} - f_{32})(h_{31}x_4 + h_{32}x_6) \end{bmatrix} \tag{4.72}$$

Let

$$\alpha_3 = \frac{f_{11} - f_{31}}{h_{31}f_{11} + h_{32}f_{12}},$$

$$\beta_3 = \frac{f_{12} - f_{32}}{h_{31} f_{11} + h_{32} f_{12}} \tag{4.73}$$

then

$$\begin{bmatrix} x_3^{new} & x_4^{new} \\ x_5^{new} & x_6^{new} \end{bmatrix} = \begin{bmatrix} x_3 & x_4 \\ x_5 & x_6 \end{bmatrix} - \begin{bmatrix} \alpha_3 h_{31} x_3 + \alpha_3 h_{32} x_5 & \alpha_3 h_{31} x_4 + \alpha_3 h_{32} x_6 \\ \beta_3 h_{31} x_3 + \beta_3 h_{32} x_5 & \beta_3 h_{31} x_4 + \beta_3 h_{32} x_6 \end{bmatrix} \tag{4.74}$$

The nonstandard finite difference scheme is:

$$\begin{aligned} x_1^{new} &= x_1 + h x_2 \\ x_2^{new} &= \left\{ x_2 + h f_{22}\left( x_1^{new}, x_2 \right) \right\} \end{aligned} \tag{4.75}$$

when $\alpha_3 h_{31} > 0$, let

$$\begin{aligned} x_3 &= 2 x_3^{new} - x_3 \\ x_4 &= 2 x_4^{new} - x_4 \end{aligned} \tag{4.76}$$

then

$$\begin{aligned} x_3^{new} &= \left\{ \left(1 + \alpha_3 h_{31}\right) x_3 - \alpha_3 h_{32} x_5 \right\} / \left(1 + 2\alpha_3 h_{31}\right) \\ x_4^{new} &= \left\{ \left(1 + \alpha_3 h_{31}\right) x_4 - \alpha_3 h_{32} x_6 \right\} / \left(1 + 2\alpha_3 h_{31}\right) \end{aligned} \tag{4.77}$$

when $\alpha_3 h_{31} < 0$, let

$$\begin{aligned} x_3 &= 2 x_3 - x_3^{new} \\ x_4 &= 2 x_4 - x_4^{new} \end{aligned} \tag{4.78}$$

then

$$\begin{aligned} x_3^{new} &= \left\{ \left(1 - 2\alpha_3 h_{31}\right) x_3 - \alpha_3 h_{32} x_5 \right\} / \left(1 - \alpha_3 h_{31}\right) \\ x_4^{new} &= \left\{ \left(1 - 2\alpha_3 h_{31}\right) x_4 - \alpha_3 h_{32} x_6 \right\} / \left(1 - \alpha_3 h_{31}\right) \end{aligned} \tag{4.79}$$

when $\beta_3 h_{32} > 0$, let

$$\begin{aligned} x_5 &= 2 x_5^{new} - x_5 \\ x_6 &= 2 x_6^{new} - x_6 \end{aligned} \tag{4.80}$$

then

$$x_5^{new} = \left\{(1+\beta_3 h_{32})x_5 - \beta_3 h_{31} x_3^{new}\right\}/(1+2\beta_3 h_{32})$$
$$x_6^{new} = \left\{(1+\beta_3 h_{32})x_6 - \beta_3 h_{31} x_4^{new}\right\}/(1+2\beta_3 h_{32}) \quad (4.81)$$

when $\beta_3 h_{32} < 0$, let

$$x_5 = 2x_5 - x_5^{new}$$
$$x_6 = 2x_6 - x_6^{new} \quad (4.82)$$

then

$$x_5^{new} = \left\{(1-2\beta_3 h_{32})x_5 - \beta_3 h_{31} x_3^{new}\right\}/(1-\beta_3 h_{32})$$
$$x_6^{new} = \left\{(1-2\beta_3 h_{32})x_6 - \beta_3 h_{31} x_4^{new}\right\}/(1-\beta_3 h_{32}) \quad (4.83)$$

Following the same procedure described in Region 1, Lyapunov exponents can be calculated.

***At $t = t_4$, Region3 Switches to Region1***

Indicator function is

$$h_4 = h_3 = \tau_{ctr} - \tau_{lower} = 0 \quad (4.84)$$

Jacobian of indicator function is

$$H_4 = H_3 = \left[\frac{\partial h_3}{\partial x_1} \quad \frac{\partial h_3}{\partial x_2}\right] = \left[h_{31} \quad h_{32}\right] \quad (4.85)$$

Jacobian of transition condition is

$$G_4 = G_3 = \begin{bmatrix} 1 & 0 \\ 0 & 1 \end{bmatrix} \quad (4.86)$$

The transition condition of the linearized equations is:

$$\delta x(t_4^+) = G_4(x^-)\delta x(t_4^-) - \left[G_4(x^-) f_3(x(t_4^-)) - f_1(x(t_4^+)\right] \frac{H_4(x^-)\delta x(t_4^-)}{H_4(x^-) f_3(x(t_4^-))} \quad (4.87)$$

where "+" and "_" sign denote the time just after and before switch instants $t_4$.

$$\begin{bmatrix} x_3^{new} & x_4^{new} \\ x_5^{new} & x_6^{new} \end{bmatrix}$$

$$= \begin{bmatrix} 1 & 0 \\ 0 & 1 \end{bmatrix} \begin{bmatrix} x_3 & x_4 \\ x_5 & x_6 \end{bmatrix} - \left\{ \begin{bmatrix} 1 & 0 \\ 0 & 1 \end{bmatrix} \begin{bmatrix} f_{31} \\ f_{32} \end{bmatrix} - \begin{bmatrix} f_{11} \\ f_{12} \end{bmatrix} \right\} \frac{\begin{bmatrix} h_{31} & h_{32} \end{bmatrix} \begin{bmatrix} x_3 & x_4 \\ x_5 & x_6 \end{bmatrix}}{\begin{bmatrix} h_{31} & h_{32} \end{bmatrix} \begin{bmatrix} f_{31} \\ f_{32} \end{bmatrix}}$$

$$= \begin{bmatrix} x_3 & x_4 \\ x_5 & x_6 \end{bmatrix} - \left\{ \begin{bmatrix} f_{31} \\ f_{32} \end{bmatrix} - \begin{bmatrix} f_{11} \\ f_{12} \end{bmatrix} \right\} \frac{\begin{bmatrix} h_{31}x_3 + h_{32}x_5 & h_{31}x_4 + h_{32}x_6 \end{bmatrix}}{h_{31}f_{31} + h_{32}f_{32}}$$

$$= \begin{bmatrix} x_3 & x_4 \\ x_5 & x_6 \end{bmatrix} - \frac{1}{h_{31}f_{31} + h_{32}f_{32}} \begin{bmatrix} f_{31} - f_{11} \\ f_{32} - f_{12} \end{bmatrix} \begin{bmatrix} h_{31}x_3 + h_{32}x_5 & h_{31}x_4 + h_{32}x_6 \end{bmatrix}$$

$$= \begin{bmatrix} x_3 & x_4 \\ x_5 & x_6 \end{bmatrix} - \frac{1}{h_{31}f_{31} + h_{32}f_{32}} \begin{bmatrix} (f_{31} - f_{11})(h_{31}x_3 + h_{32}x_5) & (f_{31} - f_{11})(h_{31}x_4 + h_{32}x_6) \\ (f_{32} - f_{12})(h_{31}x_3 + h_{32}x_5) & (f_{32} - f_{12})(h_{31}x_4 + h_{32}x_6) \end{bmatrix} \tag{4.88}$$

Let

$$\alpha_4 = \frac{f_{31} - f_{11}}{h_{31}f_{31} + h_{32}f_{32}},$$

$$\beta_4 = \frac{f_{32} - f_{12}}{h_{31}f_{31} + h_{32}f_{32}} \tag{4.89}$$

then

$$\begin{bmatrix} x_3^{new} & x_4^{new} \\ x_5^{new} & x_6^{new} \end{bmatrix} = \begin{bmatrix} x_3 & x_4 \\ x_5 & x_6 \end{bmatrix} - \begin{bmatrix} \alpha_4 h_{31}x_3 + \alpha_4 h_{32}x_5 & \alpha_4 h_{31}x_4 + \alpha_4 h_{32}x_6 \\ \beta_4 h_{31}x_3 + \beta_4 h_{32}x_5 & \beta_4 h_{31}x_4 + \beta_4 h_{32}x_6 \end{bmatrix} \tag{4.90}$$

The nonstandard finite difference scheme is:

$$\begin{aligned} x_1^{new} &= x_1 + hx_2 \\ x_2^{new} &= \left\{ x_2 + hf_{22}\left(x_1^{new}, x_2\right) \right\} \end{aligned} \tag{4.91}$$

when $\alpha_4 h_{31} > 0$, let

$$\begin{aligned} x_3 &= 2x_3^{new} - x_3 \\ x_4 &= 2x_4^{new} - x_4 \end{aligned} \tag{4.92}$$

then

$$x_3^{new} = \{(1+\alpha_4 h_{31})x_3 - \alpha_4 h_{32} x_5\}/(1+2\alpha_4 h_{31})$$
$$x_4^{new} = \{(1+\alpha_4 h_{31})x_4 - \alpha_4 h_{32} x_6\}/(1+2\alpha_4 h_{31}) \quad (4.93)$$

when $\alpha_4 h_{31} < 0$, let

$$x_3 = 2x_3 - x_3^{new}$$
$$x_4 = 2x_4 - x_4^{new} \quad (4.94)$$

then

$$x_3^{new} = \{(1-2\alpha_4 h_{31})x_3 - \alpha_4 h_{32} x_5\}/(1-\alpha_4 h_{31})$$
$$x_4^{new} = \{(1-2\alpha_4 h_{31})x_4 - \alpha_4 h_{32} x_6\}/(1-\alpha_4 h_{31}) \quad (4.95)$$

when $\beta_4 h_{32} > 0$, let

$$x_5 = 2x_5^{new} - x_5$$
$$x_6 = 2x_6^{new} - x_6 \quad (4.96)$$

then

$$x_5^{new} = \{(1+\beta_4 h_{32})x_5 - \beta_4 h_{31} x_3^{new}\}/(1+2\beta_4 h_{32})$$
$$x_6^{new} = \{(1+\beta_4 h_{32})x_6 - \beta_4 h_{31} x_4^{new}\}/(1+2\beta_4 h_{32}) \quad (4.97)$$

when $\beta_4 h_{32} < 0$, let

$$x_5 = 2x_5 - x_5^{new}$$
$$x_6 = 2x_6 - x_6^{new} \quad (4.98)$$

then

$$x_5^{new} = \{(1-2\beta_4 h_{32})x_5 - \beta_4 h_{31} x_3^{new}\}/(1-\beta_4 h_{32})$$
$$x_6^{new} = \{(1-2\beta_4 h_{32})x_6 - \beta_4 h_{31} x_4^{new}\}/(1-\beta_4 h_{32}) \quad (4.99)$$

Following the same procedure described in Region 1, Lyapunov exponents can be calculated.

## 4.5 Numerical Results and Discussion

In this section, the numerical results of angular displacements, angular velocities, control torques, control bounds and stability regions determined using Lyapunov exponents are presented and discussed. The simulation program is written using Matlab. Numerical integration time step-size $h = 0.0005$ second, the time series includes 20,000 data values or points. All simulations were conducted using the same physical parameters as those from the reference (Pai and Patton 1997), which together with the control gains, are listed in Table 4.1.

Table 4.1 Physical parameters and control gains

| | |
|---|---|
| Body height | H = 1.78 m |
| Body mass | mass = 80 kg |
| Foot-link mass | $m_f$ = 2*0.0145*mass = 2.32 kg |
| Pendulum mass | m = mass - $m_f$ = 77.68 kg |
| Length of ankle-to-center of mass | r = 0.575*H = 1.02 m |
| Foot-link length | $L_f$ = 0.152*H = 0.27 m |
| Horizontal ankle-to-heel distance | a = 0.19*$L_f$ = 0.05 m |
| Vertical ankle height | b = 0.039*H = 0.07 m |
| Horizontal ankle-to-center of foot-link | c = 0.5*$L_f$ – a = 0.085 m |
| Pendulum length | L = H – b = 1.71 m |
| Coefficient of friction | $\mu = 0.5$ |
| Gravity acceleration | g = 9.80 m/$s^2$ |
| Control gain | $K_p$ = 10000 Nm |
| Control gain | $K_d$ = 2000 Nms |

### 4.5.1 Comparison of conventional PD control and switching state control

To demonstrate the importance of satisfying the constraints between the foot-link and the ground for the control design, a conventional PD controller, designed without the consideration of the constraints, is compared with our state-switching controller. Simulation results are shown in Figure 4.2.

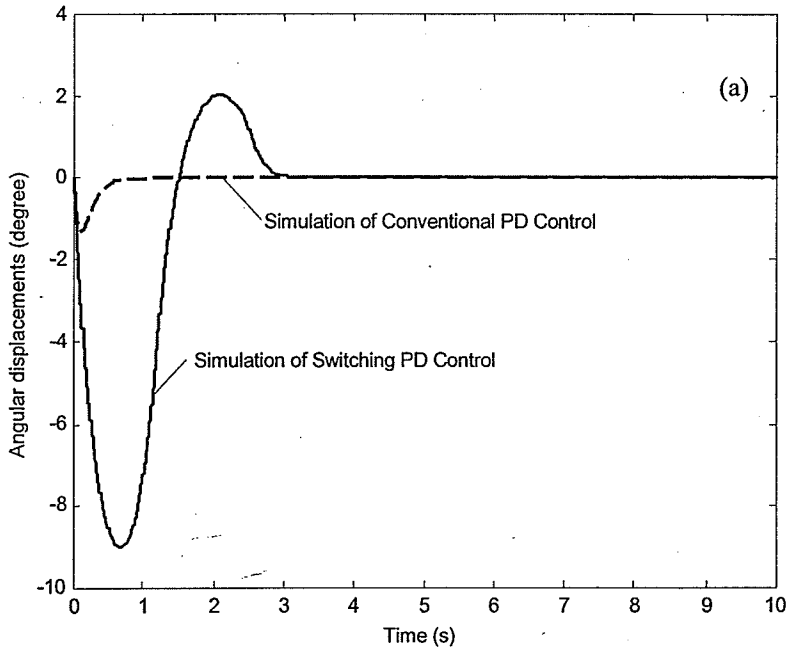

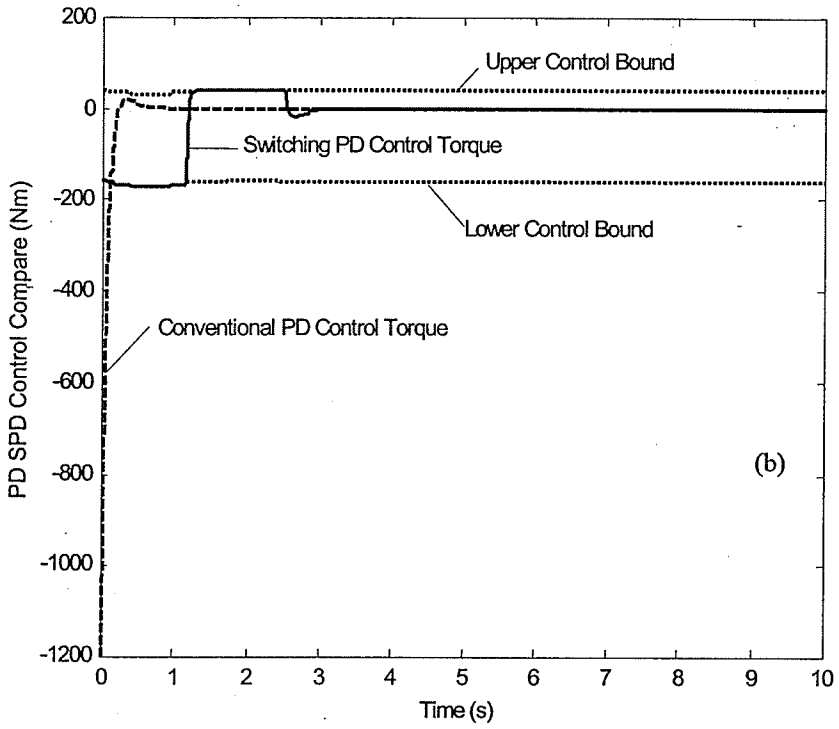


Figure 4.2 Simulation results using a conventional PD controller and the PD-based switching state feedback control, (a) Simulated angular displacements, (b) Control torques.

Figure 4.2a shows the simulated angular displacements using a conventional PD feedback controller and our PD-based switching state feedback controller to stabilize the biped from the initial states $\theta_0 = 0rad$ and $\dot{\theta}_0 = -0.6rad/sec$ to the upright position. Same control gains were used for both controllers. The horizontal axis is simulation time, and the vertical axis is the angular displacement. The solid line represents the angular displacement from our switching state controller, and the dash line represents the one from the conventional PD controller. From Figure 4.2a, one can see that using the conventional PD controller, the biped is stabilized to the upright position within 0.5 second, while using our PD-based switching state controller, the biped oscillates approximately 3 seconds, and then settles down at the upright position. The transient

period from the switching state control system is longer due to the control bounds determined by the constraints.

Figure 4.2b shows the control torques from our PD-based switching state controller (the solid line), the conventional PD controller (the dash line) and the control bounds (dotted lines) satisfying the constraints. The horizontal axis is simulation time, and the vertical axis is the values of the control torque. Figure 4.2b shows that the control torque, determined from our switching state feedback controller, is always within the control bounds, indicating that the constraints between the foot-link and the ground are satisfied, while the control torque from the conventional PD controller is below the lower bound of the control torque. This indicates that if the foot-link is not fixed on the ground, the constraints, shown in Inequality (3.4)., will be violated, and stabilization of the biped robot is out of the question. While for a human subject, he/she can use hip control strategy, upper body and arms movements, even change the base of support to prevent falls.

Together with the simulated angular displacement shown by the solid line in Figure 4.2a, it can be concluded that our PD-based switching state feedback controller can stabilize the biped at the upright position meanwhile satisfying the constraints shown in Inequality (3.4). The simulation results, shown in Figure 4.2, indicate the importance to consider the constraints between the foot-link and the ground when the balance control law is designed.

### 4.5.2 Stability analysis and stability region

Two Lyapunov exponents for the control system shown in Equation (4.2) were calculated. Since Lyapunov exponents involve long-term averaged behaviours of the

system, through simulations, it was observed that for the system with parameters given in Table 4.1, after 100 seconds, the largest Lyapunov exponent converges to $-10.3318$, and the second Lyapunov exponent converges to $-18.0704$. Thus, the control system shown in Equation (4.2) is exponentially stable about the equilibrium point, which is the upright position.

Since Lyapunov exponents remain the same values within the same stability region, the determination of the stability region become an important part of the stability analysis. To determine the stability region, the algorithm developed by Nusse and Yorke (1998) is adapted, where the region of interest is first divided into grid boxes. The grid box at the origin of the state-space (also called 'center box') contains the stable equilibrium point. Next, the size of neighboring grid boxes is chosen and Lyapunov exponents are calculated using the initial states from each neighboring box. If the same convergent and negative exponents are obtained, the neighboring grid box belongs to the stability region. In this work the stability region around the states $\{0rad, -0.6rad/sec\}$ was determined based on the largest Lyapunov exponent. The biped leaning posteriorly was considered only, *i.e.*, the angular displacement ranged from $0^0$ to positive $63^0$ since leaning posteriorly is considered more dangerous.

The region $\Gamma := \{\theta, \dot{\theta}; 0^0 \le \theta < 63^0 \;\&\; -3.0rad/s \le \dot{\theta} \le 0.7rad/s\}$ was divided into grid boxes neighboring the center box with sizes of $5^0$ and 0.1 rad/s for $\theta$ and $\dot{\theta}$, respectively.

The determined stability region is compared with the previous work (Pai and Patton 1997) based on a different stability definition. In their work, the stability was defined based on the clinical observations on balance control of human subjects. From an initial

position, with an initial angular velocity, if the center of mass of the biped can be moved by the control torque determined by an optimal algorithm into a region between the heel and the toe within a short time period (1s) and with a zero angular velocity, this initial state is included in stability region they defined. Both results are shown in Figure 4.3.

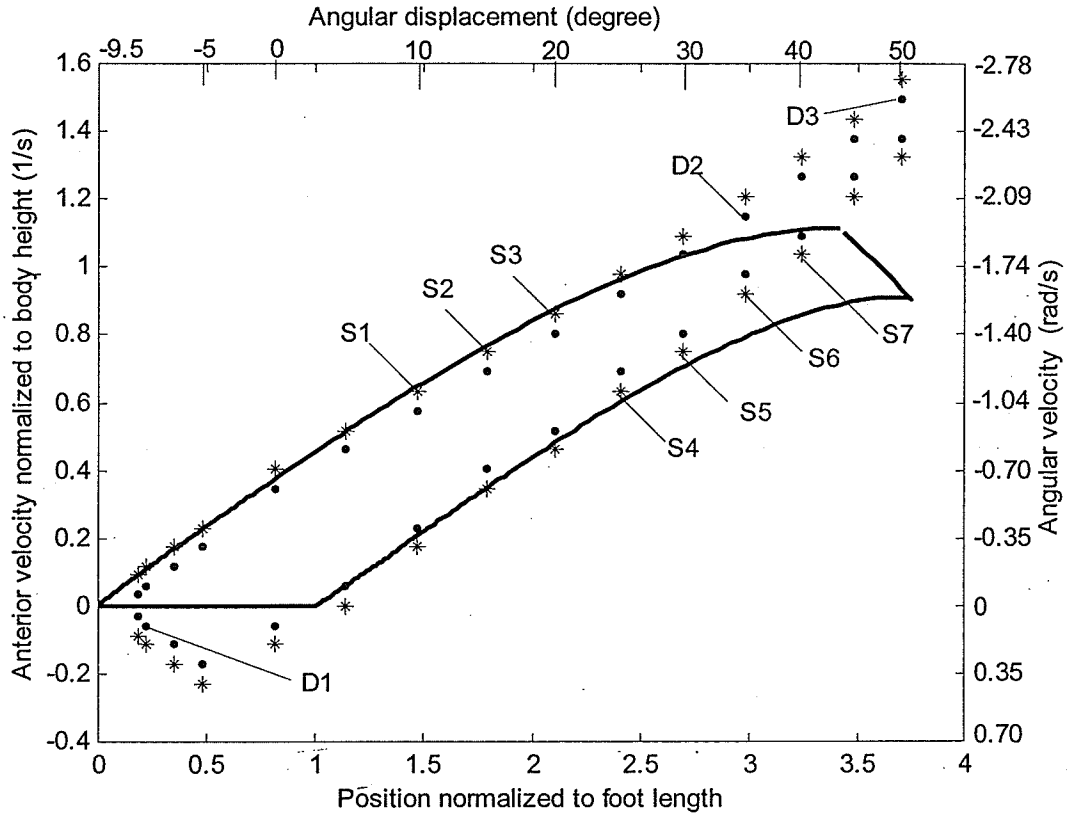


Figure 4.3 Stability regions determined by Lyapunov exponents and from previous work (Pai and Patton 1997).

In Figure 4.3, the horizontal axis on the top is the angular displacement, and the vertical axis on the right is the angular velocity of the biped. The horizontal axis at the bottom of Figure 4.3 is the position of the center of mass normalized to the length of the foot-link, and the vertical axis on the left is the velocity of the mass center normalized to body height, as defined in the reference (Pai and Patton 1997). In Figure 4.3, the region surrounded by the solid curve represents the stability region obtained in the previous

work (Pai and Patton 1997) where neither forward falls nor backward falls of a human subject would be initiated. Dots are the initial states such that convergent and negative Lyapunov exponents were obtained using our PD-based switching state feedback controller, while stars are initial states such that convergent Lyapunov exponents cannot be obtained. Our simulations show that the region surrounded by the dots is a stability region, *i.e.*, the bipedal model can be stabilized at the upright position with the foot-link remaining stationary. Note that such a region surrounded by dots is a part of the stability region, but not necessarily the entire stability region. Finding the entire stability region is important, but it is off the scope of this work. For the region outside the stars, convergent Lyapunov exponents cannot be obtained. Our simulation results further show that in the region outside the stars, failure to obtain convergent Lyapunov exponents is due to the violation of the constraints between the foot-link and the ground. This is because our PD-based switching state controller cannot keep the angular velocity below the critical value. With the constraints violated, the biped collapses, which terminates the simulation.

Although the definitions on stability and the criteria in determining the stability regions, used in this work and the previous one (Pai and Patton 1997), are significantly different, Figure 4.3 shows that both stability regions agree overall reasonably well. Especially as the angular displacement below $30^{\circ}$ and as the value of the angular velocity lower than *1rad/s*, the stability region from our work is almost identical to the one from the previous work (Pai and Patton 1997). Note that the definition of the stability used in the previous work was based on the observations of balancing control of human subjects and was intended to developing a clinical tool to assess a person's ability to maintain standing posture. Such a definition only concerns the system performance within a short

time period, while Lyapunov stability deals with long-term dynamic behaviour. The agreement between the two stability regions suggests that the two stability concepts are related and, to certain extent, are equivalent. The equivalence indicates that the concept of Lyapunov exponents has great potential to be used as a measure for assessing a person's ability to maintain the upright posture during disturbed/undisturbed standing.

## 4.6 Further Discussion on Stability Region

In spite of the agreement, there are some differences in the two stability regions. In the stability region surrounded by the solid curve (Pai and Patton 1997), there are stars ($S_1$, $S_2$, ... , $S_7$), where, based on the concept of Lyapunov exponents, the biped cannot be stabilized at the upright position. Simulation results of the angular displacement and velocity using our PD-based switching state controller are shown in Figure 4.4, with the initial states $\theta_0 = 10^\circ$ and $\dot{\theta}_0 = -1.1 rad/sec$, corresponding to the star $S_1$ in Figure 4.3.

In Figure 4.4a, the solid line represents the angular displacement, and the dotted lines represent the angular displacements of the biped when its center of mass is above the base of support. In Figure 4.4b, the solid line represents the angular velocity and the dash line represents the zero angular velocity, which is one of the requirements for determining the stability region (Pai *et al.* 1997). Figure 4.4 shows that the center of mass of the biped moves into the region between the heel and the toe within 0.3 second. The angular velocity reaches close to zero at approximate 1 second (*-0.08rad/sec*). According to the criteria from the previous work (Pai and Patton 1997), star $S_1$ is in the stability region. However, as one observes the bipedal movement for a longer period of time, the controller cannot keep the biped close to the upright position due to the limited control torque. As the biped falls out of the stability region determined from the previous work

(Pai and Patton 1997), the angular velocity increases, which causes the violation of the constraints. Once the constraints are violated, balance control is out of the question; simulation is terminated and Lyapunov exponents cannot be determined.

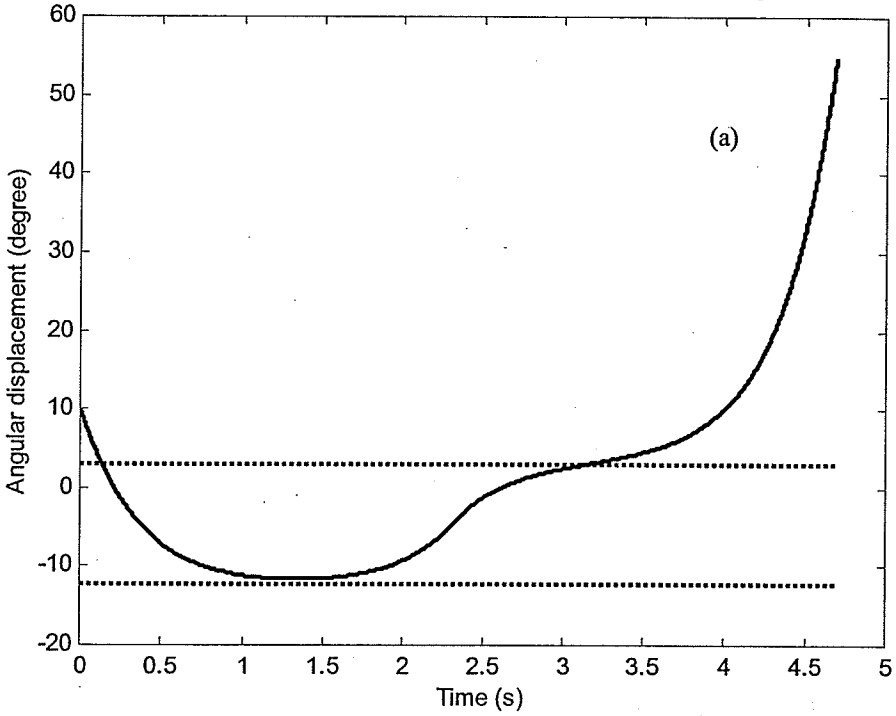

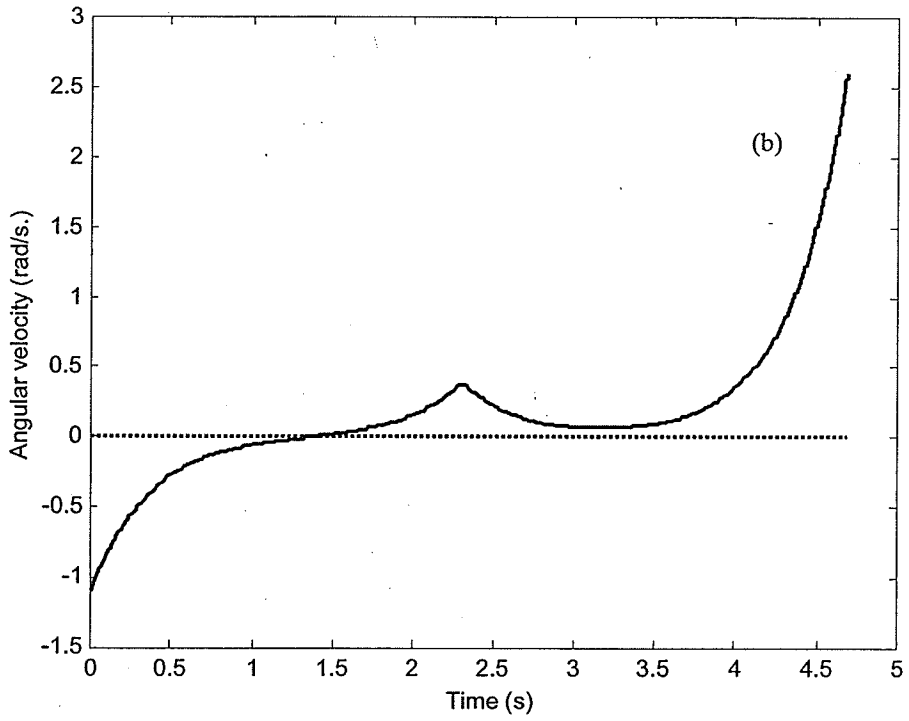


Figure 4.4 Simulated motion of $S_1$ in Figure 4.3.
(a) Angular displacement, (b) Angular velocity.

On the other hand, outside the stability region from the previous work (Pai and Patton 1997), there are dots, such as $D_1$, $D_2$, and $D_3$, *etc.*, shown in Figure 4.3, where Lyapunov exponents converge and are negative, indicating that the biped can be stabilized about the upright position. Simulation results of the angular displacement and velocity using our PD-based switching state controller are shown in Figure 4.5, with the initial states $\theta_0 = 50^\circ$ and $\dot{\theta}_0 = -2.6 rad/sec$, corresponding to the dot $D_3$ in Figure 4.3.

Figure 4.5 shows that the angular displacement (the solid line in Figure 4.5a) reaches the region where the center of mass of the biped is above the heel within the time period of 1 second, but the angular velocity is below zero (*-0.14rad/sec*). Based on the criteria in the previous work (Pai and Patton 1997), dot $D_3$ is outside the stability region. However, the simulation results show that the biped can be stabilized around the upright position

with the transient period of approximately 1.6 seconds while keeping the foot-link stationary. This is also supported by the fact that the Lyapunov exponents are all negative.

The discrepancy between our work and the previous work (Pai and Patton 1997) occurs mainly in the region where the biped leans posteriorly with a large angle ($\theta_0 > 30^o$) and with a high value of the angular velocity ($\dot{\theta}_0 < -1.4 rad/sec$). It is unrealistic that humans and bipedal robots lean posteriorly about the ankle keeping the knees and the hip straight at such a large angle and with such a high angular velocity. Note that in the previous work (Pai and Patton 1997), the stability region with only negative angular velocity was determined. Thus, no comparison can be made as the biped model is around the upright position, within $-9^o$ and $3^o$.

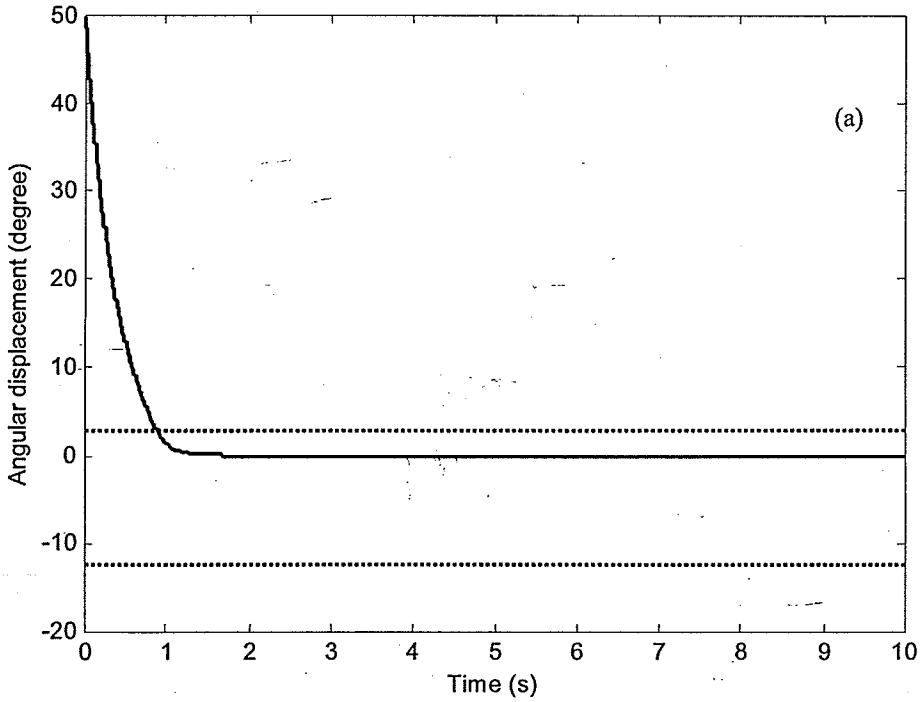

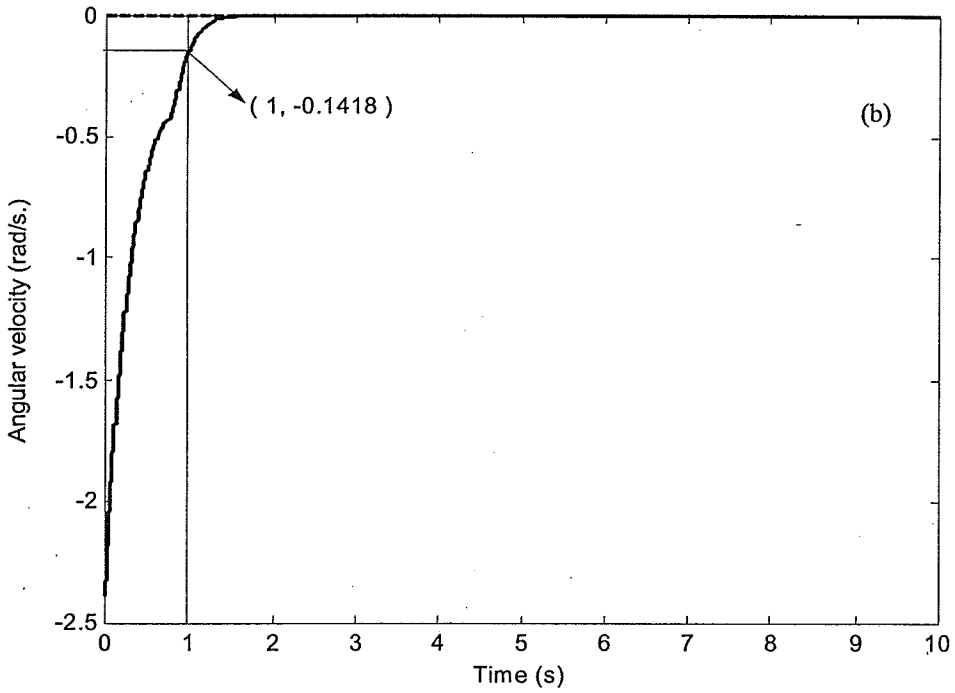


Figure 4.5 Simulated motion of $D_3$ in Figure 4.3
(a) angular displacement, (b) angular velocity.

The comparison of the stability region determined by the Lyapunov exponent with the "controllable regions", defined as the regions that it is possible to design a controller to stabilize the biped to upright position and to maintain the foot-link still on the ground is shown in Figure 4.6. Such "controllable regions" are determined by satisfying all constraints (refer Section 3.5 in Chapter 3 for detailed discussions).

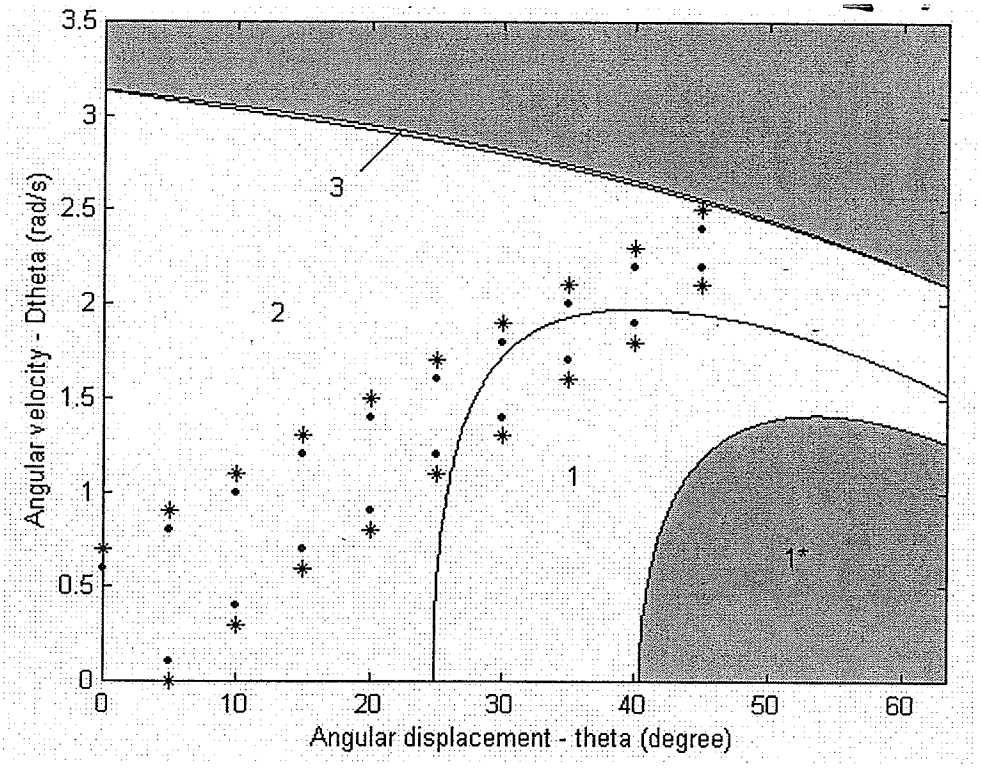


Figure 4.6 Stability region

In Figure 4.6, x-axis is the angular displacement of the biped, and y-axis is the angular velocity. Only the biped leaning posteriorly is considered, *i.e.*, the angular foot displacement ranges from $0^0$ to positive $63^0$ since leaning posteriorly is considered more dangerous. The grey regions are termed as "uncontrollable regions", while the "controllable regions" is shown as the white regions. Both white and grey regions are further divided into sub-regions, where the control bounds are determined by different constraints (refer Section 3.5 in Chapter 3 for detailed discussions). In the grey regions, regardless of the controllers, the constraints between the foot-link and the ground will be violated. Thus, it is impossible to design any controllers to stabilize the biped while keeping the foot-link stationary. Dots and stars in Figure 4.6 are defined the same as those in Figure 4.3. Thus, the region surrounded by dots represents the stability regions using our PD-based switching state controller. The biped with the states in the region outside

the stars is unstable. Our simulations show that, in the region outside the stars, the limited control torque is not adequate to balance the biped. As the biped deviates from the upright position, the angular velocity increases higher than the critical value, *i.e.*, the biped falls in the "uncontrollable region", where the constraints between the foot-link and the ground are violated.

Results, shown in Figure 4.6, raise two important issues. One is that the stability region only takes a small portion of the "controllable region". This is due to the simple PD-based switching state control. Thus, designing an advanced nonlinear controller that can stabilize the biped in a large portion of the "controllable region" is highly desirable. Another issue is that the instability region outside the stars is dictated by the condition on the angular velocity. This is because the controller was designed to satisfy the control bounds. The condition imposed on the angular velocity was not considered in the control design, but it was checked and once it is violated, the simulation was terminated, and the biped was considered collapsed. This finding indicates that the consideration of the condition imposed on the angular velocity in the control design is important.

## 4.7 Summary

In this chapter, the balance control of disturbed bipedal standing is investigated. A simple PD-based switching state feedback control is proposed, which determine the ankle torque to stabilize the biped at the upright posture while satisfying the constraints between the foot-link and the ground. The importance of consideration of the constraints between the foot-link and the ground when designing the balance control law is demonstrated. The same inverted pendulum model presented in Chapter 3 is used. The stability of such a control system is analyzed using the concept of Lyapunov exponents, and a stability

region is determined. Since Lyapunov exponents are calculated numerically, a nonstandard finite difference scheme is constructed in detail to ensure the numerical stability and improve the computational efficiency. Non-smooth instants are expressed using Müller's method. Stability region is determined using the concept of Lyapunov exponent based on the mathematical model and basin of attraction method. Furthermore, the stability region is compared and agrees well with the one from the previous work that predicts the feasible movement during which balance of human standing can be maintained. This agreement shows the potential of the concept of Lyapunov exponents to be used as a measure of balance control of human standing. The work contributes to bipedal balance control, which is important in the development of bipedal walking machines.

# Chapter 5

# Stability Analysis of Bipedal Standing via Lyapunov Exponents Calculated from a Time Series Using Nonlinear Mapping – A Case Study

## 5.1 Introduction

In this chapter, a method for stability analysis based on Lyapunov exponents calculated from time series for potentially stable engineering systems is described. The time series used in this paper is obtained from numerical simulation of the mathematical model, which is derived for balancing of a bipedal robot subjected to the constraints between the foot-link and the ground (detailed in reference Yang and Wu 2005, 2006a, 2006b, 2006c). The method of higher order Taylor series expansion for generating local neighbour-to-neighbour mapping in order to construct more accurate mapping matrices *Js* is presented in detail. This work belongs to step 2 and step 3 in the procedure described in Chapter 2, whole spectra of Lyapunov exponents can be obtained.

## 5.2 Method

In this section, the main procedure of calculating Lyapunov exponents based on time series given in Chapter 2 is reviewed and the problem that prohibits the applications are pointed out. Next, how to use higher-order Taylor series expansion getting more accurate

local neighborhood-to-neighborhood mapping is introduced, and then second-order Taylor series expansion is taken as an example to demonstrate how to obtain local neighborhood-to-neighborhood mapping, the coefficients which are needed for describing the mapping and how to construct the mapping matrices *Js*, which play an important role on calculating Lyapunov exponents.

The reconstruction method has been developed for the construction of the phase space in which the dynamics of the system dwells. The result of this reconstruction is a $d_E$-dimensional embedding space (phase space) in which one may observe the attractor. One can view the evolution in the reconstructed phase space of the many dimensional dynamics in a quantitative fashion in the time domain. The $d_E$-dimensional embedding space enclosing the attractor should be sufficiently large than the dimension of the real system $d$ that all the geometric information about the attractor is exposed in the embedding space. Takens' formal result requires $d_E > 2d+1$ assuring one of a faithful representation of the $m$ dimensional attractor as seen in the $d_E$-dimensional embedding space, but often, in practice, $d_E > d$ will do. The method of phase space reconstruction seeks to construct from the $x(n)$'s $d_E$-dimensional vectors which, when embedded in $R^{dE}$ describes the full dynamical evolution of the system.

In this work, the author assumes that the embedding dimension $d_E$ is known, the data set is accurate and long enough. The noise is absent from the time series when we receive them.

Following the developmental work of numerous others (Wolf *et al.* 1985, Eckmann *et al.* 1986, Bryant *et al.* 1990, Rauf and Ahmed 1991, Abarbanel *et al.* 1991, 1992, 1996, Sano and Sawada 1995, Williams 1997, Sakai *et al.* 2003), a set of lagged variables $x(n), x(n+T_{lag}), x(n+2T_{lag}),\ldots, x(n+(d_E-1)T_{lag})$ is used. They act as the coordinates in a $d_E$-dimensional space in which the dynamics producing the $x(n)$'s is fully captured or embedded.

The procedure of calculating Lyapunov exponents from a time series includes the following steps (Williams 1997, Brown *et al.* 1991):

*1.* Reconstructing the dynamics in a finite dimensional space.

Choose an embedding dimension $d_E$ and construct a $d_E$-dimensional orbit representing the time evolution of the system by the time-lag method. This means we define

$$\vec{y}_i = (x_i, x_{i+T_{lag}}, \ldots, x_{i+(d_E-1)T_{lag}}) \tag{5.1}$$

where $T_{lag}$ is the time lag. This provides the fuducial trajectory for the analysis of Lyapunov exponents.

*2.* Determining the neighbors of $\vec{y}_i$, *i.e.*, the point $\vec{y}_j$ of the orbit which are contained in a shell of suitable radius $r$, and $r_{min}$ centered at $\vec{y}_i$,

$$r_{\min} \le \left\| \vec{y}_j - \vec{y}_i \right\| \le r \tag{5.2}$$

*3.* Determining the $d_E \times d_E$ matrix $J_i$ which describes how the time evolution sends small vectors around $\vec{x}_i$ to small vectors around $\vec{x}_{i+1}$. The matrix $J_i$ is obtained by looking for neighbors $\vec{x}_j$ of $\vec{x}_i$, and imposing

$$J_i(\vec{x}_j - \vec{x}_i) \approx \vec{x}_{j+1} - \vec{x}_{i+1} \tag{5.3}$$

The elements of $J_i$ are obtained by a least-squares fit (described later)

*4.* Step 3 gives a sequence of matrices $J_i$, $J_{i+T_1}$, $J_{i+2T_1}$, .... Using QR decomposition, one determines successively orthogonal matrices $Q_{(j)}$ and upper triangular matrices $R_{(j)}$ with positive diagonal elements such that $Q_{(0)}$ is the unit matrix and

$$\begin{aligned} J_1 Q_{(0)} &= Q_{(1)} R_{(1)} \\ J_{1+T_1} Q_{(1)} &= Q_{(2)} R_{(2)} \\ &\cdots \\ J_{1+jT_1} Q_{(j)} &= Q_{(j+1)} R_{(j+1)} \end{aligned} \tag{5.4}$$

This decomposition is unique except in the case of zero diagonal elements. Then Lyapunov exponents $\lambda_k^i$ are given by

$$\lambda_k^i = \frac{1}{Tk} \sum_{j=0}^{K-1} \ln R_{(j)ii} \tag{5.5}$$

Where K is the available number of matrices, $T$ is sampling time step, $i = 1,2,...,d_E$

*5.* Repeating Step 2 through Step 4 along the fiducial trajectory, until the convergent Lyapunov exponents are achieved.

Within these five steps, it is believed that the linear Taylor series expansion of the embedded system prevent the applicability of the method of Lyapunov exponents to stable systems. Nonlinear expressions, *i.e.*, the higher-order expansions instead of the linear expression will be used. Since in principle, using higher-order expansions, the local neighborhood-to-neighborhood mapping one obtained includes more information of underlying dynamical system than just using local linear mapping, and more accurate description of the system will be achieved.

### 5.2.1 Generation of higher order mappings

In the Taylor series expansion, the relationship among the order of the Taylor series, $N_{Tay}$, the embedding dimension of the phase space, $d_E$, and the minimum number of parameters $N_p$ is given by the following equation (Zeng *et al.* 1992):

$$N_p = \left[ \prod_{k=1}^{N_{Tay}} \frac{d_E + k}{k} \right] - 1 = \frac{(d_E + N_{Tay})!}{d_E! N_{Tay}!} - 1 \tag{5.6}$$

Partial results based on Equation (5.6) are shown in Table 5.1. From Table 5.1, it is observed that $N_p$ grows rather rapidly with the order of Taylor series $N_{Tay}$ and the dimensions of reconstructed phase space $d_E$. The minimum number of parameters $N_p$ is also the minimum number of neighbors required to calculate values for the fitting parameters in the expansion. Using less than $N_p$ neighbors would result in un-determined least-squares fit.

Table 5.1 The minimum number of parameter $N_p$

| $N_p$ | $d_E$ =1 | 2 | 3 | 4 | 5 | 6 | 7 | 8 |
|---|---|---|---|---|---|---|---|---|
| $N_{Tay}$=1 | 1 | 2 | 3 | 4 | 5 | 6 | 7 | 8 |
| $N_{Tay}$=2 | 2 | 5 | 9 | 14 | 20 | 27 | 35 | 44 |
| $N_{Tay}$=3 | 3 | 9 | 19 | 34 | 55 | 83 | 119 | 164 |
| $N_{Tay}$=4 | 4 | 14 | 34 | 69 | 125 | 209 | 329 | 494 |
| $N_{Tay}$=5 | 5 | 20 | 55 | 125 | 251 | 461 | 791 | 1286 |
| $N_{Tay}$=6 | 6 | 27 | 83 | 209 | 461 | 923 | 1715 | 3002 |
| $N_{Tay}$=7 | 7 | 35 | 119 | 329 | 791 | 1715 | 3431 | 6434 |

For a fiducial orbit $y(n)$, its $r^{\text{th}}$ neighbor is defined as $y^r(n)$, the small displacement between $y^r(n)$ and $y(n)$ is represented by $Z^r(n;T_0)$, after time-step $T_1$, the small displacement is represented by $Z^r(n;T_1)$. In the embedding phase space, $Z^r(n;T_1)$ have $d_E$ components.

Let $Z^r_\alpha(n;T_1)$ be the $\alpha^{th}$ component of $Z^r(n;T_1)$. Expanding the local neighborhood-to-neighborhood mapping $F$ (which is a nonlinear function) in a Taylor series about the fiducial orbit $y(n)$, one has

$$Z^r_\alpha(n;T_1) = DF_{\alpha\beta}(n)Z^r_\beta(n;T_0) + DF^{(2)}_{\alpha\beta\gamma}(n)Z^r_\beta(n;T_0)Z^r_\gamma(n;T_0) + \ldots \tag{5.7}$$

where
$$DF^{(2)}_{\alpha\beta}(n) = \frac{\partial F_\alpha}{\partial F_\beta}, \tag{5.8a}$$

$$DF^{(2)}_{\alpha\beta\gamma}(n) = \frac{1}{2!}\frac{\partial^2 F_\alpha}{\partial y_\beta \partial y_\gamma} \tag{5.8b}$$

In summary, one can get the common form of Matrix $J$ for any dimension $d_E$, as follows:

$$J_{k,l} = \partial F_{kl} + \frac{1}{2}\sum_{\alpha=1}^{d_E} \partial F_{kl\alpha} Z^r_\alpha, \quad k,l = 1,\ldots,d_E \tag{5.9}$$

For example,

If $d_E$=2, $$J_{12} = \partial F_{12} + \frac{1}{2}\left\{\partial F_{121} Z_1^r + \partial F_{122} Z_2^r\right\} \quad (5.10a)$$

If $d_E$=3, $$J_{12} = \partial F_{12} + \frac{1}{2}\left\{\partial F_{121} Z_1^r + \partial F_{122} Z_2^r + \partial F_{123} Z_3^r\right\} \quad (5.10b)$$

If $d_E$=4, $$J_{12} = \partial F_{12} + \frac{1}{2}\left\{\partial F_{121} Z_1^r + \partial F_{122} Z_2^r + \partial F_{123} Z_3^r + \partial F_{124} Z_4^r\right\} \quad (5.10c)$$

Once the matrix, *J*s, at each time instant, is determined, Lyapunov exponents are obtained using Equations (5.4) and (5.5). In this work, the second-order mapping, *i.e.*, the order of Taylor series $N_{Tay}$ is equal to 2, is used for constructing the mapping matrices *J*s, and the derivation is presented in details when the dimension of reconstructed phase space $d_E$ is equal to 2, because the case studied here is a two dimensional system. To the best of the author's knowledge, this is the first time the 2nd order mapping is used to calculate the negative Lyapunov exponents.

### 5.2.2 Construction of mapping matrix *Js* for $N_{Tay} = 2$, and $d_E = 2$

From Equation (5.6), the minimum number of parameters $N_p$ is equal to five, thus 5 neighbors, and 10 coefficients should be determined. In Equation (5.7), $\alpha = 1,2$, so, Equation (5.7) can be written as

$$Z_1^r(n;T_1) = \partial F_{11} Z_1^r(n;T_0) + \partial F_{12} Z_2^r(n;T_0) + \frac{1}{2!}\left\{\partial F_{111} Z_1^r(n;T_0) Z_1^r(n;T_0) + 2\partial F_{112} Z_1^r(n;T_0) Z_2^r(n;T_0) + \partial F_{122} Z_2^r(n;T_0) Z_2^r(n;T_0)\right\} \quad (5.11a)$$

$$Z_2^r(n;T_1) = \partial F_{21} Z_1^r(n;T_0) + \partial F_{22} Z_2^r(n;T_0) + \frac{1}{2!}\left\{\partial F_{211} Z_1^r(n;T_0) Z_1^r(n;T_0) + 2\partial F_{212} Z_1^r(n;T_0) Z_2^r(n;T_0) + \partial F_{222} Z_2^r(n;T_0) Z_2^r(n;T_0)\right\} \quad (5.11b)$$

Re-writing Equation (5.11) in a matrix form, one has

$$\begin{pmatrix} Z_1^r(n;T_1) \\ Z_2^r(n;T_1) \end{pmatrix} = \begin{bmatrix} J_{11} & J_{12} \\ J_{21} & J_{22} \end{bmatrix} \begin{pmatrix} Z_1^r(n;T_0) \\ Z_2^r(n;T_0) \end{pmatrix} \tag{5.12}$$

where

$$\begin{aligned} J_{11} &= \partial F_{11} + \frac{1}{2!}[\partial F_{111} Z_1^r(n;T_0) + \partial F_{112} Z_2^r(n;T_0)] \\ J_{12} &= \partial F_{12} + \frac{1}{2!}[\partial F_{112} Z_1^r(n;T_0) + \partial F_{122} Z_2^r(n;T_0)] \\ J_{21} &= \partial F_{21} + \frac{1}{2!}[\partial F_{211} Z_1^r(n;T_0) + \partial F_{212} Z_2^r(n;T_0)] \\ J_{22} &= \partial F_{22} + \frac{1}{2!}[\partial F_{212} Z_1^r(n;T_0) + \partial F_{222} Z_2^r(n;T_0)] \end{aligned} \tag{5.13}$$

From Equation (5.11), 10 coefficients should be determined. These coefficients can be determined using the least-square method, which minimizes the following distance

$$\Pi = \sum_{i=1}^{N_p} \left\| Z^i(n;T_1) - JZ^i(n;T_0) \right\|^2 \tag{5.14}$$

To simplify the expression of Equation (5.13), let

$$\begin{aligned} &\partial F_{11} = a_1,\ \partial F_{111} = a_2,\ \partial F_{112} = a_3,\ \partial F_{12} = a_4,\ \partial F_{122} = a_5,\ \partial F_{21} = b_1,\ \partial F_{211} = b_2, \\ &\partial F_{212} = b_3,\ \partial F_{22} = b_4,\ \partial F_{222} = b_5, Z_\alpha^r(n;T_0) = v_\alpha^r \end{aligned} \tag{5.15}$$

Then Equation (5.13) can be written as

$$\begin{aligned} J_{11} &= a_1 + \frac{1}{2!}\left(a_2 v_1^i + a_3 v_2^i\right) = a_1 + \frac{1}{2} a_2 v_1^i + \frac{1}{2} a_3 v_2^i \\ J_{12} &= a_4 + \frac{1}{2!}\left(a_3 v_1^i + a_5 v_2^i\right) = a_4 + \frac{1}{2} a_3 v_1^i + \frac{1}{2} a_5 v_2^i \\ J_{21} &= b_1 + \frac{1}{2!}\left(b_2 v_1^i + b_3 v_2^i\right) = b_1 + \frac{1}{2} b_2 v_1^i + \frac{1}{2} b_3 v_2^i \\ J_{22} &= b_4 + \frac{1}{2!}\left(b_3 v_1^i + b_5 v_2^i\right) = b_4 + \frac{1}{2} b_3 v_1^i + \frac{1}{2} b_5 v \end{aligned} \tag{5.16}$$

The procedure of obtaining coefficients $a_i, b_i, (i=1,...,5)$ is derived in details. First, two sets of linear equations are derived by minimizing the distance based on the least-square method, and then the solutions to the linear equations are obtained.

The lease-square method to show the distance is:

$$\begin{aligned}\Pi &= \sum_{i=1}^{N_p}\left\|Z^i(n;T_1)-JZ^i(n;T_0)\right\|^2 = \sum_{i=1}^{N_p}\left\|Z^i - Jv^i\right\|^2 \\ &= \sum_{i=1}^{N_p}\left\{\left(Z_1^i - J_{11}v_1^i - J_{12}v_2^i\right)^2 + \left(Z_2^i - J_{21}v_1^i - J_{22}v_2^i\right)^2\right\} \\ &= \sum_{i=1}^{N_p}\left\{Z_1^i - \left(a_1 + \frac{1}{2}a_2v_1^i + \frac{1}{2}a_3v_2^i\right)v_1^i - \left(a_4 + \frac{1}{2}a_3v_1^i + \frac{1}{2}a_5v_2^i\right)v_2^i\right\}^2 \\ &+ \sum_{i=1}^{N_p}\left\{Z_2^i - \left(b_1 + \frac{1}{2}b_2v_1^i + \frac{1}{2}b_3v_2^i\right)v_1^i - \left(b_4 + \frac{1}{2}b_3v_1^i + \frac{1}{2}b_5v_2^i\right)v_2^i\right\}^2\end{aligned} \tag{5.17}$$

where $a_i, b_i, v_\alpha^i, (i=1,...,5), (\alpha=1,2)$, are defined in Equation (5.15), $J_{ij}, (i,j=1,2)$ are defined in Equation (5.16).

To minimize the above distance, the following linear equations are obtained:

$$\frac{\partial\Pi}{\partial a_1} = \sum_{i=1}^{N_p} 2\left[Z_1^i - \left(a_1 + \frac{1}{2}a_2v_1^i + \frac{1}{2}a_3v_2^i\right)v_1^i - \left(a_4 + \frac{1}{2}a_3v_1^i + \frac{1}{2}a_5v_2^i\right)v_2^i\right]v_1^i = 0 \tag{5.18a}$$

$$\frac{\partial\Pi}{\partial a_2} = \sum_{i=1}^{N_p} 2\left[Z_1^i - \left(a_1 + \frac{1}{2}a_2v_1^i + \frac{1}{2}a_3v_2^i\right)v_1^i - \left(a_4 + \frac{1}{2}a_3v_1^i + \frac{1}{2}a_5v_2^i\right)v_2^i\right]\frac{1}{2}v_1^iv_1^i = 0 \tag{5.18b}$$

$$\frac{\partial\Pi}{\partial a_3} = \sum_{i=1}^{N_p} 2\left[Z_1^i - \left(a_1 + \frac{1}{2}a_2v_1^i + \frac{1}{2}a_3v_2^i\right)v_1^i - \left(a_4 + \frac{1}{2}a_3v_1^i + \frac{1}{2}a_5v_2^i\right)v_2^i\right]v_1^iv_2^i = 0 \tag{5.18c}$$

$$\frac{\partial\Pi}{\partial a_4} = \sum_{i=1}^{N_p} 2\left[Z_1^i - \left(a_1 + \frac{1}{2}a_2v_1^i + \frac{1}{2}a_3v_2^i\right)v_1^i - \left(a_4 + \frac{1}{2}a_3v_1^i + \frac{1}{2}a_5v_2^i\right)v_2^i\right]v_2^i = 0 \tag{5.18d}$$

$$\frac{\partial\Pi}{\partial a_5} = \sum_{i=1}^{N_p} 2\left[Z_1^i - \left(a_1 + \frac{1}{2}a_2v_1^i + \frac{1}{2}a_3v_2^i\right)v_1^i - \left(a_4 + \frac{1}{2}a_3v_1^i + \frac{1}{2}a_5v_2^i\right)v_2^i\right]\frac{1}{2}v_2^iv_2^i = 0 \tag{5.18e}$$

$$\frac{\partial \Pi}{\partial b_1} = \sum_{i=1}^{N_p} 2\left[ Z_2^i - \left( b_1 + \frac{1}{2} b_2 v_1^i + \frac{1}{2} b_3 v_2^i \right) v_1^i - \left( b_4 + \frac{1}{2} b_3 v_1^i + \frac{1}{2} b_5 v_2^i \right) v_2^i \right] v_1^i = 0 \tag{5.18f}$$

$$\frac{\partial \Pi}{\partial b_2} = \sum_{i=1}^{N_p} 2\left[ Z_2^i - \left( b_1 + \frac{1}{2} b_2 v_1^i + \frac{1}{2} b_3 v_2^i \right) v_1^i - \left( b_4 + \frac{1}{2} b_3 v_1^i + \frac{1}{2} b_5 v_2^i \right) v_2^i \right] \frac{1}{2} v_1^i v_1^i = 0 \tag{5.18g}$$

$$\frac{\partial \Pi}{\partial b_3} = \sum_{i=1}^{N_p} 2\left[ Z_2^i - \left( b_1 + \frac{1}{2} b_2 v_1^i + \frac{1}{2} b_3 v_2^i \right) v_1^i - \left( b_4 + \frac{1}{2} b_3 v_1^i + \frac{1}{2} b_5 v_2^i \right) v_2^i \right] v_1^i v_2^i = 0 \tag{5.18h}$$

$$\frac{\partial \Pi}{\partial b_4} = \sum_{i=1}^{N_p} 2\left[ Z_2^i - \left( b_1 + \frac{1}{2} b_2 v_1^i + \frac{1}{2} b_3 v_2^i \right) v_1^i - \left( b_4 + \frac{1}{2} b_3 v_1^i + \frac{1}{2} b_5 v_2^i \right) v_2^i \right] v_2^i = 0 \tag{5.18i}$$

$$\frac{\partial \Pi}{\partial b_5} = \sum_{i=1}^{N_p} 2\left[ Z_2^i - \left( b_1 + \frac{1}{2} b_2 v_1^i + b_3 v_2^i \right) v_1^i - \left( b_4 + b_3 v_1^i + \frac{1}{2} b_5 v_2^i \right) v_2^i \right] \frac{1}{2} v_2^i v_2^i = 0 \tag{5.18j}$$

The above linear equations can be written as matrix form as

$$U_A = CA, U_B = CB$$

where

$$A = (a_1, a_2, a_3, a_4, a_5)^T \tag{5.19a}$$

$$B = (b_1, b_2, b_3, b_4, b_5)^T \tag{5.19b}$$

$$U_A = \left( \sum_{i=1}^{N_p} Z_1^i v_1^i, \sum_{i=1}^{N_p} Z_1^i \left( v_1^i \right)^2, \sum_{i=1}^{N_p} Z_1^i v_1^i v_2^i, \sum_{i=1}^{N_p} Z_1^i v_2^i, \sum_{i=1}^{N_p} Z_1^i \left( v_2^i \right)^2 \right)^T \tag{5.19c}$$

$$U_B = \left( \sum_{i=1}^{N_p} Z_2^i v_1^i, \sum_{i=1}^{N_p} Z_2^i \left( v_1^i \right)^2, \sum_{i=1}^{N_p} Z_2^i v_1^i v_2^i, \sum_{i=1}^{N_p} Z_2^i v_2^i, \sum_{i=1}^{N_p} Z_2^i \left( v_2^i \right)^2 \right)^T \tag{5.19d}$$

$$C=\begin{pmatrix} \sum_{i=1}^{N_p}(v_1^i)^2 & \frac{1}{2}\sum_{i=1}^{N_p}(v_1^i)^3 & \sum_{i=1}^{N_p}(v_1^i)^2 v_2^i & \sum_{i=1}^{N_p} v_1^i v_2^i & \frac{1}{2}\sum_{i=1}^{N_p} v_1^i (v_2^i)^2 \\ \sum_{i=1}^{N_p}(v_1^i)^3 & \frac{1}{2}\sum_{i=1}^{N_p}(v_1^i)^4 & \sum_{i=1}^{N_p}(v_1^i)^3 v_2^i & \sum_{i=1}^{N_p}(v_1^i)^2 v_2^i & \frac{1}{2}\sum_{i=1}^{N_p}(v_1^i)^2 (v_2^i)^2 \\ \sum_{i=1}^{N_p}(v_1^i)^2 v_2^i & \frac{1}{2}\sum_{i=1}^{N_p}(v_1^i)^3 v_2^i & \sum_{i=1}^{N_p}(v_1^i)^2 (v_2^i)^2 & \sum_{i=1}^{N_p} v_1^i (v_2^i)^2 & \frac{1}{2}\sum_{i=1}^{N_p} v_1^i (v_2^i)^3 \\ \sum_{i=1}^{N_p} v_1^i v_2^i & \frac{1}{2}\sum_{i=1}^{N_p}(v_1^i)^2 v_2^i & \sum_{i=1}^{N_p} v_1^i (v_2^i)^2 & \sum_{i=1}^{N_p}(v_2^i)^2 & \frac{1}{2}\sum_{i=1}^{N_p}(v_2^i)^3 \\ \sum_{i=1}^{N_p} v_1^i (v_2^i)^2 & \frac{1}{2}\sum_{i=1}^{N_p}(v_1^i)^2 (v_2^i)^2 & \sum_{i=1}^{N_p} v_1^i (v_2^i)^3 & \sum_{i=1}^{N_p}(v_2^i)^3 & \frac{1}{2}\sum_{i=1}^{N_p}(v_2^i)^4 \end{pmatrix} \quad (5.19e)$$

The solutions of the coefficients, $a_i$ and $b_i$ listed in vectors $A$ and $B$, can be determined provided that matrix $C$ is invertible. In this work, it only occurred at some isolated points that matrix $C$ is not invertible, which have been neglected. It was found that the selection of the time lag, $T_{lag}$, and evolving time, $T_{evol}$, can affect the occurrence of non-invertible matrix, C. However, more in-depth research on the invertibility of matrix, C, is needed, which remains as future work.

After getting these coefficients, the mapping matrices $Js$ can be constructed according to Equation (5.16)

$$J=\begin{bmatrix} J_{11} & J_{12} \\ J_{21} & J_{22} \end{bmatrix} \quad (5.20)$$

These mapping matrices $Js$ work as the acting functions. Under the action of these mapping functions, the small hyper-sphere will change to hyper-ellipsoid, and then following the procedure described in Wolf *et al.* (1985), the spectrum of Lyapunov exponents will be achieved.

## 5.3 Numerical Results and Discussions

To demonstrate that the second-order local neighborhood-to-neighborhood mapping has more advantages than the local linear mapping in calculating Lyapunov exponents, the numerical results of all Lyapunov exponents calculated from the same time series using the second-order local neighborhood-to-neighborhood mapping and the local linear mapping are presented. Their relative errors with respect to the Lyapunov exponents computed from the mathematical model are also compared and discussed here. The bipedal balancing control system during standing subjected to constraints between the foot-link and the ground is used as an example. The time series is generated from the mathematical model, of which the simulation program is written using Matlab. The initial conditions are $\theta_0 = \pi/36$ rad., $\dot{\theta}_0 = -0.1$ rad/sec. Numerical integration time step-size $h = 0.0005$ seconds, the time series includes 20,000 data. The simulation results of the bipedal balancing control system are shown in Figure 5.1. In Figure 5.1a, the horizontal axis is the simulation time, and the vertical axis is the angular displacement. The solid line represents the angular displacement from the switching state controller. Figure 5.1b shows the control torque from PD-based switching-state controller and the control bounds satisfying the constraints. From Figure 4a, we can see that using the PD-based switching state controller, the biped settles down at the upright position after around 15 seconds. Figure 5.1b shows that the control torque, determined from switching state feedback controller, is always within the control bounds, indicating that the constraints between the foot-link and the ground are satisfied. Together with the angular displacement shown in Figure 5.1a, it can be concluded that PD-based switching state feedback controller can

stabilize the biped at the upright position meanwhile satisfying the constraints shown in Equation (3.4).

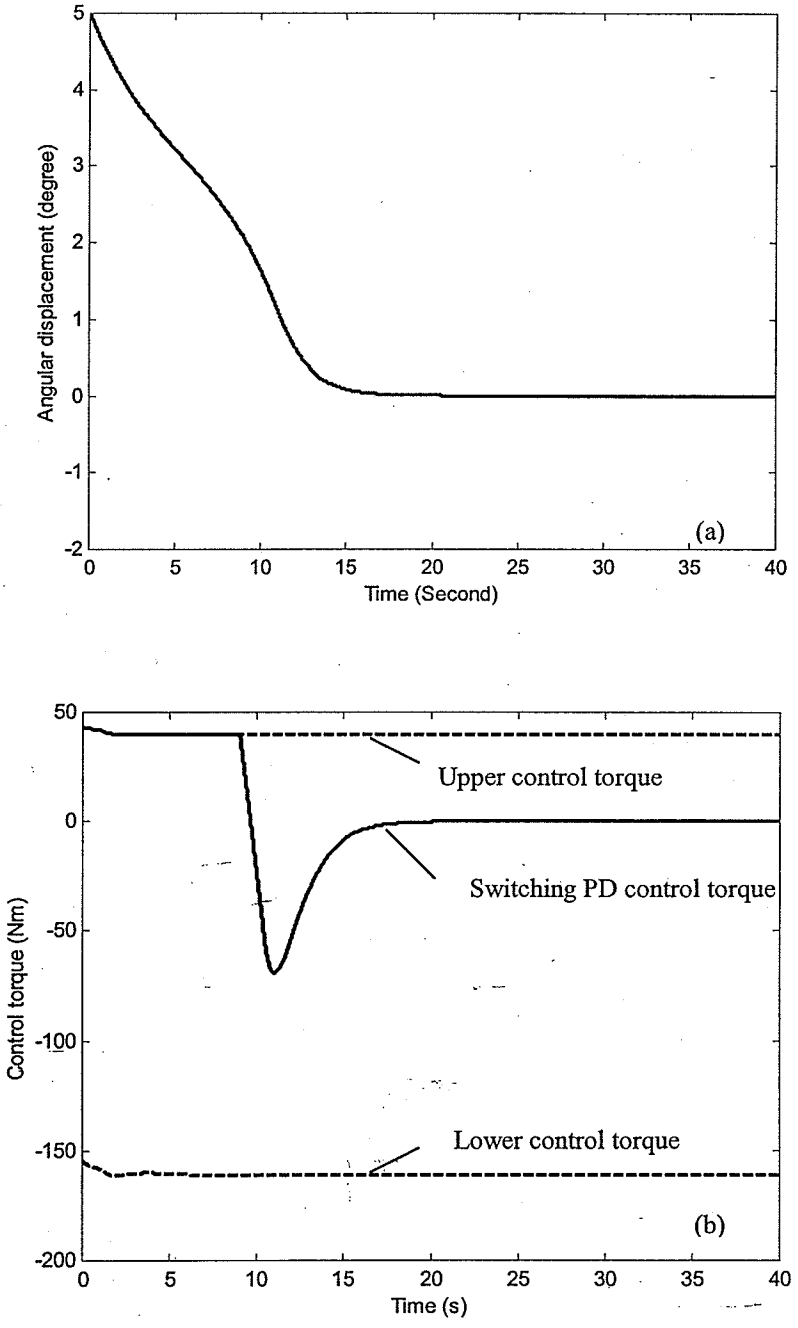


Figure 5.1 Simulation results using PD-based switching state feedback control, (a) simulated angular displacement, (b) control torque.

The two Lyapunov exponents calculated from the mathematical model of the constrained biped with respect to time is shown in Figure 5.2. It can be seen that in the steady state, both exponents are always negative, and converge to -10.3318 and -18.0704, respectively.

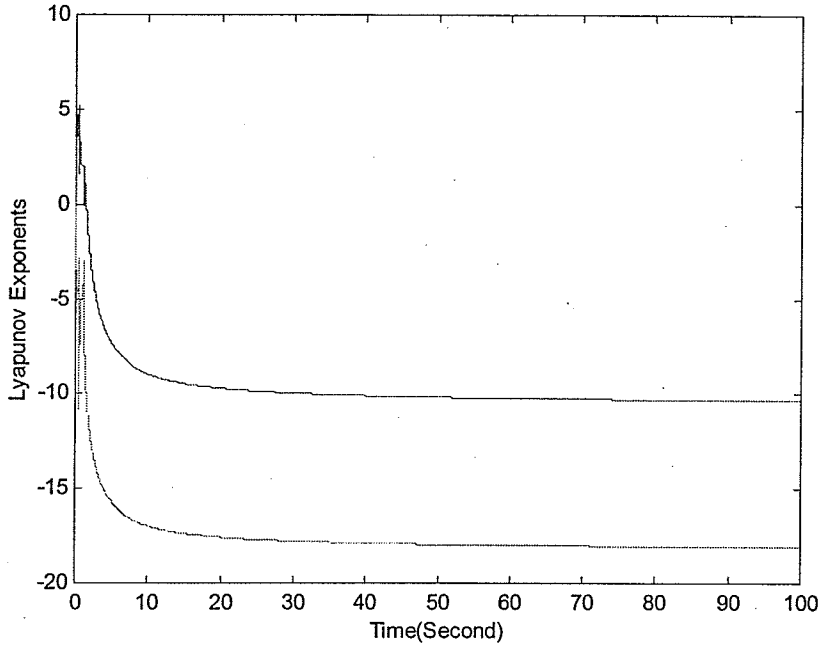


Figure 5.2. Lyapunov exponents calculated from the mathematical model

Note that in calculating Lyapunov exponents based on a time series, the value of time lag ($T_{lag}$), which determines the number of the data points to be used in the analysis, has significant effects on the accuracy of the calculated Lyapunov exponents. Takens' results indicate that, in principle, any choice of lags $T_{lag}$ will do. However, If $T_{lag}$ is too small, the coordinates at the successive points in the phase space represent almost the same information. On the other hand, if $T_{lag}$ is too large, the successive points represent distinct uncorrelated descriptions of the embedding phase space (Nusse and Yorke 1998). Another important parameter is the evolving time, $T_{evol}$. The question of proper

selections of the above parameters still remains open. In order to demonstrate that the nonlinear mapping truly improves the accuracy of the calculated Lyapunov exponents and leads to true negative exponents, in this work, large ranges of the key parameters, from 100 to 900 for both the time-lag ($T_{lag}$) and evolving time ($T_{evol}$) are used, and the results are presented.

### 5.3.1 Spectrum of Lyapunov exponents and relative errors using local linear mapping

From the previous work (Yang and Wu 2005, 2006a, 2006b, and 2006c), the bipedal robot subjected to three constraints is a 2-dimensional nonlinear non-smooth system. When calculating Lyapunov exponents using the linear mapping, the embedding dimension should follow Takens' theorem (Takens 1981), *i.e.*, in order to preserve the dynamical properties of the original attractor, theoretically the embedding dimension should satisfy $d_E \geq 2[d]+1$, where $d$ is the fractal dimension and $[d]$ is the lowest integer greater than $d$. However, there has been a misunderstanding that in practice the minimum embedding dimension can be taken below $2[d]+1$ (Nusse and Yorke 1998). Thus first the importance of following Takens' theorem was demonstrated. For the bipedal system under study, a 2-dimensional phase space system based on the time delay embedding method was reconstructed, while according to Takens' theorem, the minimum dimension of the embedding phase space should be 5. Then, the local linear mapping is first used to construct mapping matrices and calculate the Lyapunov exponents of this 2-dimensional embedding system. The values of two Lyapunov exponents and the relative

error with respect to the values obtained from mathematical model are shown in Table 5.2.

Table 5.2 Lyapunov exponents and relative errors using the local linear mapping embedding in 2-dimensional phase space ($\lambda_1^* = -10.3318, \lambda_2^* = -18.0704$)

| $T_{evol}$ | $T_{lag}$ | $\lambda_1$ | Error % | $\lambda_2$ | Error % |
|---|---|---|---|---|---|
| 400 | 100 | -3.0286 | 70.69 | -3.9217 | 78.30 |
| | 200 | -3.4420 | 66.69 | -4.3993 | 75.65 |
| | 300 | -2.5035 | 75.77 | -4.8993 | 72.89 |
| | 400 | -1.6060 | 84.46 | -4.6540 | 74.25 |
| | 500 | -1.4051 | 86.40 | -4.5415 | 74.87 |
| 500 | 100 | -2.7081 | 73.79 | -4.1002 | 77.31 |
| | 200 | -2.4541 | 76.25 | -4.7122 | 73.92 |
| | 300 | -1.9481 | 81.14 | -5.6142 | 68.93 |
| | 400 | -1.9017 | 81.59 | -5.5429 | 69.33 |
| | 500 | -1.7689 | 82.88 | -5.4910 | 69.61 |
| 600 | 100 | -3.0858 | 70.13 | -4.4933 | 75.13 |
| | 200 | -2.5334 | 75.48 | -5.2282 | 71.07 |
| | 300 | -2.8566 | 72.35 | -5.6717 | 68.61 |
| | 400 | -2.7713 | 73.18 | -5.1070 | 71.74 |
| | 500 | -2.3163 | 77.58 | -5.7342 | 68.27 |

From Table 5.2, it is found that the minimum relative error is 67%. Thus, the results are not acceptable, which demonstrates that it is important to follow Takens' embedding theorem (Takens 1981), *i.e.*, using the local linear mapping or the linearization method to reconstruct the system from a time series, the embedding dimension $d_E$ should not be lower than $2d+1$ if the real system is $d$-dimensional system.

The phase space systems were reconstructed with the dimensions ranging from two to ten, mapping matrices are constructed using the local linear mapping, and then calculated the whole spectrum of Lyapunov exponents. It was found, based on these results, that there are no significant improvements on the accuracy of the Lyapunov exponents when

the embedding dimension is above 5. On the other hand, the larger the embedding dimension we chose, the more spurious Lyapunov exponents will be conducted. So in this work, only the results of 5-dimensional embedding phase space are presented. Since the number of the Lyapunov exponents is equal to the dimension of the embedding system, five Lyapunov exponents will be conducted. All of them are shown in Figure 5.3. Triangles, stars, plus signs, squares and diamonds represent the $i^{th}$ Lyapunov exponent (where $i = 1,...,5$).

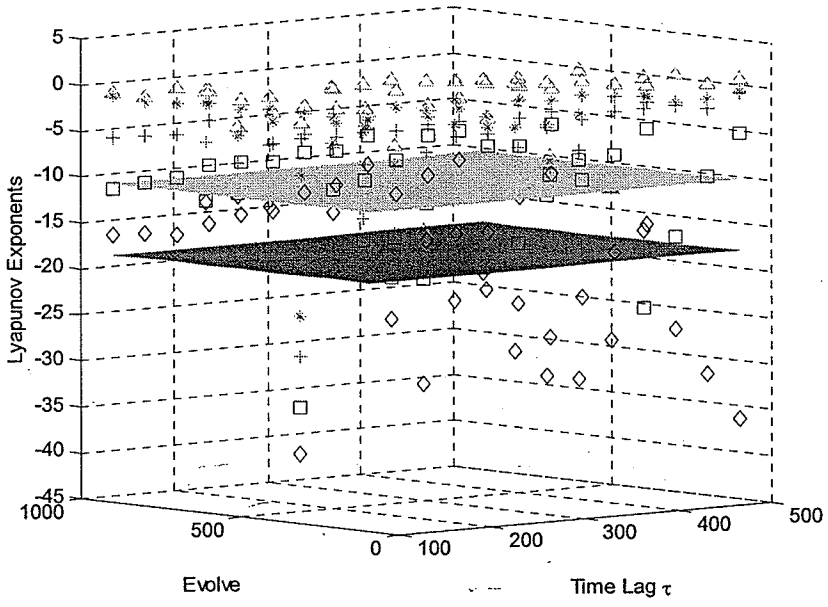


Figure 5.3 Spectrum of Lyapunov exponents using 1st order mapping embedding in 5-dimensional phase space (Triangles represent the first exponent; stars represent the second exponent; plus signs represent the third exponent; squares represent the fourth exponent and diamonds represent the fifth exponent).

Among these five Lyapunov exponents, only two of them are the true Lyapunov exponents, and the remaining three are spurious exponents. Identifying the actually two Lyapunov exponents from all these five Lyapunov exponents remains a challenge. Although some techniques have been proposed to identify the true exponents, their

applicability depends on the individual systems. On the other hand, when excessively large dimensions are used, not only spurious exponents will be generated, but also in some cases, the accuracy of the true exponents will be affected (Müller 1995). From Figure 5.3, we observed that the fourth exponent (squares) and the fifth exponent (diamonds) are much closer to the values calculated from mathematical model. Since in this work, the focus is to demonstrate the advantages of nonlinear mapping, the fourth and fifth exponents, which are the closest to those calculated from the mathematical model, were assumed to be the "true" Lyapunov exponents representing the balancing of constrained bipedal robot standing. These two Lyapunov exponents determined from times series and their relative errors with respect to the values obtained from the mathematical model are shown in Table 5.3. The standard for acceptable Lyapunov exponents was set as that the individual relative error should be below 15%, the average relative error of two exponents should be below 10%.

Table 5.3 Lyapunov exponents and relative errors using 5D local linear mapping $(\lambda_1^* = -10.3318, \lambda_2^* = -18.0704)$

| $T_{evol}$ | $T_{lag}$ | $\lambda_4$ | Error % | $\lambda_5$ | Error % |
|---|---|---|---|---|---|
| 400 | 100 | -6.0906 | 41.05 | -11.3631 | 37.12 |
| | 200 | -8.8755 | 14.10 | -10.8925 | 39.72 |
| | 300 | -10.3733 | 0.40 | -15.6721 | 13.27 |
| | 400 | -10.0746 | 2.49 | -27.7914 | 53.80 |
| | 500 | -16.9300 | 63.86 | -25.4629 | 40.91 |
| 500 | 100 | -6.3917 | 38.14 | -12.1951 | 32.51 |
| | 200 | -10.2626 | 0.67 | -12.8257 | 29.02 |
| | 300 | -12.7572 | 23.48 | -16.6464 | 7.88 |
| | 400 | -17.9346 | 73.59 | -24.4320 | 35.20 |
| | 500 | -12.5367 | 21.34 | -29.4321 | 62.87 |
| 600 | 100 | -7.1900 | 30.41 | -13.6164 | 24.65 |
| | 200 | -10.6688 | 3.26 | -10.7559 | 40.48 |
| | 300 | -16.8478 | 63.07 | -19.5681 | 8.29 |
| | 400 | -19.1858 | 85.70 | -23.3168 | 29.03 |
| | 500 | -10.0056 | 3.16 | -34.0555 | 88.46 |

From Table 5.3, it is found that the relative errors decrease as compared with the values in Table 5.2. The minimum average relative error is 6.84% when time lag is 300; evolving time is 400, while the individual relative errors are 0.40% and 13.27%, respectively. This result implies that using the local linear mapping, the accuracy of the Lyapunov exponents can be improved with the increase in the embedding dimension. Thus, using sufficiently high embedding dimensions, *i.e.,* satisfying Takens' embedding theorem (Takens 1981), is crucial when the linear mapping is used for calculating Lyapunov exponents. However, it is observed that the accuracy of the Lyapunov exponents is very sensitive to the choice of the time lag and evolving time. Thus, selection of proper parameters, such as time lag $T_{lag}$, and evolving time, $T_{evol}$, for computing Lyapunov exponents, is still a very challenging problem. Another problem is that since the dimension of embedding phase space is large than the dimension of the robot system, three spurious exponents are generated. How to identify the true exponents remains challenging.

### 5.3.2 Spectrum of Lyapunov exponents and relative errors using second-order mapping

In this section, the Lyapunov exponents of the bipedal control system are presented where the second-order local neighborhood-to-neighborhood mapping was used to construct more accurate mapping matrices *Js*. Since Takens' embedding theorem is meant for linear mapping and since for nonlinear mapping, more information of the original system is captured, the embedding dimension is chosen as two, which is equal to the dimension of bipedal system under study. The time history of two exponents with time

lag $T_{lag} = 600$ and evolving time $T_{evol} = 400$ is shown in Figure 5.4. Their values and the relative errors with respect to the values obtained from the mathematical model are shown in Table III.

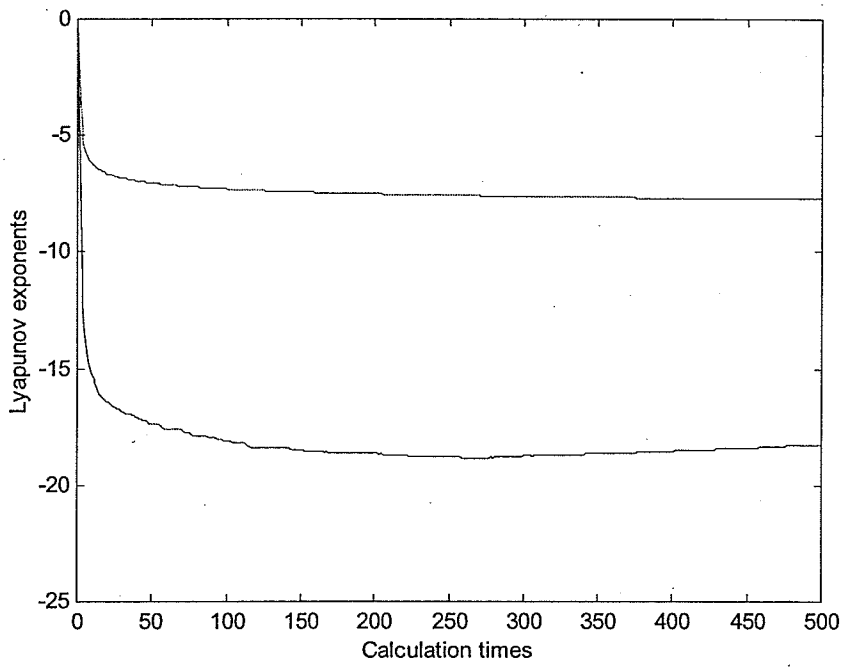


Figure 5.4 Lyapunov exponents using 2nd order mapping embedding in 2-dimensional phase space when time lag $T_{lag} = 600$, evolving time $T_{evol} = 400$

Figure 5.4 shows that in the steady state phase, the exponents always remain negative and converges to -7.7221 and -18.1672. The property of the exponents remaining negative indicates that the nearby trajectories converge consistently. Such a property is an important condition for system stability. Otherwise, the stability of the systems cannot be guaranteed even if the average exponents are negative. Examples of Lyapunov stability refer Slotine and Li (1991).

Two Lyapunov exponents and their relative errors with respect to the values obtained from the mathematical model are shown in Table 5.4.

Table 5.4 Lyapunov exponents and relative errors using 2nd order mapping embedding in 2-dimensional phase space ($\lambda_1^* = -10.3318, \lambda_2^* = -18.0704$)

| $T_{evol}$ | $T_{lag}$ | $\lambda_1$ | Error % | $\lambda_2$ | Error % |
|---|---|---|---|---|---|
| 400 | 100 | -7.7220 | 25.26 | -18.3770 | 1.70 |
| | 200 | -7.7734 | 24.76 | -17.9987 | 0.40 |
| | 300 | -7.7804 | 24.69 | -18.0775 | 0.04 |
| | 400 | -7.7779 | 24.72 | -18.1034 | 0.18 |
| | 500 | -7.7605 | 24.89 | -18.2308 | 0.89 |
| 500 | 100 | -9.2915 | 10.07 | -19.7182 | 9.12 |
| | 200 | -9.3494 | 9.51 | -18.8249 | 4.18 |
| | 300 | -9.3515 | 9.49 | -18.9325 | 4.77 |
| | 400 | -9.3256 | 9.74 | -19.0590 | 5.47 |
| | 500 | -9.2921 | 10.06 | -19.1059 | 5.73 |
| 600 | 100 | -10.5810 | 2.41 | -22.5561 | 24.82 |
| | 200 | -10.7262 | 3.82 | -20.2052 | 11.81 |
| | 300 | -10.7365 | 3.92 | -19.7989 | 9.57 |
| | 400 | -10.7184 | 3.74 | -19.8684 | 9.95 |
| | 500 | -10.6537 | 3.12 | -19.9426 | 10.36 |

Based on the results shown in Table 5.4, it is found that using the second-order mapping; firstly, the relative overall errors of the Lyapunov exponents decrease significantly as compared with those using the local linear mapping. The minimum average relative error is 6.74% when time lag, $T_{lag}$, is 500, evolving time, $T_{evol}$, is 600, while the individual relative errors are 3.12% and 10.36%, respectively. Secondly, the results are not sensitive to the values of time lag, $T_{lag}$, and evolving time, $T_{evol}$, nine sets of results have met the requirement we set within the range of time lag, $T_{lag}$, from 100 to 500, and evolving time, $T_{evol}$, from 500 to 600. Thirdly, since the reconstructed phase space system is 2-dimensional, only two Lyapunov exponents are conducted. No spurious exponents are generated. Thus, using the second-order local neighborhood-to-

neighborhood mapping can avoid the identification of the true Lyapunov exponents from spurious ones.

## 5.4 Discussions

Stability analysis and stability control are important for the development of robotic systems. Due to the limitations on the derivations of Lyapunov functions, stability analysis and control of robotic systems have been extremely limited. On the other hand, Lyapunov exponents, which can be calculated from the mathematical models of the systems or a time series, are independent from the initial conditions and can characterize the system stability provided that the numerical artifact is under control (Sekhavat 2004). The most attractive advantage of using a time series is that the data for only one state is required, which can often be measured experimentally (Wolf *et al* 1985, Sano and Sawada 1985, Kantz and Schreiber 2004). However, it has been documented that the current methods for calculating Lyapunov exponents using a time series are valid for chaotic systems, *i.e.*, for calculating positive Lyapunov exponents. They have been considered not reliable for calculating negative and zero exponents.

It was believed that the first-order Taylor series expression used in current methods for calculating Lyapunov exponents based on a time series becomes unacceptable for potentially stable systems (Wolf *et al* 1985, Brown *et al* 1991, Zeng *et al* 1992). Thus, using a higher order Taylor series expression for generating local neighborhood-to-neighborhood mapping was proposed to calculate Lyapunov exponents based on a time series. A control system of a biped during standing has been used as an example to demonstrate the proposed method. Two Lyapunov exponents have been calculated using a second-order local neighborhood-to-neighborhood mapping. The results have been

compared with those determined using a linear mapping and those obtained from the mathematical model of the bipedal control system under study. Since the time lag $T_{lag}$ and the evolving time $T_{evolv}$ have significant effects on the calculated Lyapunov exponents, and there are no methods available on the selection of such parameters, a large range of such parameters have been used to ensure the results truly approximate the Lyapunov exponents.

As demonstrated in Section 5.3, the nonlinear mapping has following advantages:

(1) The accuracy of the negative Lyapunov exponents calculated using the nonlinear mapping is significantly improved as compared with those from the linear mapping;

(2) The sensitivity of the calculated Lyapunov exponents is significantly reduced to the time lag and the evolving time as compared to those from the linear mapping;

(3) No spurious Lyapunov exponent is generated since the dimension of the embedding phase space is the same as the true dimension of the original bipedal system.

The importance of satisfying Takens' embedding theorem is also demonstrated when the linear mapping is used.

In addition to calculating negative Lyapunov exponents, one of the issues preventing the applications of the concept of Lyapunov exponents to potentially stable systems is that Lyapunov exponents are the average divergent/convergent rates of close-by trajectories. The evaluation of system stability based on the final average value may be problematic because there might be some strange trajectories that escape from or oscillate around the boundary of the attracting region. We then propose to examine the time history of the exponents rather than just the final average values for determining the system stability as

discussed in Section 5.3 in that the exponents should remain negative during the whole steady state phase.

Although Lyapunov exponents are calculated from a specific trajectory, they are independent from any initial conditions and specific trajectories within the same stability region (Oseledec 1968, Dieci *et al* 1997). Thus, determination of the stability region is an important part when Lyapunov exponents are used for stability analysis. An effective and practical algorithm for determining stability region, developed by Nusse and Yorke (1998), is recommended here.

Although conceptually, Lyapunov exponents are related to the eigenvalues of the linear systems, stability analysis using Lyapunov exponents is fundamentally different from linear stability analysis in that, for linear stability analysis, the nonlinear system is first linearized in a region around an operating point, and the eigenvalues of the linear system are calculated. In the cases that the region of interests is not close to the operating point or the nonlinear systems cannot be linearized, such as non-smooth systems, linear stability analysis does not work. The concept of Lyapunov exponents provides a generalization of the linear stability analysis for perturbations of steady state solutions to time-dependent solutions. Although linearization is involved, it is around the points on the trajectory, rather than around an operating point.

Applying Lyapunov's second method to engineering systems, which are highly nonlinear systems, is well-known challenging due to the lack of constructive method for deriving a Lyapunov function. The method of calculating Lyapunov exponents developed in this work is both systematic and constructive. Furthermore, the method is not restricted

to bipedal robotic systems. It can be used to general nonlinear potentially stable systems, especially for practical engineering systems.

# Chapter 6

# Conclusions and Future Work

## 6.1 Contributions of This Thesis

The contributions of this thesis include three aspects. The first contribution is that the effects of constraints on balance control of bipedal standing have been investigated rigorously. The second contribution is that the balance control of constrained bipedal standing has been studied. The stability of this control system has been analyzed using the concept of Lyapunov exponents based on the mathematical model. The third contribution is that a method for analyzing potentially stable engineering systems based on the concept of Lyapunov exponents using a time series has been developed. Each contribution is further elaborated below.

### 6.1.1 Effects of constraints on balancing of bipedal standing

The effects of constraints between the foot-link and the ground on balancing of bipedal standing have been investigated. To the best of the author's knowledge, this is the first systematic study on this subject. Analytical solutions to the bounds of the controlled ankle torque have been determined satisfying each individual constraint, the gravity and friction constraints simultaneously. The control bounds satisfying all three constraints have been obtained using a numerical method. The regions in the state space satisfying all the constraints have been determined. More importantly, the regions that can not satisfy the constraints have also been identified. If the states of the biped fall in such regions,

regardless of the control torque, the constraints will be violated and stabilization cannot be achieved. The changes in the range of the control torque versus the angle and the angular velocity have been obtained. Furthermore, the results of control bounds have shown explicitly the specific constraint causing such bounds, which, in turn, predicts the specific constraint to be violated and the potential movement of the foot-link once the constraint is violated. The solutions to the control bounds are important for designing balancing control laws. They are also helpful for preparing protective measures for the bipedal robots.

The investigation of the effects of constraints on the bipedal robot provides valuable information about the role of each individual constraint and their interactions on the bipedal standing. This information is very helpful to gain an in-depth understanding of the mechanics of bipedal standing. It also provides a guideline to design suitable control laws for balancing the bipedal standing.

### 6.1.2 Balance control and stability analysis of constrained bipedal standing

The balancing control of constrained disturbed bipedal standing has been investigated. To demonstrate the effects of constraints on balancing of bipedal standing, a PD-based switching state controller has been designed, and has been used to stabilize the biped from some initial states to upright posture while satisfying all constraints between the feet and the ground. A conventional PD controller, designed without the consideration of the constraints, has been compared with the state-switching controller. Simulation results have shown that the control torque, determined from the switching state feedback

controller, was always within the control bounds, indicating that the constraints between the foot-link and the ground are satisfied. The control torque from the conventional PD controller was below the lower bound of the control torque. This indicates that if the foot-link is not fixed on the ground, the constraints will be violated, and stabilization of the biped is out of the question. The simulation results indicate the importance to consider the constraints between the foot-link and the ground when the balance control law is designed.

The stability of PD-based switching state control system has been analyzed using the concept of Lyapunov exponents based on a mathematical model, and a stability region has been determined. Furthermore, the stability region has been compared and agreed well with the one from the previous work that predicts the feasible movement during which balance of human standing can be maintained. This agreement shows the potential of the concept of Lyapunov exponents to be used as a measure of balance control of human standing. The work contributes to bipedal balance control, which is important in the development of bipedal walking machines.

### 6.1.3 Stability analysis using Lyapunov exponents based on a time series

Stability analysis and stability control are important for the development of robotic systems. Lyapunov's stability analysis for engineering systems is well-known challenging due to the lack of constructive method for deriving a Lyapunov function. Methods for calculating the Lyapunov exponents based on a time series have been developed primarily for analyzing chaotic systems, where at least one Lyapunov exponent is positive. Such

methods are not reliable for studying potentially stable systems, where the largest Lyapunov exponent is negative or zero. It is believed that the local linear mapping leads to inaccurate matrices which are essential for calculating the spectrum of Lyapunov Exponents. In this research, the method on stability analysis for potential stable engineering systems using Lyapunov exponents based on a time series has been developed. Higher order Taylor expansions have been used in the local neighbour-to-neighbour mapping to obtain more accurate mapping matrices. A control system of a biped during standing has been used as an example to demonstrate the proposed method. The whole spectrum of Lyapunov exponents has been numerically obtained. The results have been compared with those determined using a linear mapping and those obtained from the mathematical model of the bipedal control system under study. It has been shown that a significant improvement in the accuracy is achieved. The results show that the nonlinear mapping has the following advantages for calculating Lyapunov exponents:

1. The accuracy of the negative Lyapunov exponents calculated using the nonlinear mapping is significantly improved as compared with those from the linear mapping.
2. The sensitivity of the calculated Lyapunov exponents is significantly reduced to the time lag and the evolving time as compared to those from the linear mapping.
3. No spurious Lyapunov exponent is generated since the dimension of the embedding phase space is the same as the true dimension of the original bipedal system.

Hence, the proposed method for calculating Lyapunov exponents based on time series has a great potential for obtaining negative Lyapunov exponents and has significant

practical applications in engineering systems. The method of calculating Lyapunov exponents developed in this work is both systematic and constructive. Furthermore, the method is not restricted to bipedal robotic systems. It can be used to general nonlinear potentially stable systems, especially for practical engineering systems.

## 6.2 Future Work

Several recommendations are made for future work.

(1) In order to use the proposed methodology to analyze the stability of potential stable systems using the concept of Lyapunov exponents based on a time series, the biped model needs to be expanded to multi-linkage system.

(2) An advanced nonlinear controller satisfying both the control bounds and the condition on the angular velocity needs to be designed to enlarge the stability region. Since one limitation of the present work is that, the controller was designed satisfying only the control bounds. The condition, imposed on the angular velocity, was not considered in the control design; rather it was used to terminate the controller and simulations if the magnitude of the angular velocity was above the critical value.

(3) The derivation and programming on computing Lyapunov exponents based on a time series for arbitrary order of Taylor series expression and for any dimensional phase space need to be developed.

With the above future developments, the proposed method may be used as an efficient stability analysis tool for potentially stable engineering systems.

# REFERENCES


Abel, M., Ahnert, K., Kurths, J., and Mandelj, S., "Additive nonparametric reconstruction of dynamical systems from time series", *arXiv:nlin.CD/0408003 v2 30Nov 2004*

Abarbanel, H.D.I., Brown, R., and Kennel, M.B., "Prediction in chaotic nonlinear systems: methods for time series with broadband Fourier spectra", *Journal of Nonlinear Science physical Review A* **41**(4), 1782- 1807 (1990)

Abarbanel, H.D.I., Brown, R., and Kennel, M.B., "Variation of Lyapunov exponents on a strange attractor", *Journal of Nonlinear Science* **1,** 175-199 (1991)

Abarbanel, H.D.I., Brown, R., and Kennel, M.B., "Local Lyapunov exponents computed from observed data", *Journal of Nonlinear Science* **2,** 343-365 (1992)

Abarbanel, H.D.I., *Analysis of Observed Chaotic Data*, Springer, New York, (1996)

Abarbanel, H.D.I., Gilpin, M.E. and Rotenberg, M., *Analysis of Observed Chaotic Data*, Springer, New York, (1997)

Abo-Shanab, R.F., Sepehri, N. and Wu, Q., "Application of nonstandard finite difference schemes to the simulation studies of robotic systems", Advances in the Applications of *Nonstandard Finite Difference Schemes*, edited by Mickens, R.E., World Scientific Publishing Co. Pte. Ltd., New Jersey, (2005)

Awrejcewicz, J., and Dzyubak, L., "Quantifying smooth and nonsmooth regular and chaotic dynamics", *International Journal of Bifurcation and Chaos* **15** (6), 2041-2055 (2005)

Baker, G.L. and Gollub, J.P. *Chaotic Dynamics an Introduction*, 2nd edition, Cambridge University Press, New York, (1996)

Benettin, G., Galgani, L., Giorgilli, A. and Strelcyn, J-M., "Lyapunov characteristic exponents for smooth dynamical systems: a method for computing all of them. Part 1: theory", *Meccanica* **15,** 9-20 (1980)

Barbasin, E.A., "The construction of Liapunov functions for non-linear systems", *Proceedings of 1st International Congress of IFAC*, Moscow, 943-947 (1960),

Bersini, H. and Gorrini, V., "A simplification of the backpropagation-through-time algorithm for optimal neuron-control", *IEEE, Transaction on Neural Networks* **8,** 437-441 (1997)

Brown, R., Bryant, P. and Abarbanel, H. D. I., "Computing the Lyapunov spectrum of a dynamical system from an observed time", *Physical Review A* **43(6)**, 2787-2806 (1991)

Bryant, P., Brown, R. and Abarbanel, H. D. I., "Lyapunov exponents from observed time series", *Physics Review Letter* **65**, 1523 (1990)

Burian, K, "Stability and limit cycles of nonlinear systems", *Ph.D. Thesis, Northwestern University,* (1959), University Microfilms, Inc., Ann Arbor, Michigan, 1961

Carretero-González , R., Ørstavik, S. and Stark, J., "Quasi-diagonal approach to the estimation of Lyapunov spectra for spatiotemporal systems from multivariate time series", *Physical Review E* **62**(5), 6429-6439 (2000)

Caux, S., and Zapata, R., "Modeling and control of biped robot dynamics", *Robotica* **17**, 413-426 (1999)

Channon, P.H., Hopkins, S.H., and Phan, D.T., "Derivation of optimal walking motions for a biped walking robot", *Robotica* **10**, 165-172 (1992)

Chen, Z.-M., Djidjeli, K., and Price, W.G., "Computing Lyapunov exponents based on the solution expression of the variational system", *Applied Mathematics and Computation* **174** (2), 982–996 (2006)

Chevallereau, C., Formal'sky, A., and Perrin, B., "Low energy cost reference trajectories for a biped robot", *Proceedings of IEEE International Conference on Robotics and Automation* **3**, 1398-1404 (1998)

Chevallereau, C., Aoustin, Y., and Formal'sky, A., "Optimal reference trajectories for a biped", *Proceedings of the First Workshop on Robot Motion and Control*, 171-176 (1999)

Chevallereau, C., and Aoustin, Y., "Optimal reference trajectories for walking and running of a biped robot", *Robotica* **19**, 557-569 (2001)

Chew, C.M. and Pratt, G.A., "Adaptation to load variations of a planar biped: height control using robust adaptive control", *Robotics and Autonomous Systems* **35**(1), 1-22 (2001)

Chin, P.S.M., "A genera method to derive Lyapunov function for non-linear systems", *International Journal of Control* **44**, 381-393 (1986)

Chin, P.S.M., "Scalar-Lyapunov-function method for single- and multi-machine problems in power system", *International Journal of Control* **45**, 1737-1749 (1987)

Chin, P.S.M., "Generalized integral method to derive Lyapunov functions for non-linear systems", *International Journal of Control* **46**, 933-943 (1987)

Chin, P.S.M., "Stability of non-linear systems via the intrinsic method", *International Journal of Control* **48**, 1561-1567 (1988)

Chin, P.S.M., "Stability results for the solutions of certain fourth-order autonomous differential equations", *International Journal of Control* **49**, 1163-1173 (1989)

Chow, C.K. and Jacobson, D.H., "Further studies of human locomotion: postural stability and control", *Mathematical Biosciences* **15,** 93-108 (1972),

Cong, N. D., and Son, D. T., "An open set of unbounded cocycles with simple lyapunov spectrum and no exponential separation", *Stochastics and Dynamics* **7** (3), 335-355 (2007)

Cover, T.M. and Thomas, J.A., *Elements of Information Theory*, Wiley-Interscience, (1991)

Dieci, L, Russell, R.D., and Van Vleck, E.S, "On the computation of Lyapunov exponents for continuous dynamical systems", *SIAM Journal of Numerical Analysis* **34**(1), 402-423 (1997)

Eckmann, J.-P. and Ruelle, D., " Ergodic theory of chaos and strange attractor", *Reviews of Modern Physics* **57,** 617 (1985)

Eckmann, J.-P., Kamphorst, S.O., Ruelle, D., and Ciliberto, S., "Liapunov exponents from time series", *Physical Review A* **34,** 4971 (1986)

Furusho, J. and Sano, A., "Sensor-based control of a nine-link biped", *International Journal of Robotics Research* **9,** 83-98 (1990)

Giannerini, S., Rosa, R., and Gonzalez, D. L., "Testing chaotic dynamics in systems with two positive lyapunov exponents: a bootstrap solution", *International Journal of Bifurcation and Chaos* **17** (1), 169-182 (2007)

Golliday, C.L. and Hemami, H., "Posture stability of the two-degree-of freedom biped by general linear feedback", *IEEE Transactions on Automatic Control* **21**, 74-79 (1976)

Goswami, A., "Postural stability of biped robots and the foot-rotation indicator point", *International Journal of Robotics Research* **18**(6), 523-533 (1999)

Grüne, L., "A uniform exponential spectrum for linear flows on vector bundles", *Journal of Dynamics and Differential Equations* **12**(2), 435-448 (2000)

Hemami, H. and Camana, P.C., "Nonlinear feedback in simple locomotion systems", *IEEE Transactions on Automatic Control,* 835-860 (1976)

Hemami, H. and Golliday, C. Jr., "The inverted pendulum and biped stability", *Mathematical Bioscience* **34**, 95-110 (1977a)

Hemami, H. and Cvetkovic, V.S., "Postural stability of two biped models via Lyapunov second method", *IEEE Transactions on Automatic Control* **22**, 66-70 (1977b)

Hemami, H. and Farnsworth, R.L., "Postural and gait stability of a planar five link biped by simulation", *IEEE Transactions on Automatic Control* **22**, 452-458 (1977c)

Hemami, H., Weimer, F.C., Robinson, C.S., Stokewell, C.W. and Cvetkovič, V.S., "Biped stability considerations with vestibular models", *IEEE Transactions on Automatic Control, AC*-**23**, 1074-1079 (1978)

Hemami, H. and Wyman, B.F., "Modeling and control of constrained dynamic systems with application to biped locomotion in the frontal plane", *IEEE Transactions on Automatic Control* **24,** 526-535 (1979a)

Hemami, H. and Wyman, B.F., "Indirect control of the forces of constraint in dynamic systems", *Journal of Dynamic Systems, Measurement, and Control* **1,** 335-360 (1979b)

Hemami, H. and Katbab, A., "Constrained inverted pendulum model of evaluating upright postural stability", *Journal of Dynamic Systems, Measurement, and Control* **104**, 343-349 (1982)

Hemami, H. and Stokes, B.T., "A qualitative discussion of mechanisms of feedback and feedforward in the control of locomotion", *IEEE Transactions on Biomedical Engineering, BME*-**30**, 681-688 (1983)

Hemami, H., and Utkin, V.I., "On the dynamics and Lyapunov stability of constrained and embedded rigid bodies", *International Journal of Control* **75**(6), 408-420 (2002)

Hemami, H., Barin, K., Jallics, L., and Heiss, D., "Dynamics, stability, and control of stepping", *Annuas of Biomechanical Engineering* **32**(8), 1153-1160 (2004)

Hemami, H., Barin, K., and Pai, Y.-C., "Quantitative analysis of the ankle strategy under translational platform disturbance", *IEEE Transactions on Neural Systems and Rehabilitation Engineering* **14**(4), 470-480 (2006)

Hirai, K., Hirose, M., Haikawa, Y., and Takenaka, T., "The development of Honda humanoid robot", *Proceedings of IEEE International Conference on Robotics and Automation*, 1321-1326 (1998)

Holzfuss, J and Lauterborn, W., "Lyapunov exponents from a time series of acoustic chaos", *Physical Review A* **39(4),** 2146-2152 (1989)

Honda Motor Co., Ltd, http://world.honda.com/HDTV/ASIMO/ (2005)

Huang, Q., Yokoi, K., Kajita, S., Kaneko, K., Arai, H., Koyachi, N., and Tanie, K., "Planning walking patterns for a biped robot", *IEEE Transactions on Robotics and Automation* **17**, 280-289 (2001)

Huang, W., Ding, W.X., Feng, D.L. and Yu, C.X., "Estimation of a Lyapunov exponent spectrum of plasma chaos", *Physical Review E* **50**(2), 1062 - 1069 (1994)

Huaux, A., "On the construction of Lyapunov functions", *IEEE Transactions on Automation and Control* **12**, 465 (1967),

Hurmuzlu, Y. and Moskowiz, "Bipedal locomotion stabilized by impact and switching: I. two- and three-dimensional, three-element models", *Dynamics and Stability of Systems* **2,** 75-96 (1987a)

Hurmuzlu, Y. and Moskowiz, "Bipedal locomotion stabilized by impact and switching: II. Structural stability analysis of a four-element bipedal locomotion model", *Dynamics and Stability of Systems* **2,** 98-112 (1987b)

Hurmuzlu, Y., "Dynamics of bipedal gait: Part I - Objective functions and contact event of a planar five-link biped", *Journal of Applied Mechanics* **60**, 331-336 (1993a)

Hurmuzlu, Y., "Dynamics of bipedal gait: Part II – Stability analysis of a planar five-link biped", *Journal of Applied Mechanics* **60**, 337-343 (1993b)

Iqbal, K. and Pai, Y.C., "Predicted region of stability for balance recovery: Motion at the knee joint can improve termination of forward movement", *Journal of Biomechanics* **33**, 1619-1627 (2000)

Iqbal, K. Hemami, H., and Simon, S., "Stability and control of a frontal four-link biped system", *IEEE Transactions on Biomechanical Engineering* **40**(10), 1007-1018 (1993)

Kajita, S., and Tanie, K., "Study of dynamic biped locomotion on rugged terrain", *IEEE Proceedings of 1991 International Conference on Robotics and Automation*, 1405-1411 (1991)

Kantz, H., and Schreiber, T., *Nonlinear Time Series Analysis*, Cambridge, UK: Cambridge Univ. Press. (2004), 2nd Edition

Katoh, R., and Mori, M., "Control method of biped locomotion giving asymptotic stability of trajectory", *Automatica* **20**(4), 405-414 (1984)

Kinsner, W., *Fractal and Chaos Engineering*, Lecture notes. Department of Electrical and Computer Engineering, University of Manitoba, 1996, 760 pages

Kinsner, W., "Characterizing Chaos through Lyapunov metrics", *Proceedings of the Second IEEE International Conference on Cognitive Informatics*, 189-201 (2003)

Kinsner, W., "Characterizing Chaos through Lyapunov metrics", *IEEE Transactions on Systems, Man, and Cybernetics-Part C: Applications and Reviews* **36** (2), 141-151 (2006)

Kinsner, W., *Microcontroller, Microprocessor, and Microcomputer Interfacing for Real-Time Systems.* Winnipeg, MB: University of Manitoba, 2007, 788 pages

Kunze, M., "On Lyapunov exponents for non-smooth dynamical systems with an application to a pendulum with dry friction", *Journal of Dynamics and Differential Equations* **12**(1), 31-116 (2000)

Kuo, A.D., "An optimal control model for analyzing human posture balance", *IEEE Transactions on Biomedical Engineering* **42**, 87-101 (1995)

Kuperstein, M. and Wang, J., "Neural controller for adaptive movements with unforeseen payloads", *IEEE Transactions on Neural Networks* **1**,137-142 (1990)

Lai, Y-C., and Ye, N., "Recent developments in chaotic time series analysis", *International Journal of Bifurcation and Chaos* **13** (6), 1383-1422 (2003)

Liu, W.D., Ren, K.F., Meunier-Guttin-Cluzel, S. and Gouesbet, G., "Global vector-field reconstruction of nonlinear dynamical systems from a time series with SVD method and validation with Lyapunov exponents", *Chinese Physics* **12**(12), 1366-1373 (2003).

Liu, Z. and Li, C., "Fuzzy neural networks quadratic stabilization output feedback control for biped robots via H_infiniti approach", *IEEE Transactions on Systems, Man, and Cybernetics—Part B: Cybernetics* **33(1)**, 67-84 (2003)

Lyapunov, A.M., 1892, "The general problem of the stability of motion", Translated by Fuller, A.T., *International Journal of Control* **52**, 531-773; also (London: Taylor & Francis, 1992)
Ma, B. and Wu, Q., "Parametric study of repeatable gait for a planar five-link biped", *Robotica* **20**, 493-498 (2002)

Mane, R., "On the dimension of the compact invariant sets of certain nonlinear maps", *Dynamical Systems and Turbulence, Lecture Notes in Mathematics*, Springer, NY, 898, 230-242 (1981)

Marchese, S., Muscate, G. and Virk, G.S., "Dynamically stable trajectory synthesis for a biped robot during the single-support phase", *IEEE/ASME International Conference on Advanced Intelligent Mechatronics Proceedings,* 953-958 (2001)

Marino, R., and Nicosia, S., "Hamiltonian-type Lyapunov functions", *IEEE Transactions on Automatic Control* **28**, 1055-1057 (1983)

McCown-McClintick, B.E., and Moskowitz, G.D., "The behavior of a biped walking gait on irregular terrain", *International Journal of Robotics Research* **17**, 43-55 (1998)

Mickens, R.E., *Nonstandard Finite Difference Models of Differential Equations,* World Scientific Publishing Company, Inc. (1994)

Mickens, R.E., "Nonstandard finite difference schemes for differential equations", *Journal of Difference Equation and Applications* **8**, 823-847 (2002)

Mickens,R.E. and Gumel, A.B., "Construction and analysis of a nonstandard finite difference scheme for the Burgers-Fisher equation", *Journal of Sound and Vibration* **257**, 791-797 (2002)

Miksovsky, J. and Raidl, A., "Multivariate phase space reconstruction of meteorological systems", *Geophysical Research Abstracts* **5,** 01916 (2003)

Miksovsky, J., "On some meteorogical applications of nonlinear time series methods", Extended Abstract of Doctoral Thesis, Charles University, Prague, (2004)

Miura, H., and Shimoyama, I., "Dynamic walking of a biped locomotion", *International Journal of Robotics Research* **3**, 60-73 (1984)

Most, T., Bucher, C. and Schorling, Y., "Dynamic stability analysis of non-linear structures with geometrical imperfections under random loading", *Journal of Sound and Vibration* **276**, 381-400 (2004)

Mu, X. and Wu,Q., "Development of a complete dynamic model of a planar five-link biped and sliding mode control of its locomotion during the double support phase", *International Journal of Control* **77**, 789-799 (2004)

Mu, X., "Dynamic modeling and motion regulation of a five-link biped robot walking in the sagittal plane", *Ph.D. Thesis, University of Manitoba* (2005)

Murray, R.N., Li, Z., and Saatry, S.S., *A Mathematical Introduction to Robotic Manipulation,* CRC Press Inc., London (1993)

Müller, P.C., "Calculation of Lyapunov exponents for dynamic systems with discontinuities", *Chaos, Solitans and Fractals* **5**, 1671-1681 (1995)

Narendra, K.S. and Parthasarathy, K., "Identification and control of dynamic systems using neural networks", *IEEE Transactions on Neural Networks* **1**, 4-27 (1990)

Nicolis, C. and Nicolis, G., "Reconstruction of the dynamics of the climatic system from time-series data", *Proceedings of the National Academy of Sciences, USA* **(83)**, 536-540 (1986)

Nusse, H.E. and Yorke, J.A., *Dynamics: Numerical Explorations*, Springger-Verlag, New York (1998)

Oseledec, V.I., "A multiplicative ergodic theorem: Lyapunov characteristic numbers for dynamical systems", *Trans. Moscow Math. Soc.* **19**, 197 (1968)

Packard, N.H., Crutchfeld, J.P., Farmer, J.D. and Shaw, R.S., "Geometry from a time series," *Physical Review Letters* 45(9), 712-716 (1980)

Paden, B.E., and Sastry, S.S., "A calculus for computing Filippov's differential inclusion with application to the variable structure control of robot manipulators", *IEEE Transactions on Circuits and Systems* **34**, 73-82 (1987)

Pai, Y.C. and Patton, J., "Center of mass velocity-position predictions for balance control", *Journal of Biomechanics* **30**, 347-354 (1997)

Pai, Y.C. and Iqbal, K., "Simulated movement termination for balance recovery: Can movement strategies be sought to maintain stability in the presence of slipping or forced sliding?" *Journal of Biomechanics* **32**, 779-786 (1999)

Paradopoulos, E.G. and Rey, D.A., "A new measurement of tip-over stability margin for mobile manipulator", *Proceedings of IEEE International Conference on Robotics and Automation,* 3111-3116 (1996)

Parlitz, U., "Identification of true and spurious Lyapunov exponents from time series", *International Journal of Bifurcation and Chaos* **2,**155 (1992)

Paul , M. R., Einarsson, M. I., Fischer, P. F., and Cross, M. C. "Extensive chaos in Rayleigh-Bénard convection", *Physics Review E* **75**, 045203 (2007) (4 pages)

Pavlov, A.N., Yanson, N.B., and Anishchenko, V.S., "Application of statistical methods to solve global reconstruction problems", *Technical physics Letters* **23,** 297 (1997)

Pavlov, A.N., Yanson, N.B., Kapitaniak, T., and Anishchenko, V.S., "Reconstruction of dynamic systems using short signals", *Technical physics Letters* **25**(6), 424-426 (1999)

Ponzo, P.J., "On the stability of certain non-linear differential equations", *IEEE Transactions on Automatic Control* **10**, 470 (1965),

Porcher, R. and Guy Thomas, G, "Estimating Lyapunov exponents in biomedical time series", *Physical Review E* **64**(1), 010902 (2001)

Raibert, M. H., Brown, H. B., "Experiments in balance with a 2d one-legged hopping machine", *ASME Journal of Dynamic Systems, Measurement, and Control* **106**, 75-81 (1984)

Raibert, M. H., "Running with symmetry", *International Journal of Robotics Research* **5**, 3-19 (1986)

Rauf, F, and Ahmed, H.M., "Calculation of Lyapunov exponents through nonlinear adaptive filters", *Proceedings IEEE International Symposium on Circuits and Systems*, Singapore (1991)

Sakai, M., Homma, N., Yano, M. and Abe, K., "Lyapunov spectrum analysis of reconstructed attractors from observed time series", *SICE Annual Conference in Fukui*, (2003)

Sano, M. and Sawada, Y., "Measurement of the Lyapunov spectrum from chaotic time series", *Physics Review Letter* **55,** 1082 (1985)

Sauer, Timothy D, *Numerical Analysis*, Pearson Education, Inc. New York, (2006) 566-579

Sauer, T.D. and Yorke, J.A., "Reconstructing the Jacobian from data with observational noise", *Physics Review Letter* **83**(7), 1331-1334 (1999)

Sekhavat, P., "Design and stability analysis of a switching contact task control for hydraulic actuators", *Ph.D. Thesis, University of Manitoba* (2004)

Sekhavat, P., Sepehri, N. and Wu, Q., "Calculation of Lyapunov exponents using nonstandard finite difference discretization scheme: a case study", *Journal of Difference Equations and Applications* **10**(4), 369-378 (2004)

Sekhavat, P., Wu, Q. and Sepehri, N., "Impact control in hydraulic actuators", *ASME Journal of Dynamic Systems, Measurement, and Control* 127(2), 197-205 (2005)

Shenoi, B.A., *Introduction to Digital Signal Processing and Filter Design*, John Wiley & Sons. Inc. (2006)

Shevitz, D. and Paden, B., "Lyapunov stability theory of non-smooth systems", *IEEE Transactions on Automatic Control* **39**, 1910-1914 (1994)

Shih, C.L., Chuing, S., Lee, T.T., and Gruver, W.A., "Trajectory synthesis and physical admissibility for a biped robot during the single-support phase", *Proceedings of IEEE International Conference on Robotics and Automation*, 1646-1651 (1990)

Silva, F.M. and Machado, J.A.T., "Goal oriented biped walking based on force interaction control", *Proceedings of the IEEE International Conference on Robotics and Automation,* 4122-4127, (2001)

Slotine, J-J.E., and Li, W, *Applied Nonlinear Control,* Prentice Hall, (1991)
Small, M., *Applied Nonlinear Time Series Analysis: Applications in Physics, Physiology and Finance*, World Scientific, (2005)

Sony Corp. http://www.youtube.com/watch?v=33a33XEVHKE, (2006)

Southwood, S.C., Radcliffe, C.J., and MacCluer, C.R., "robust non-linear stick-slip friction compensation", *ASME Journal of Dynamic systems, Measurement, and Control* **113**, 639-644 (1990)

Takens, F., "Dynamical systems and turbulence", *Lecture Notes in Mathematics* **898**, edited by Rand, D.A., and Young L.-S. Springer-Verlag, Berlin (1981)

Thiffeault, J.L. and Boozer, A.H., "Geometrical constraints on finite-time Lyapunov exponents in two and three dimensions", *Chaos* **11**, 16-28 (2001) ISSN 1054-1500

Vukobratović, M., Frank, A.A. and Juricic, D., "On the stability of anthropomorphic systems", *Mathematical Biosciences* **15**, 1-37 (1970)

Vukobratović, M. and Ekalo, Y., "Mathematical model of general anthropomorphic systems", *Mathematical Biosciences* **17**, 191-242 (1973)

Vukobratović, M. and Borovać, B., "Zero-moment point -thirty years of its life", *International Journal of Humanoid Robotics* **1 (1)**, 157-173 (2004)

Williams, G.P., *Chaos Theory Tamed*, Joseph Henry Press, Washington, D.C. (1997)

Wolf, A., Swift, J.B. Swinney, H.L. and Vastano, J.A., "Determining Lyapunov exponents from a time series", *Physics* **16D**, 285-317 (1985)

Wright, J., "Method for calculating a Lyapunov exponent", *Physical Review A* **29** (5), 2924-2927 (1984)

Wu, Q., Sepehri, N., Thornton-Trump, A.B. and Onyshko, S., "An extended integral method to derive Lyapunov functions for nonlinear systems", *International Journal of Control* 62, 717-736 (1995)

Wu, Q., "Lyapunov stability analysis of a class of base-excited inverted pendulums with application to bipedal locomotion systems", *Ph.D. Thesis, University of Manitoba* (1996)

Wu, Q., Thornton-Trump, A.B. and Sepehri, N., "Lyapunov stability control of inverted pendulums with general base point motion", *International Journal of Non-Linear Mechanics* **33**, 801-818 (1998a)

Wu, Q., Onyshko, S., Sepehri, N. and Thornton-Trump, A.B., "On construction of smooth Lyapunov functions for non-smooth systems", *International Journal of Control* **69**, 443-457 (1998b)

Wu, Q., Sepehri, N., Thornton-Trump, A.B. and Alexander, M., "Stability and control of human trunk movement during walking", *Computer Methods in Biomechanics and Biomechanical Engineering* **1**, 247-259 (1998c)

Wu, Q. and Sepehri, N., "On Lyapunov's stability analysis of non-smooth systems with applications to control engineering", *International Journal of Nonlinear Mechanics* **36**, 1153-1161 (2001)

Wu, Q. and Chan, C.Y.A., "Design of energy efficient joint profiles for a planar five-link biped robot", *Proceedings of 2001 IEEE International Symposium on Computational Intelligence in Robotics and Automation,* 35-40, (2001)

Wu, Q., and Swain, R., "A mathematical model of stability control of human thorax and pelvis movements during walking", *Computer Methods in Biomechanics and Biomechanical Engineering* **5**, 67-74 (2002)

Wu, Q., Sepehri, N., Sekhavat, P. and Peles, S., "On design of continuous Lyapunov's feedback control", *Journal of Franklin Institute* **342**(6), 702-723 (2005)

Yang, C. and Wu, Q., "Effects of gravity and friction constraints on bipedal balance control", *Proceedings of 2005 IEEE International Conference on Control Applications,* Toronto, Ontario, Canada, August 28-31, 1093-1098 (2005)

Yang, C. and Wu, Q., "Effects of constraints on bipedal balance control", *Proceedings of the 2006 American Control Conference*, Minneapolis, Minnesota, USA, June 14-16, 2510-2515 (2006a)

Yang, C. and Wu, Q., "On stabilization of bipedal robots during disturbed standing using the concept of Lyapunov exponents", *Proceedings of the 2006 American Control Conference*, Minneapolis, Minnesota, USA, June 14-16, 2516-2521 (2006b)

Yang, C. and Wu, Q., "On stabilization of bipedal robots during disturbed standing using the concept of Lyapunov exponents", *Robotica*, (2006c)

Zeng,X., Pielke, R.A., And Eykholt, R., "Extracting Lyapunov exponents from short time series of low precision", *Modern Physics Letters B* **6**(2), 55-75 (1992)

Zheng, Y.F., and Shen, J., "Gait synthesis for the sd-2 biped robot to climb sloping surface", *IEEE Transactions on Robotics and Automation* **6**, 86-96 (1990)

Zeni, A.R., and Gallas, J.A.C., "Lyapunov exponents for a Duffing oscillator", *Physics D* **89**, 71-82 (1995)

Zhi L.,and Chunwen L., "Fuzzy neural networks quadratic stabilization output feedback control for biped robots via h_infiniti approach", *IEEE Transactions on Systems, Man, and Cybernetics*—Part B: Cybernetics **33**(1), Feb. 2003.

# Appendix A

## Determination of the Minimum Critical Angular Velocity

In this section, the minimum critical angular velocity between $\dot{\theta}_{cr1}$ and $\dot{\theta}_{cr2}$ is determined analytically when $-\theta^* \le \theta \le \theta^*$. Where $\dot{\theta}_{cr1}$ and $\dot{\theta}_{cr2}$ are critical angular velocities determined by friction constraint and Center of Pressure (COP) constraint, respectively, which are defined in Equations (3.11c) and (3.23b).

Subtracting square of Equation (3.11c) from square of Equation (3.23b), one has:

$$\dot{\theta}_{cr2}{}^2 - \dot{\theta}_{cr1}{}^2 = \frac{g\sin\theta}{mr(M\cos\theta + mrb)}(cmm_f r + M(m+m_f)\sin\theta - m^2r^2\sin\theta) \qquad \text{(A1)}$$

Since the denominator in Equation (A1) is always positive, the numerator determines the sign.

Examining the numerator shows two possible cases: $\theta \ge 0$, and $\theta < 0$.

**Case 1:** $0 \le \theta \le \theta^*$

Since $M = I + mr^2$, $M(m+m_f) = (I+mr^2)(m+m_f) > m^2r^2$.

As $\sin\theta \ge 0$, the numerator is always positive, one has:

$$\dot{\theta}_{cr2} \ge \dot{\theta}_{cr1} \qquad \text{(A2)}$$

So, the minimum critical angular velocity is determined by the friction constraint.

**Case 2:** $-\theta^* \le \theta \le 0$

Following the similar procedure to the case 1, and considering that $\sin\theta \le 0$, one has:

$$\dot{\theta}_{cr2} > \dot{\theta}_{cr1} \quad \text{when} \quad -\theta^* \le \theta < \tilde{\theta} \qquad \text{(A3)}$$

$$\dot{\theta}_{cr2} < \dot{\theta}_{cr1} \quad \text{when} \quad \tilde{\theta} < \theta < 0 \qquad \text{(A4)}$$

where:

$$\tilde{\theta} = -\arcsin\left(\frac{cmm_f r}{I(m+m_f)+mm_f r^2}\right) = -\arcsin\left(\frac{1}{\frac{I}{cr}(\frac{1}{m_f}+\frac{1}{m})+\frac{r}{c}}\right) \quad \text{(A5)}$$

Furthermore, as $r >> c$, $\frac{r}{c} >> 1$, thus $\tilde{\theta}$ will have a very low value.

Using parameters shown in Table 3.3, $\tilde{\theta} = 0.52^0$

# Appendix B

## Derivation of Coefficients in Mapping Matrices

In this section, the whole procedure of calculating coefficients for mapping matrices is given. First, minimize the distance based on least-square method, and then solve two sets of linear equations.

### Construction of Jacobian Matrix for $N_{Tay} = 2$, and $d_E = 3$

From Equation (5.6), the minimum number of parameters $N_p$ is equal to nine, thus nine neighbors, and 27 coefficients should be determined. Since $d_E = 3$, Equation (5.7) can be written as

$$\begin{aligned} Z_1^r(n;T_1) = {} & \partial F_{11} Z_1^r(n;T_0) + \partial F_{12} Z_2^r(n;T_0) + \partial F_{13} Z_3^r(n;T_0) \\ & + \frac{1}{2!}\{\partial F_{111}\left(Z_1^r(n;T_0)\right)^2 + \partial F_{112} Z_1^r(n;T_0) Z_2^r(n;T_0) + \partial F_{113} Z_1^r(n;T_0) Z_3^r(n;T_0) \\ & + \partial F_{121} Z_2^r(n;T_0) Z_1^r(n;T_0) + \partial F_{122}\left(Z_2^r(n;T_0)\right)^2 + \partial F_{123} Z_2^r(n;T_0) Z_3^r(n;T_0) \\ & + \partial F_{131} Z_3^r(n;T_0) Z_1^r(n;T_0) + \partial F_{132} Z_3^r(n;T_0) Z_2^r(n;T_0) + \partial F_{133}\left(Z_3^r(n;T_0)\right)^2\} \end{aligned} \tag{B1a}$$

$$\begin{aligned} Z_2^r(n;T_1) = {} & \partial F_{21} Z_1^r(n;T_0) + \partial F_{22} Z_2^r(n;T_0) + \partial F_{23} Z_3^r(n;T_0) \\ & + \frac{1}{2!}\{\partial F_{211}\left(Z_1^r(n;T_0)\right)^2 + \partial F_{212} Z_1^r(n;T_0) Z_2^r(n;T_0) + \partial F_{213} Z_1^r(n;T_0) Z_3^r(n;T_0) \\ & + \partial F_{221} Z_2^r(n;T_0) Z_1^r(n;T_0) + \partial F_{222}\left(Z_2^r(n;T_0)\right)^2 + \partial F_{223} Z_2^r(n;T_0) Z_3^r(n;T_0) \\ & + \partial F_{231} Z_3^r(n;T_0) Z_1^r(n;T_0) + \partial F_{232} Z_3^r(n;T_0) Z_2^r(n;T_0) + \partial F_{233}\left(Z_3^r(n;T_0)\right)^2\} \end{aligned} \tag{B1b}$$

$$Z_3^r(n;T_1)=\partial F_{31}Z_1^r(n;T_0)+\partial F_{32}Z_2^r(n;T_0)+\partial F_{33}Z_3^r(n;T_0)$$
$$+\frac{1}{2!}\{\partial F_{311}\left(Z_1^r(n;T_0)\right)^2+\partial F_{312}Z_1^r(n;T_0)Z_2^r(n;T_0)+\partial F_{313}Z_1^r(n;T_0)Z_3^r(n;T_0)$$
$$+\partial F_{321}Z_2^r(n;T_0)Z_1^r(n;T_0)+\partial F_{322}\left(Z_2^r(n;T_0)\right)^2+\partial F_{323}Z_2^r(n;T_0)Z_3^r(n;T_0)$$
$$+\partial F_{331}Z_3^r(n;T_0)Z_1^r(n;T_0)+\partial F_{332}Z_3^r(n;T_0)Z_2^r(n;T_0)+\partial F_{333}\left(Z_3^r(n;T_0)\right)^2\} \quad \text{(B1c)}$$

Re-writing Equation (B1) in matrix form, one has

$$\begin{pmatrix} Z_1^r(n;T_1) \\ Z_2^r(n;T_1) \\ Z_3^r(n;T_1) \end{pmatrix}=\begin{bmatrix} J_{11} & J_{12} & J_{13} \\ J_{21} & J_{22} & J_{23} \\ J_{31} & J_{32} & J_{33} \end{bmatrix}\begin{pmatrix} Z_1^r(n;T_0) \\ Z_2^r(n;T_0) \\ Z_3^r(n;T_0) \end{pmatrix} \quad \text{(B2)}$$

where

$$J_{11}=\partial F_{11}+\frac{1}{2}\{\partial F_{111}Z_1^r+\partial F_{112}Z_2^r+\partial F_{113}Z_3^r\}$$
$$J_{12}=\partial F_{12}+\frac{1}{2}\{\partial F_{121}Z_1^r+\partial F_{122}Z_2^r+\partial F_{123}Z_3^r\}$$
$$J_{13}=\partial F_{13}+\frac{1}{2}\{\partial F_{131}Z_1^r+\partial F_{132}Z_2^r+\partial F_{133}Z_3^r\}$$
$$J_{21}=\partial F_{21}+\frac{1}{2}\{\partial F_{211}Z_1^r+\partial F_{212}Z_2^r+\partial F_{213}Z_3^r\}$$
$$J_{22}=\partial F_{22}+\frac{1}{2}\{\partial F_{221}Z_1^r+\partial F_{222}Z_2^r+\partial F_{223}Z_3^r\} \quad \text{(B3)}$$
$$J_{23}=\partial F_{23}+\frac{1}{2}\{\partial F_{231}Z_1^r+\partial F_{232}Z_2^r+\partial F_{233}Z_3^r\}$$
$$J_{31}=\partial F_{31}+\frac{1}{2}\{\partial F_{311}Z_1^r+\partial F_{312}Z_2^r+\partial F_{313}Z_3^r\}$$
$$J_{32}=\partial F_{32}+\frac{1}{2}\{\partial F_{321}Z_1^r+\partial F_{322}Z_2^r+\partial F_{323}Z_3^r\}$$
$$J_{33}=\partial F_{33}+\frac{1}{2}\{\partial F_{331}Z_1^r+\partial F_{332}Z_2^r+\partial F_{333}Z_3^r\}$$

The coefficients $N_p \times d = 9 \times 3 = 27$ can be determined using the least-square method which minimize the following distance

$$\Pi = \sum_{i=1}^{N_p} \left\| Z^i(n;T_1) - JZ^i(n;T_0) \right\|^2 \tag{B4}$$

To simplify the expression of Equation (B3), we let

$$\begin{aligned}
&\partial F_{11} = a_1, \partial F_{111} = a_2,\ \partial F_{112} = a_3,\ \partial F_{113} = a_4,\ \partial F_{12} = a_5,\\
&\partial F_{122} = a_6, \partial F_{123} = a_7, \partial F_{13} = a_8, \partial F_{133} = a_9\\
&\partial F_{21} = b_1, \partial F_{211} = b_2,\ \partial F_{212} = b_3,\ \partial F_{213} = b_4,\ \partial F_{22} = b_5,\\
&\partial F_{222} = b_6, \partial F_{223} = b_7, \partial F_{23} = b_8, \partial F_{233} = b_9\\
&\partial F_{31} = c_1,\ \partial F_{311} = c_2,\ \partial F_{312} = c_3,\ \partial F_{313} = c_4,\ \partial F_{32} = c_5,\\
&\partial F_{322} = c_6, \partial F_{323} = c_7, \partial F_{33} = c_8, \partial F_{333} = c_9\\
&Z^i(n;T_0) = v^i
\end{aligned} \tag{B5}$$

Then Equation (B3) can be written as:

$$\begin{aligned}
J_{11} &= a_1 + \frac{1}{2}\left\{a_2 v_1^i + a_3 v_2^i + a_4 v_3^i\right\}\\
J_{12} &= a_5 + \frac{1}{2}\left\{a_3 v_1^i + a_6 v_2^i + a_7 v_3^i\right\}\\
J_{13} &= a_8 + \frac{1}{2}\left\{a_4 v_1^i + a_7 v_2^i + a_9 v_3^i\right\}\\
J_{21} &= b_1 + \frac{1}{2}\left\{b_2 v_1^i + b_3 v_2^i + b_4 v_3^i\right\}\\
J_{22} &= b_5 + \frac{1}{2}\left\{b_3 v_1^i + b_6 v_2^i + b_7 v_3^i\right\}\\
J_{23} &= b_8 + \frac{1}{2}\left\{b_4 v_1^i + b_7 v_2^i + b_9 v_3^i\right\}\\
J_{31} &= c_1 + \frac{1}{2}\left\{c_2 v_1^i + c_3 v_2^i + c_4 v_3^i\right\}\\
J_{32} &= c_5 + \frac{1}{2}\left\{c_3 v_1^i + c_6 v_2^i + c_7 v_3^i\right\}\\
J_{33} &= c_8 + \frac{1}{2}\left\{c_4 v_1^i + c_7 v_2^i + c_9 v_3^i\right\}
\end{aligned} \tag{B6}$$

The procedure of obtaining coefficients $a_i, b_i, c_i, (i = 1,...,9)$ is derived in details. First, minimize the distance based on least-square method, and then solve two sets of linear equations.

The lease-square method to show the distance is:

$$
\begin{aligned}
\Pi &= \sum_{i=1}^{N_p} \left\| Z^i(n;T_2) - JZ^i(n;0) \right\| = \sum_{i=1}^{N_p} \left\| Z^i - Jv^i \right\|^2 \\
&= \sum_{i=1}^{N_p} \{ \left( Z_1^i - J_{11}v_1^i - J_{12}v_2^i - J_{13}v_3^i \right)^2 + \left( Z_2^i - J_{21}v_1^i - J_{22}v_2^i - J_{23}v_3^i \right)^2 \\
&+ \left( Z_3^i - J_{31}v_1^i - J_{32}v_2^i - J_{33}v_3^i \right)^2 \} \\
&= \sum_{i=1}^{N_p} \{ Z_1^i - \left( a_1 + \frac{1}{2}\left\{ a_2v_1^i + a_3v_2^i + a_4v_3^i \right\} \right)v_1^i - \left( a_5 + \frac{1}{2}\left\{ a_3v_1^i + a_6v_2^i + a_7v_3^i \right\} \right)v_2^i \\
&- \left( a_8 + \frac{1}{2}\left\{ a_4v_1^i + a_7v_2^i + a_9v_3^i \right\} \right) \}^2 \\
&+ \sum_{i=1}^{N_p} \{ Z_2^i - \left( b_1 + \frac{1}{2}\left\{ b_2v_1^i + b_3v_2^i + b_4v_3^i \right\} \right)v_1^i - \left( b_5 + \frac{1}{2}\left\{ b_3v_1^i + b_6v_2^i + b_7v_3^i \right\} \right)v_2^i \\
&- \left( b_8 + \frac{1}{2}\left\{ b_4v_1^i + b_7v_2^i + b_9v_3^i \right\} \right) \}^2 \\
&+ \sum_{i=1}^{N_p} \{ Z_3^i - \left( c_1 + \frac{1}{2}\left\{ c_2v_1^i + c_3v_2^i + c_4v_3^i \right\} \right)v_1^i - \left( c_5 + \frac{1}{2}\left\{ c_3v_1^i + c_6v_2^i + c_7v_3^i \right\} \right)v_2^i \\
&- \left( c_8 + \frac{1}{2}\left\{ c_4v_1^i + c_7v_2^i + c_9v_3^i \right\} \right) \}^2
\end{aligned}
\tag{B7}
$$

where $a_i, b_i, c_i, v_\alpha^i, (i = 1,...,9), (\alpha = 1,2,3)$ , are defined in Equation (B5), $J_{ij}, (i, j = 1,2,3)$ are defined in Equation (B6).

To minimize the above distance, the following linear equations are obtained:

$$\frac{\partial \Pi}{\partial a_1} = \sum_{i=1}^{N_p} 2\{Z_1^i - \left(a_1 + \frac{1}{2}\{a_2 v_1^i + a_3 v_2^i + a_4 v_3^i\}\right) v_1^i - \left(a_5 + \frac{1}{2}\{a_3 v_1^i + a_6 v_2^i + a_7 v_3^i\}\right) v_2^i - \left(a_8 + \frac{1}{2}\{a_4 v_1^i + a_7 v_2^i + a_9 v_3^i\}\right) v_3^i\} v_1^i = 0$$

$$\frac{\partial \Pi}{\partial a_2} = \sum_{i=1}^{N_p} 2\{Z_1^i - \left(a_1 + \frac{1}{2}\{a_2 v_1^i + a_3 v_2^i + a_4 v_3^i\}\right) v_1^i - \left(a_5 + \frac{1}{2}\{a_3 v_1^i + a_6 v_2^i + a_7 v_3^i\}\right) v_2^i - \left(a_8 + \frac{1}{2}\{a_4 v_1^i + a_7 v_2^i + a_9 v_3^i\}\right) v_3^i\} \frac{1}{2} v_1^i v_1^i = 0$$

$$\frac{\partial \Pi}{\partial a_3} = \sum_{i=1}^{N_p} 2\{Z_1^i - \left(a_1 + \frac{1}{2}\{a_2 v_1^i + a_3 v_2^i + a_4 v_3^i\}\right) v_1^i - \left(a_5 + \frac{1}{2}\{a_3 v_1^i + a_6 v_2^i + a_7 v_3^i\}\right) v_2^i - \left(a_8 + \frac{1}{2}\{a_4 v_1^i + a_7 v_2^i + a_9 v_3^i\}\right) v_3^i\} v_1^i v_2^i = 0$$

$$\frac{\partial \Pi}{\partial a_4} = \sum_{i=1}^{N_p} 2\{Z_1^i - \left(a_1 + \frac{1}{2}\{a_2 v_1^i + a_3 v_2^i + a_4 v_3^i\}\right) v_1^i - \left(a_5 + \frac{1}{2}\{a_3 v_1^i + a_6 v_2^i + a_7 v_3^i\}\right) v_2^i - \left(a_8 + \frac{1}{2}\{a_4 v_1^i + a_7 v_2^i + a_9 v_3^i\}\right) v_3^i\} v_1^i v_3^i = 0$$

$$\frac{\partial \Pi}{\partial a_5} = \sum_{i=1}^{N_p} 2\{Z_1^i - \left(a_1 + \frac{1}{2}\{a_2 v_1^i + a_3 v_2^i + a_4 v_3^i\}\right) v_1^i - \left(a_5 + \frac{1}{2}\{a_3 v_1^i + a_6 v_2^i + a_7 v_3^i\}\right) v_2^i - \left(a_8 + \frac{1}{2}\{a_4 v_1^i + a_7 v_2^i + a_9 v_3^i\}\right) v_3^i\} v_2^i = 0$$

$$\frac{\partial \Pi}{\partial a_6} = \sum_{i=1}^{N_p} 2\{Z_1^i - \left(a_1 + \frac{1}{2}\{a_2 v_1^i + a_3 v_2^i + a_4 v_3^i\}\right) v_1^i - \left(a_5 + \frac{1}{2}\{a_3 v_1^i + a_6 v_2^i + a_7 v_3^i\}\right) v_2^i - \left(a_8 + \frac{1}{2}\{a_4 v_1^i + a_7 v_2^i + a_9 v_3^i\}\right) v_3^i\} \frac{1}{2} v_2^i v_2^i = 0$$

$$\frac{\partial \Pi}{\partial a_7} = \sum_{i=1}^{N_P} 2\{Z_1^i - \left(a_1 + \frac{1}{2}\{a_2 v_1^i + a_3 v_2^i + a_4 v_3^i\}\right) v_1^i - \left(a_5 + \frac{1}{2}\{a_3 v_1^i + a_6 v_2^i + a_7 v_3^i\}\right) v_2^i$$
$$- \left(a_8 + \frac{1}{2}\{a_4 v_1^i + a_7 v_2^i + a_9 v_3^i\}\right) v_3^i\} v_2^i v_3^i$$
$$= 0$$

$$\frac{\partial \Pi}{\partial a_8} = \sum_{i=1}^{N_P} 2\{Z_1^i - \left(a_1 + \frac{1}{2}\{a_2 v_1^i + a_3 v_2^i + a_4 v_3^i\}\right) v_1^i - \left(a_5 + \frac{1}{2}\{a_3 v_1^i + a_6 v_2^i + a_7 v_3^i\}\right) v_2^i$$
$$- \left(a_8 + \frac{1}{2}\{a_4 v_1^i + a_7 v_2^i + a_9 v_3^i\}\right) v_3^i\} v_3^i$$
$$= 0$$

$$\frac{\partial \Pi}{\partial a_9} = \sum_{i=1}^{N_P} 2\{Z_1^i - \left(a_1 + \frac{1}{2}\{a_2 v_1^i + a_3 v_2^i + a_4 v_3^i\}\right) v_1^i - \left(a_5 + \frac{1}{2}\{a_3 v_1^i + a_6 v_2^i + a_7 v_3^i\}\right) v_2^i$$
$$- \left(a_8 + \frac{1}{2}\{a_4 v_1^i + a_7 v_2^i + a_9 v_3^i\}\right) v_3^i\} \frac{1}{2} v_3^i v_3^i$$
$$= 0$$

$$\frac{\partial \Pi}{\partial b_1} = \sum_{i=1}^{N_P} 2\{Z_2^i - \left(b_1 + \frac{1}{2}\{b_2 v_1^i + b_3 v_2^i + b_4 v_3^i\}\right) v_1^i - \left(b_5 + \frac{1}{2}\{b_3 v_1^i + b_6 v_2^i + b_7 v_3^i\}\right) v_2^i$$
$$- \left(b_8 + \frac{1}{2}\{b_4 v_1^i + b_7 v_2^i + b_9 v_3^i\}\right) v_3^i\} v_1^i$$
$$= 0$$

$$\frac{\partial \Pi}{\partial b_2} = \sum_{i=1}^{N_P} 2\{Z_2^i - \left(b_1 + \frac{1}{2}\{b_2 v_1^i + b_3 v_2^i + b_4 v_3^i\}\right) v_1^i - \left(b_5 + \frac{1}{2}\{b_3 v_1^i + b_6 v_2^i + b_7 v_3^i\}\right) v_2^i$$
$$- \left(b_8 + \frac{1}{2}\{b_4 v_1^i + b_7 v_2^i + b_9 v_3^i\}\right) v_3^i\} \frac{1}{2} v_1^i v_1^i$$
$$= 0$$

$$\frac{\partial \Pi}{\partial b_3} = \sum_{i=1}^{N_P} 2\{Z_2^i - \left(b_1 + \frac{1}{2}\{b_2 v_1^i + b_3 v_2^i + b_4 v_3^i\}\right) v_1^i - \left(b_5 + \frac{1}{2}\{b_3 v_1^i + b_6 v_2^i + b_7 v_3^i\}\right) v_2^i$$
$$- \left(b_8 + \frac{1}{2}\{b_4 v_1^i + b_7 v_2^i + b_9 v_3^i\}\right) v_3^i\} v_1^i v_2^i$$
$$= 0$$

$$\frac{\partial \Pi}{\partial b_4} = \sum_{i=1}^{N_p} 2\{Z_2^i - \left(b_1 + \frac{1}{2}\{b_2 v_1^i + b_3 v_2^i + b_4 v_3^i\}\right) v_1^i - \left(b_5 + \frac{1}{2}\{b_3 v_1^i + b_6 v_2^i + b_7 v_3^i\}\right) v_2^i$$
$$- \left(b_8 + \frac{1}{2}\{b_4 v_1^i + b_7 v_2^i + b_9 v_3^i\}\right) v_3^i\} v_1^i v_3^i$$
$$= 0$$

$$\frac{\partial \Pi}{\partial b_5} = \sum_{i=1}^{N_p} 2\{Z_2^i - \left(b_1 + \frac{1}{2}\{b_2 v_1^i + b_3 v_2^i + b_4 v_3^i\}\right) v_1^i - \left(b_5 + \frac{1}{2}\{b_3 v_1^i + b_6 v_2^i + b_7 v_3^i\}\right) v_2^i$$
$$- \left(b_8 + \frac{1}{2}\{b_4 v_1^i + b_7 v_2^i + b_9 v_3^i\}\right) v_3^i\} v_2^i$$
$$= 0$$

$$\frac{\partial \Pi}{\partial b_6} = \sum_{i=1}^{N_p} 2\{Z_2^i - \left(b_1 + \frac{1}{2}\{b_2 v_1^i + b_3 v_2^i + b_4 v_3^i\}\right) v_1^i - \left(b_5 + \frac{1}{2}\{b_3 v_1^i + b_6 v_2^i + b_7 v_3^i\}\right) v_2^i$$
$$- \left(b_8 + \frac{1}{2}\{b_4 v_1^i + b_7 v_2^i + b_9 v_3^i\}\right) v_3^i\} \frac{1}{2} v_2^i v_2^i$$
$$= 0$$

$$\frac{\partial \Pi}{\partial b_7} = \sum_{i=1}^{N_p} 2\{Z_2^i - \left(b_1 + \frac{1}{2}\{b_2 v_1^i + b_3 v_2^i + b_4 v_3^i\}\right) v_1^i - \left(b_5 + \frac{1}{2}\{b_3 v_1^i + b_6 v_2^i + b_7 v_3^i\}\right) v_2^i$$
$$- \left(b_8 + \frac{1}{2}\{b_4 v_1^i + b_7 v_2^i + b_9 v_3^i\}\right) v_3^i\} v_2^i v_3^i$$
$$= 0$$

$$\frac{\partial \Pi}{\partial b_8} = \sum_{i=1}^{N_p} 2\{Z_2^i - \left(b_1 + \frac{1}{2}\{b_2 v_1^i + b_3 v_2^i + b_4 v_3^i\}\right) v_1^i - \left(b_5 + \frac{1}{2}\{b_3 v_1^i + b_6 v_2^i + b_7 v_3^i\}\right) v_2^i$$
$$- \left(b_8 + \frac{1}{2}\{b_4 v_1^i + b_7 v_2^i + b_9 v_3^i\}\right) v_3^i\} v_3^i$$
$$= 0$$

$$\frac{\partial \Pi}{\partial b_9} = \sum_{i=1}^{N_p} 2\{Z_2^i - \left(b_1 + \frac{1}{2}\{b_2 v_1^i + b_3 v_2^i + b_4 v_3^i\}\right) v_1^i - \left(b_5 + \frac{1}{2}\{b_3 v_1^i + b_6 v_2^i + b_7 v_3^i\}\right) v_2^i$$
$$- \left(b_8 + \frac{1}{2}\{b_4 v_1^i + b_7 v_2^i + b_9 v_3^i\}\right) v_3^i\} \frac{1}{2} v_3^i v_3^i$$
$$= 0$$

$$\frac{\partial \Pi}{\partial c_1} = \sum_{i=1}^{N_P} 2\{Z_3^i - \left(c_1 + \frac{1}{2}\{c_2 v_1^i + c_3 v_2^i + c_4 v_3^i\}\right) v_1^i - \left(c_5 + \frac{1}{2}\{c_3 v_1^i + c_6 v_2^i + c_7 v_3^i\}\right) v_2^i$$
$$- \left(c_8 + \frac{1}{2}\{c_4 v_1^i + c_7 v_2^i + c_9 v_3^i\}\right) v_3^i \} v_1^i$$
$$= 0$$

$$\frac{\partial \Pi}{\partial c_2} = \sum_{i=1}^{N_P} 2\{Z_3^i - \left(c_1 + \frac{1}{2}\{c_2 v_1^i + c_3 v_2^i + c_4 v_3^i\}\right) v_1^i - \left(c_5 + \frac{1}{2}\{c_3 v_1^i + c_6 v_2^i + c_7 v_3^i\}\right) v_2^i$$
$$- \left(c_8 + \frac{1}{2}\{c_4 v_1^i + c_7 v_2^i + c_9 v_3^i\}\right) v_3^i \} \frac{1}{2} v_1^i v_1^i$$
$$= 0$$

$$\frac{\partial \Pi}{\partial c_3} = \sum_{i=1}^{N_P} 2\{Z_3^i - \left(c_1 + \frac{1}{2}\{c_2 v_1^i + c_3 v_2^i + c_4 v_3^i\}\right) v_1^i - \left(c_5 + \frac{1}{2}\{c_3 v_1^i + c_6 v_2^i + c_7 v_3^i\}\right) v_2^i$$
$$- \left(c_8 + \frac{1}{2}\{c_4 v_1^i + c_7 v_2^i + c_9 v_3^i\}\right) v_3^i \} v_1^i v_2^i$$
$$= 0$$

$$\frac{\partial \Pi}{\partial c_4} = \sum_{i=1}^{N_P} 2\{Z_3^i - \left(c_1 + \frac{1}{2}\{c_2 v_1^i + c_3 v_2^i + c_4 v_3^i\}\right) v_1^i - \left(c_5 + \frac{1}{2}\{c_3 v_1^i + c_6 v_2^i + c_7 v_3^i\}\right) v_2^i$$
$$- \left(c_8 + \frac{1}{2}\{c_4 v_1^i + c_7 v_2^i + c_9 v_3^i\}\right) v_3^i \} v_1^i v_3^i$$
$$= 0$$

$$\frac{\partial \Pi}{\partial c_5} = \sum_{i=1}^{N_P} 2\{Z_3^i - \left(c_1 + \frac{1}{2}\{c_2 v_1^i + c_3 v_2^i + c_4 v_3^i\}\right) v_1^i - \left(c_5 + \frac{1}{2}\{c_3 v_1^i + c_6 v_2^i + c_7 v_3^i\}\right) v_2^i$$
$$- \left(c_8 + \frac{1}{2}\{c_4 v_1^i + c_7 v_2^i + c_9 v_3^i\}\right) v_3^i \} v_2^i$$
$$= 0$$

$$\frac{\partial \Pi}{\partial c_6} = \sum_{i=1}^{N_P} 2\{Z_3^i - \left(c_1 + \frac{1}{2}\{c_2 v_1^i + c_3 v_2^i + c_4 v_3^i\}\right) v_1^i - \left(c_5 + \frac{1}{2}\{c_3 v_1^i + c_6 v_2^i + c_7 v_3^i\}\right) v_2^i$$
$$- \left(c_8 + \frac{1}{2}\{c_4 v_1^i + c_7 v_2^i + c_9 v_3^i\}\right) v_3^i \} \frac{1}{2} v_2^i v_2^i$$
$$= 0$$

$$\frac{\partial \Pi}{\partial c_7} = \sum_{i=1}^{N_p} 2\{Z_3^i - \left(c_1 + \frac{1}{2}\{c_2 v_1^i + c_3 v_2^i + c_4 v_3^i\}\right) v_1^i - \left(c_5 + \frac{1}{2}\{c_3 v_1^i + c_6 v_2^i + c_7 v_3^i\}\right) v_2^i$$
$$- \left(c_8 + \frac{1}{2}\{c_4 v_1^i + c_7 v_2^i + c_9 v_3^i\}\right) v_3^i\} v_2^i v_3^i$$
$$= 0$$

$$\frac{\partial \Pi}{\partial c_8} = \sum_{i=1}^{N_p} 2\{Z_3^i - \left(c_1 + \frac{1}{2}\{c_2 v_1^i + c_3 v_2^i + c_4 v_3^i\}\right) v_1^i - \left(c_5 + \frac{1}{2}\{c_3 v_1^i + c_6 v_2^i + c_7 v_3^i\}\right) v_2^i$$
$$- \left(c_8 + \frac{1}{2}\{c_4 v_1^i + c_7 v_2^i + c_9 v_3^i\}\right) v_3^i\} v_3^i$$
$$= 0$$

$$\frac{\partial \Pi}{\partial c_9} = \sum_{i=1}^{N_p} 2\{Z_3^i - \left(c_1 + \frac{1}{2}\{c_2 v_1^i + c_3 v_2^i + c_4 v_3^i\}\right) v_1^i - \left(c_5 + \frac{1}{2}\{c_3 v_1^i + c_6 v_2^i + c_7 v_3^i\}\right) v_2^i$$
$$- \left(c_8 + \frac{1}{2}\{c_4 v_1^i + c_7 v_2^i + c_9 v_3^i\}\right) v_3^i\} \frac{1}{2} v_3^i v_3^i \qquad \text{(B8)}$$
$$= 0$$

The above linear equations can be written as matrix form as

$$U_A = VA, U_B = VB, U_C = VC \qquad \text{(B9)}$$

where

$$A = (a_1, a_2, ..., a_9)^T \qquad \text{(B10a)}$$

$$B = (b_1, b_2, ..., b_9)^T \qquad \text{(B10b)}$$

$$C = (c_1, c_2, ..., c_9)^T \qquad \text{(B10c)}$$

$$U_A = \left(\sum_{i=1}^{N_p} Z_1^i v_1^i, \sum_{i=1}^{N_p} Z_1^i (v_1^i)^2, \sum_{i=1}^{N_p} Z_1^i v_1^i v_2^i, \sum_{i=1}^{N_p} Z_1^i v_1^i v_3^i, \sum_{i=1}^{N_p} Z_1^i v_2^i, \sum_{i=1}^{N_p} Z_1^i (v_2^i)^2, \sum_{i=1}^{N_p} Z_1^i v_2^i v_3^i, v \sum_{i=1}^{N_p} Z_1^i v_3^i, \sum_{i=1}^{N_p} Z_1^i (v_3^i)^2\right)^T \qquad \text{(B10d)}$$

$$U_B = \left(\sum_{i=1}^{N_p} Z_2^i v_1^i, \sum_{i=1}^{N_p} Z_2^i (v_1^i)^2, \sum_{i=1}^{N_p} Z_2^i v_1^i v_2^i, \sum_{i=1}^{N_p} Z_2^i v_1^i v_3^i, \sum_{i=1}^{N_p} Z_2^i v_2^i, \sum_{i=1}^{N_p} Z_2^i (v_2^i)^2, \sum_{i=1}^{N_p} Z_2^i v_2^i v_3^i, v \sum_{i=1}^{N_p} Z_2^i v_3^i, \sum_{i=1}^{N_p} Z_2^i (v_3^i)^2\right)^T \qquad \text{(B10e)}$$

$$U_C = \left(\sum_{i=1}^{N_p} Z_3^i v_1^i, \sum_{i=1}^{N_p} Z_3^i (v_1^i)^2, \sum_{i=1}^{N_p} Z_3^i v_1^i v_2^i, \sum_{i=1}^{N_p} Z_3^i v_1^i v_3^i, \sum_{i=1}^{N_p} Z_3^i v_2^i, \sum_{i=1}^{N_p} Z_3^i (v_2^i)^2, \sum_{i=1}^{N_p} Z_3^i v_2^i v_3^i, v \sum_{i=1}^{N_p} Z_3^i v_3^i, \sum_{i=1}^{N_p} Z_3^i (v_3^i)^2\right)^T \qquad \text{(B10f)}$$

$$V=\begin{pmatrix}
\sum_{i=1}^{N_p}(v_1^i)^2 & \frac{1}{2}\sum_{i=1}^{N_p}(v_1^i)^3 & \sum_{i=1}^{N_p}(v_1^i)^2 v_2^i & \sum_{i=1}^{N_p}(v_1^i)^2 v_3^i & \sum_{i=1}^{N_p} v_1^i v_2^i & \frac{1}{2}\sum_{i=1}^{N_p} v_1^i (v_2^i)^2 & \sum_{i=1}^{N_p} v_1^i v_2^i v_3^i & \sum_{i=1}^{N_p} v_1^i v_3^i & \frac{1}{2}\sum_{i=1}^{N_p} v_1^i (v_3^i)^2 \\
\sum_{i=1}^{N_p}(v_1^i)^3 & \frac{1}{2}\sum_{i=1}^{N_p}(v_1^i)^4 & \sum_{i=1}^{N_p}(v_1^i)^3 v_2^i & \sum_{i=1}^{N_p}(v_1^i)^3 v_3^i & \sum_{i=1}^{N_p}(v_1^i)^2 v_2^i & \frac{1}{2}\sum_{i=1}^{N_p}(v_1^i)^2 (v_2^i)^2 & \sum_{i=1}^{N_p}(v_1^i)^2 v_2^i v_3^i & \sum_{i=1}^{N_p}(v_1^i)^2 v_3^i & \frac{1}{2}\sum_{i=1}^{N_p}(v_1^i)^2 (v_3^i)^2 \\
\sum_{i=1}^{N_p}(v_1^i)^2 v_2^i & \frac{1}{2}\sum_{i=1}^{N_p}(v_1^i)^3 v_2^i & \sum_{i=1}^{N_p}(v_1^i)^2 (v_2^i)^2 & \sum_{i=1}^{N_p}(v_1^i)^2 v_2^i v_3^i & \sum_{i=1}^{N_p} v_1^i (v_2^i)^2 & \frac{1}{2}\sum_{i=1}^{N_p} v_1^i (v_2^i)^3 & \sum_{i=1}^{N_p} v_1^i (v_2^i)^2 v_3^i & \sum_{i=1}^{N_p} v_1^i v_2^i v_3^i & \frac{1}{2}\sum_{i=1}^{N_p} v_1^i v_2^i (v_3^i)^2 \\
\sum_{i=1}^{N_p}(v_1^i)^2 v_3^i & \frac{1}{2}\sum_{i=1}^{N_p}(v_1^i)^3 v_3^i & \sum_{i=1}^{N_p}(v_1^i)^2 v_2^i v_3^i & \sum_{i=1}^{N_p}(v_1^i)^2 (v_3^i)^2 & \sum_{i=1}^{N_p} v_1^i v_2^i v_3^i & \frac{1}{2}\sum_{i=1}^{N_p} v_1^i (v_2^i)^2 v_3^i & \sum_{i=1}^{N_p} v_1^i v_2^i (v_3^i)^2 & \sum_{i=1}^{N_p} v_1^i (v_3^i)^2 & \frac{1}{2}\sum_{i=1}^{N_p} v_1^i (v_3^i)^3 \\
\sum_{i=1}^{N_p} v_1^i v_2^i & \frac{1}{2}\sum_{i=1}^{N_p}(v_1^i)^2 v_2^i & \sum_{i=1}^{N_p} v_1^i (v_2^i)^2 & \sum_{i=1}^{N_p} v_1^i v_2^i v_3^i & \sum_{i=1}^{N_p}(v_2^i)^2 & \frac{1}{2}\sum_{i=1}^{N_p}(v_2^i)^3 & \sum_{i=1}^{N_p}(v_2^i)^2 v_3^i & \sum_{i=1}^{N_p} v_2^i (v_3^i)^2 & \frac{1}{2}\sum_{i=1}^{N_p} v_2^i (v_3^i)^2 \\
\sum_{i=1}^{N_p} v_1^i (v_2^i)^2 & \frac{1}{2}\sum_{i=1}^{N_p}(v_1^i)^2 (v_2^i)^2 & \sum_{i=1}^{N_p} v_1^i (v_2^i)^3 & \sum_{i=1}^{N_p} v_1^i (v_2^i)^2 v_3^i & \sum_{i=1}^{N_p}(v_2^i)^3 & \frac{1}{2}\sum_{i=1}^{N_p}(v_2^i)^4 & \sum_{i=1}^{N_p}(v_2^i)^3 v_3^i & \sum_{i=1}^{N_p}(v_2^i)^2 v_3^i & \frac{1}{2}\sum_{i=1}^{N_p}(v_2^i)^2 (v_3^i)^2 \\
\sum_{i=1}^{N_p} v_1^i v_2^i v_3^i & \frac{1}{2}\sum_{i=1}^{N_p}(v_1^i)^2 v_2^i v_3^i & \sum_{i=1}^{N_p} v_1^i (v_2^i)^2 v_3^i & \sum_{i=1}^{N_p} v_1^i v_2^i (v_3^i)^2 & \sum_{i=1}^{N_p}(v_2^i)^2 v_3^i & \frac{1}{2}\sum_{i=1}^{N_p}(v_2^i)^3 v_3^i & \sum_{i=1}^{N_p}(v_2^i)^2 (v_3^i)^2 & \sum_{i=1}^{N_p} v_2^i (v_3^i)^2 & \frac{1}{2}\sum_{i=1}^{N_p} v_2^i (v_3^i)^3 \\
\sum_{i=1}^{N_p} v_1^i v_3^i & \frac{1}{2}\sum_{i=1}^{N_p}(v_1^i)^2 v_3^i & \sum_{i=1}^{N_p} v_1^i v_2^i v_3^i & \sum_{i=1}^{N_p} v_1^i (v_3^i)^2 & \sum_{i=1}^{N_p} v_2^i v_3^i & \frac{1}{2}\sum_{i=1}^{N_p}(v_2^i)^2 v_3^i & \sum_{i=1}^{N_p} v_2^i (v_3^i)^2 & \sum_{i=1}^{N_p}(v_3^i)^2 & \frac{1}{2}\sum_{i=1}^{N_p}(v_3^i)^3 \\
\sum_{i=1}^{N_p} v_1^i (v_3^i)^2 & \frac{1}{2}\sum_{i=1}^{N_p}(v_1^i)^2 (v_3^i)^2 & \sum_{i=1}^{N_p} v_1^i v_2^i (v_3^i)^2 & \sum_{i=1}^{N_p} v_1^i (v_3^i)^3 & \sum_{i=1}^{N_p} v_2^i (v_3^i)^2 & \frac{1}{2}\sum_{i=1}^{N_p}(v_2^i)^2 (v_3^i)^2 & \sum_{i=1}^{N_p} v_2^i (v_3^i)^3 & \sum_{i=1}^{N_p}(v_3^i)^3 & \frac{1}{2}\sum_{i=1}^{N_p}(v_3^i)^4
\end{pmatrix} \tag{B10g}$$

These equations can be solved when matrix $V$ is invertible.

$$A = V^{-1}U_A, B = V^{-1}U_B, C = V^{-1}U_C \tag{B11}$$

After getting coefficients, one can construct Jacobian matrix according to Equation (B6).

$$J = \begin{bmatrix} J_{11} & J_{12} & J_{13} \\ J_{21} & J_{22} & J_{23} \\ J_{31} & J_{32} & J_{33} \end{bmatrix} \tag{B12}$$

After obtaining the Jacobian matrix, multiplying these Jacobians together and then computing the eigenvalues. Then, (up to some constant related to the sampling time) the Lyapunov exponents can be computed as the logarithm of these eigenvalues. The entire procedure is described in reference (Abarbanel, 1996).

# Appendix C

## Description of the Structure on Calculation of Lyapunov Exponents Based on a Time Series Using Nonlinear Approximation

In this Appendix, the structure of the software implemented and used in this thesis will be provided. The time series is generated from the mathematical model detailed in Chapter 3. This time series is used to reconstruct the control system based on Takens' time delay method. Nonlinear approximation is used in Taylor expansion. Least-square method is used to obtained coefficients which are required for constructing mapping matrices. Time histories of Lyapunov exponents' spectrum is for checking the convergence of the exponents.

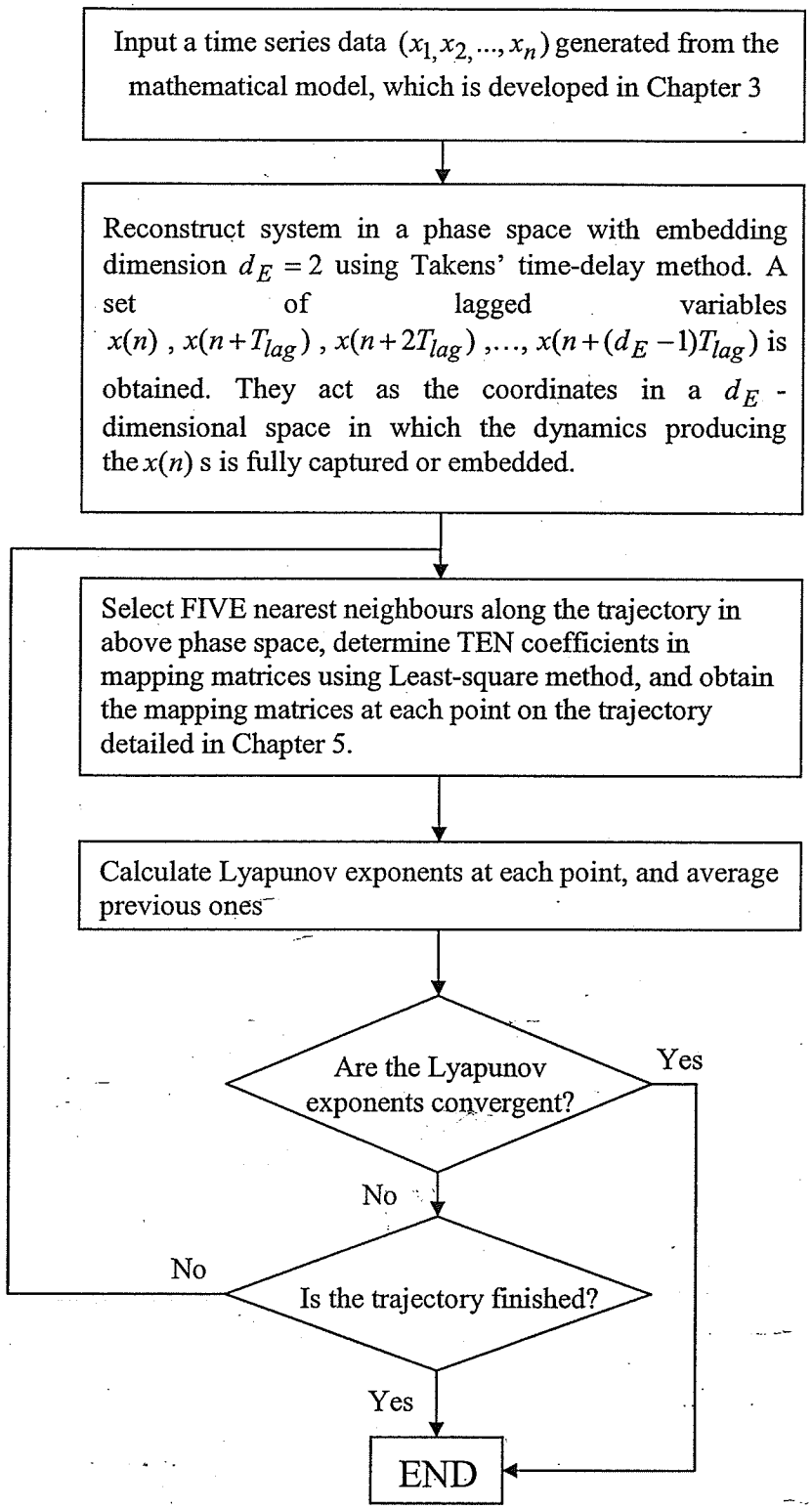
Input a time series data $(x_1, x_2, ..., x_n)$ generated from the mathematical model, which is developed in Chapter 3
Reconstruct system in a phase space with embedding dimension $d_E = 2$ using Takens' time-delay method. A set of lagged variables $x(n)$ , $x(n+T_{lag})$ , $x(n+2T_{lag})$ ,..., $x(n+(d_E-1)T_{lag})$ is obtained. They act as the coordinates in a $d_E$ - dimensional space in which the dynamics producing the $x(n)$ s is fully captured or embedded.
Select FIVE nearest neighbours along the trajectory in above phase space, determine TEN coefficients in mapping matrices using Least-square method, and obtain the mapping matrices at each point on the trajectory detailed in Chapter 5.
Calculate Lyapunov exponents at each point, and average previous ones
Are the Lyapunov exponents convergent?
Yes
No
Is the trajectory finished?
No
Yes
END